On the right track

Using neuroimaging to improve deep brain stimulation outcomes in psychiatry

Liebrand, L.C.

Publication date
2023

Document Version
Final published version

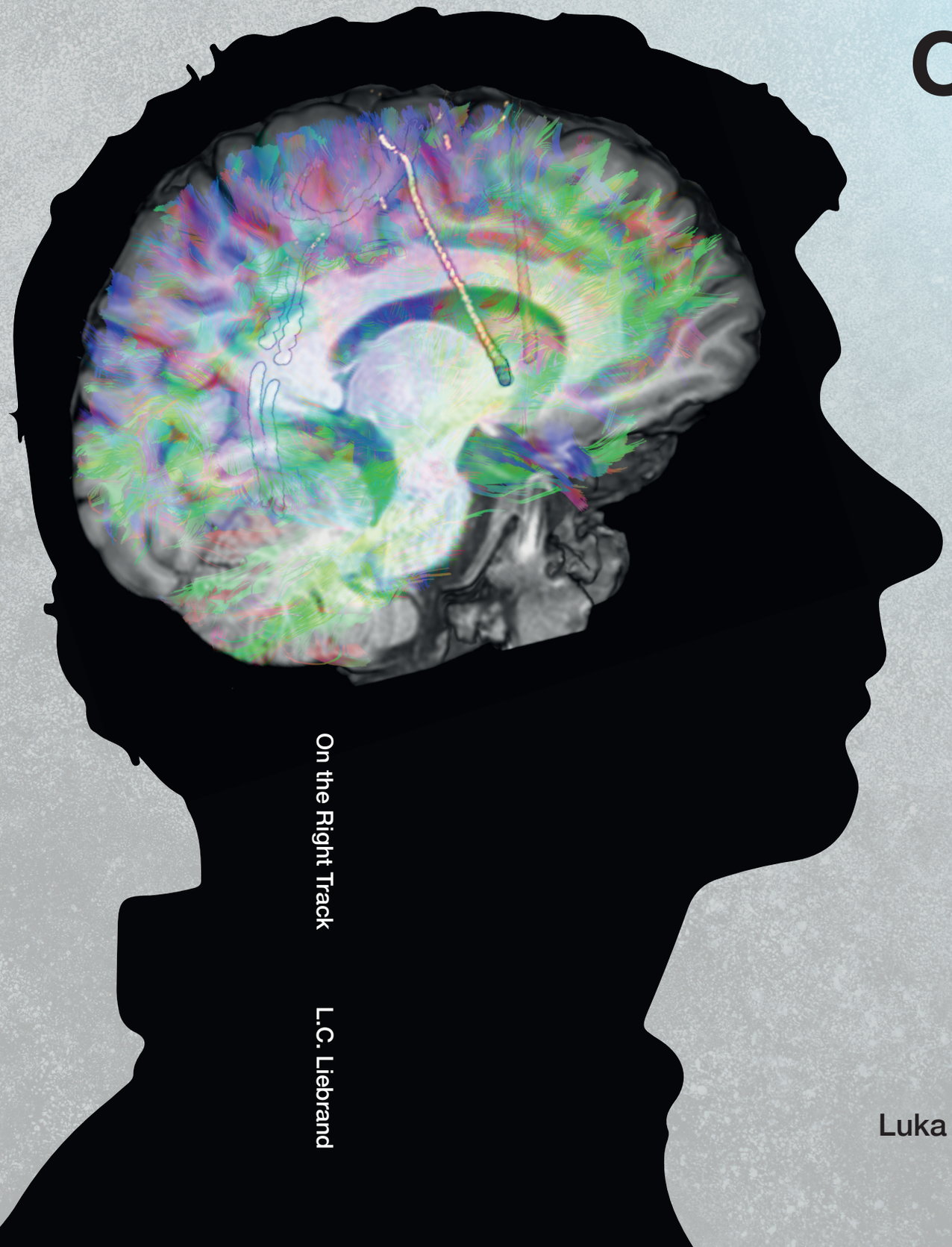

On the Right Track

Using Neuroimaging to Improve Deep Brain Stimulation Outcomes in Psychiatry

On the Right Track

L.C. Liebrand

Luka Charlie Liebrand

On the Right Track

Using Neuroimaging to Improve Deep Brain Stimulation Outcomes in Psychiatry

Luka Charlie Liebrand

The research in this thesis was supported by a research grant from the AMC (2015.011).

Cover Design: Bas Smedes

Printed by: printenbind.nl

On the Right Track

Using Neuroimaging to Improve Deep Brain Stimulation Outcomes in Psychiatry

ACADEMISCH PROEFSCHRIFT

ter verkrijging van de graad van doctor

aan de Universiteit van Amsterdam

op gezag van de Rector Magnificus

prof. dr. ir. P.P.C.C. Verbeek

ten overstaan van een door het College voor Promoties ingestelde commissie,

in het openbaar te verdedigen in de Agnietenkapel

op dinsdag 14 maart 2023, te 15.00 uur

door **Luka Charlie Liebrand**

geboren te AMSTERDAM

Promotiecommissie

Promotores:	prof. dr. G.A. van Wingen	AMC-UvA
	prof. dr. D.A.J.P. Denys	AMC-UvA
Copromotores:	dr. ir. M.W.A. Caan	AMC-UvA
Overige leden:	prof. dr. B.U. Forstmann	Universiteit van Amsterdam
	prof. dr. J. Kuhn	University of Cologne
	prof. dr. ir. A.J. Nederveen	AMC-UvA
	dr. M. Beudel	AMC-UvA
	dr. P.P. de Koning	AMC-UvA

Faculteit der Geneeskunde

Contents

I. GENERAL INTRODUCTION

Chapter 1

General Introduction

1.1 Deep brain stimulation

Deep brain stimulation (DBS) is a treatment designed to modulate brain activity. Stimulation is usually delivered through two electrodes implanted in the brain, connected to a subcutaneous electric stimulator. The DBS device is tuneable, with changeable parameters including voltage, frequency, polarity, and pulse duration. A typical DBS electrode has multiple contacts that can be activated individually; by changing which contacts are active along the electrode, even the depth of stimulation can be altered. When the stimulation parameters are adequately tuned, DBS may 'disrupt' or 'interfere with' pathological brain activity, thereby providing treatment.

Aside from DBS, multiple brain stimulation techniques are clinically used. These include electroconvulsive therapy (ECT), transcranial magnetic stimulation (TMS), transcranial alternating/direct current stimulation (TACS/TDCS) and transcranial ultrasound (TUS). Among these methods, DBS is the only one requiring surgical implantation, and could therefore be considered the most invasive. However, it also provides the most focused stimulation and could thus also be considered to be the most selective method. The main reason for implanting electrodes to deliver stimulation is to reach subcortical targets, which are difficult to reach by non-invasive stimulation modalities since they are attenuated by the skull and skin.

Some of the disorders that can be treated with DBS are also treatable with lesioning. Modern lesioning has evolved from the crude techniques used during much of the 20th century, for which large parts of the brain were severed, such as lobotomy or corpus callosotomy. Nowadays, lesioning is a precision neurosurgical procedure by which a small part of the brain tissue - usually white matter, which is effectively the brain's circuitry - is ablated to disrupt pathological brain connectivity. DBS can be considered a tuneable successor to lesioning, as it can also disrupt pathological brain circuitry. Because DBS evolved from lesioning, many DBS targets overlap with the lesioning sites, as was shown for obsessive-compulsive disorder (OCD) (Tierney et al., 2014). The main benefit of DBS with respect to lesioning is that DBS is largely reversible. A DBS-device can be turned off – instantly undoing its clinical effect in most cases (e.g., (de Koning et al., 2016)) – whereas a lesion cannot be undone.

1.2 Patients

DBS is widely applied in the treatment of movement disorders (Krack et al., 2019). In addition, DBS has become a treatment option for multiple psychiatric disorders. Treatment with DBS can range from being in an initial experimental stage to being part of clinical routine, depending on the country and the specific disorder. The most common applications of DBS in psychiatry are in OCD and major depressive disorder (MDD) (Dandekar et al., 2018; Wu et al., 2021). Other, lesser-known, applications include anorexia nervosa (Whiting et al., 2018), schizophrenia (Corripio et al., 2020), and addiction (Müller et al., 2016). In this dissertation, the focus will be on the usage of DBS for OCD and MDD.

Due to its high cost and invasive nature, DBS is only provided to patients who are treatment-resistant. Various definitions of treatment resistance exist, although they generally mean that a patient has failed to respond to multiple treatments, usually with increasing dosage, invasiveness, and impact. For example, the first step in a "stepped care" plan for a patient with OCD could consist of cognitive-behavioural therapy (CBT), or pharmacological treatment in the form of a selective serotonin reuptake inhibitor (SSRI), which are both relatively low-cost treatments with few side-effects (Diefenbach & Tolin, 2013). Next, a combination of the two could be tried, before addition of pharmacological medication such as augmentation with antipsychotic medication. If all of these steps (including multiple SSRI variants) subsequently fail, the patient is considered treatment-resistant (Denys et al., 2010).

Treatment resistance and stepped care are often captured in the inclusion criteria for DBS treatment. Besides a minimum symptom score, criteria often include a long-term disease history, and failure to respond to multiple subsequent treatments (e.g., Denys et al., 2020). It is estimated that roughly 20-50% of psychiatric patients respond to each treatment step (Rush et al., 2006). Consequently, about 20-60% of patients with OCD and MDD are estimated to be treatment-resistant (Howes et al., 2022). Upon referral to a specialist DBS centre, patients are screened to verify 1) the diagnosis is correct and OCD/MDD is the primary disorder; 2) the patient has previously received adequate treatment and is truly treatment-resistant; and 3) there are no contraindications for DBS. Contraindications are quite diverse, and could include comorbid psychiatric (personality) disorders, or conditions that make the patient unsuited for neurosurgery (Denys et al., 2020). Structural magnetic resonance imaging (MRI) scans are made to assess eligibility for surgery. Only if a patient passes all parts of the screening (including a final assessment of symptom severity) can they receive DBS treatment.

1.3 Treatment response

At the start of this project, neurosurgical targeting was commonly determined by standard atlas-based coordinates that were refined based on specific individual neuroanatomical landmarks visible on structural MRI scans (Nuttin et al., 1999; Sturm et al., 2003; van den Munckhof et al., 2013). The effect of treatment when using such targeting was highly variable from patient to patient. Similar to earlier steps in the stepped care protocol, response ranged from full remission to complete nonresponse, with approximately half of the patients responding across disorders (Alonso et al., 2015; Dandekar et al., 2018). Considering the wide variety of treatments that provided no benefit to this treatment-resistant population, it was quite remarkable that half of the patients responded to DBS.

It was unclear why some patients responded to DBS and others do not. In OCD, most common clinical features – except age at OCD onset – had been shown to not significantly correlate with treatment outcome (Alonso et al., 2015). As such, they cannot be used to explain why some patients respond and others do not. Perhaps, the answer could be found in the targeting, as treatment response possibly varied with small patient-to-patient differences in electrode placement with respect to certain – potentially unknown – features in the brain. Therefore, we turned our attention to neuroimaging, focusing on the neuroanatomical structures targeted with DBS and their surroundings.

1.4 DBS targeting

Multiple targets existed for DBS for OCD and MDD. In our hospital, OCD and TRD shared a target, which was the ventral anterior limb of the internal capsule (ventral ALIC, or vALIC). The vALIC is the white matter directly above the nucleus accumbens (NAc) (Figure 1.1). For OCD, other groups used either the vALIC, the neighbouring ventral internal capsule and ventral striatum (VC/VS) region, or the subthalamic nucleus (StN). The StN target for OCD overlapped with a DBS target for movement disorders, which showed to be effective at alleviating comorbid OCD symptoms in patients with Parkinson's disease (Mallet et al., 2002). In DBS for MDD, the subcallosal cingulate gyrus (Lozano et al., 2008) was a notable target in addition to the vALIC.

Figure 1.1. Coronal view of DBS electrodes overlaid on a structural MRI scan. The electrodes were placed so that the centre contacts are located within the vALIC. Image reprinted, with permission, from Van Westen et al. (2020).

The vALIC is an important white matter hub dorsal to the nucleus accumbens, medial to the caudate nucleus, and laterally bordering the globus pallidum. In humans, the internal capsule contains connections between the prefrontal cortex, striatum, thalamus (Nanda et al., 2017), and deeper areas of the brain such as the pons and ventral tegmental area (VTA). The entire ALIC, with our target in the ventral part, contains white matter connections from the cortex to the striatum and beyond. This structure is known to be highly variable between individuals, although following a strict set of rules (Jbabdi et al., 2013). Detailed investigations of human ALIC connectivity were sparsely available at the start of this project, even though rodent connectivity was already studied in the 1980s (Nieuwenhuys et al., 1982).

The vALIC target was originally chosen as stimulation target for OCD (Denys et al., 2010), and later also targeted when treating MDD (Bergfeld et al., 2016) due to

overlap in presented clinical symptoms and suspected effect of DBS (i.e. improvement of mood (Mantione et al., 2014)). Interestingly, our target was first introduced as NAc DBS, because of the perceived importance of the NAc in OCD pathophysiology (Denys et al., 2010). It was only later established that the clinically effective contacts were located in the vALIC white matter (van den Munckhof et al., 2013) despite landmark based targeting ensuring that the tip of the electrode ended up in the NAc.

1.5 White matter tracts as DBS targets

Interest in white matter connectivity in the context of DBS was growing at the beginning of this project. Despite DBS's roots in white matter lesioning, little research had yet been performed into white matter connections surrounding the stimulation target (e.g., (Coenen et al., 2012; Johansen-Berg et al., 2008)). The aforementioned finding that the active contacts in our cohort of "NAc DBS" patients were located in the vALIC (van den Munckhof et al., 2013) suggested white matter was the actual target, although the study could not discern the underlying connections. One way to identify white matter connections in-vivo is by using tractography analysis of diffusion MRI data (more in section 1.8.2). Initial tractography studies provided further motivation for studying the role of white matter connections in DBS. For example, (Lujan et al., 2013), which modelled stimulation in a single patient, suggested a small difference in electrode placement could drastically alter activation patterns of white matter tracts. Taken together, the question that arose was: 'Does response to DBS treatment depend on which underlying white matter connections are targeted?'

Early work on brain connectivity from the vALIC in relation to effectivity of DBS focused on "downstream" connections (Coenen et al., 2012). This work hypothesized that stimulation of the connection between the striatum and the ventral tegmental area (VTA) could be responsible for the therapeutic effect of vALIC DBS in TRD. Dubbed the supero-lateral part of the medial forebrain bundle (slMFB), this connection was assumed to be responsible for DBS response partially through a dopaminergic effect on the striatum. A study from our own group supported this reasoning, as it found an increase in striatal dopamine in OCD following DBS of the vALIC (Figee et al., 2014). The suspected role of the slMFB was yet untested, as there was no evidence relating the placement of electrodes with respect to the slMFB and the outcome of DBS.

1.6 slMFB nomenclature

Over the course of this project, the white matter tracts in the vALIC gathered much attention, largely due to their perceived therapeutic relevance in DBS (Coizet et al.,

2017; Safadi et al., 2018). The definition and the nomenclature of the slMFB (Coenen et al., 2012; Hosp et al., 2019) proved to be contentious, sparking heated debate (Haber et al., 2021). Primarily, the definition of a human (sl)MFB was considered problematic, as it is clear that this human "MFB" is not homologous to the well-studied MFB in rodents (Haynes & Haber, 2013) – something which the original authors acknowledged in their first proposition of the human MFB. Moreover, it was argued by neuroanatomists that there was no neuroanatomical basis for such an MFB in the human brain. Finding definite proof has been difficult because the gold standard in connectivity analysis is to be established by ex-vivo tracer studies, which are impossible to conduct in humans. Therefore, arguments in this debate are provided by in-vivo neuroimaging in humans and ex-vivo tracer studies in rodents and non-human primates. Recent work has again shown supportive evidence for the existence of an slMFB structure in humans (Coenen et al., 2022).

Most of the work in this thesis was already conducted before the discussion about the origin and nomenclature of the slMFB took on in earnest. At the start of this project, the slMFB appeared to be a structure which could potentially be of interest in DBS research for OCD in addition to TRD. For this reason, the term slMFB can be found throughout this dissertation.

1.7 Patient selection

In the previous sections, a potential relationship between DBS targeting and outcome was suggested. In addition, it could be possible that treatment response depends on the individual neuroanatomy of the patient. In other words, individual neuroanatomy might determine whether a patient will respond to treatment, regardless of targeting. The original DBS inclusion criteria were not very specific and the decision to treat a patient depended on clinical experience (van Westen et al., 2020). Learning whether a relationship between anatomy and treatment response exist could prove instrumental in developing accurate and objective patient selection. More on treatment prediction will follow in Section **1.9**.

1.8 Neuroimaging techniques

In this dissertation, we used neuroimaging to relate patients' brain anatomy to treatment outcome. Neuroimaging is indispensable in correct placement of DBS electrodes. It can be used to relate the position of the DBS electrodes to the individual brain, and thereby help our understanding of treatment outcome. Moreover, neuroimaging allows anatomical comparisons between different subjects to aid in patient selection.

The first subsection (**1.8.1**) covers structural imaging, which produces images showing anatomical contrast. The second subsection (**1.8.2**) contains a brief introduction to diffusion MRI, which can be used to uncover white matter orientations within each voxel and structural connections between brain regions.

1.8.1 Structural imaging

Structural MRI and CT provide 3D greyscale images of the brain. CT uses high-energy photons (x-rays) to measure differences in specific absorption rates of different tissue types. As a result, CT provides very good contrast between soft tissue, bone, and metals. On the other hand, CT provides limited contrast within the brain, since the brain is made up of soft tissues.

Magnetic resonance imaging provides a structural image of the brain by exploiting spin properties of brain tissue. A preoperative MRI exam commonly consists of a T_1-weighted, a T_2-weighted, and a fluid attenuated inversion recovery (FLAIR) scan. These provide good anatomical contrast between, respectively, grey and white matter; various grey matter nuclei; and brain tissue and blood vessels. Multiple images are typically coregistered to the highest resolution scan available, in order to combine information available from different contrasts.

In DBS, structural MRI is used for preoperative planning, and postoperative verification of lead placement is typically done with CT.

1.8.2 Diffusion-weighted MRI

Diffusion-weighted MRI (dMRI) is an advanced imaging technique that allows probing tissue microarchitecture in each voxel. Its main use in DBS is to uncover the orientations of (collections of) white matter fibres. As the name suggests, dMRI exploits the physical process of diffusion, in which particles exhibit random Brownian motion. Based on the surrounding tissue, the movement of particles is hindered to various degrees. Varying magnetic field gradients along multiple spatial orientations allows probing the degree of hindrance in each direction, since these gradients cause signal loss for moving particles. When sufficient volumes with different gradient orientations (and a reference volume) have been acquired, the preferential diffusion orientations can be modelled. The most common diffusion acquisition is a Stejskal-Tanner spin-echo sequence, which is the only dMRI sequence used in this dissertation (Stejskal & Tanner, 1965).

The sensitivity of MR images to diffusion is dependent on the number and the strength of the applied gradients, collectively termed angular resolution. A high angular resolution allows different diffusion orientations to be resolved at small angles,

whereas from low angular resolution images only large angles can be resolved (Caan et al., 2010). Spatial resolution also determines which fibre populations can be resolved, as the diffusion-weighted signal is averaged over the entire voxel. Angular and spatial resolution can both be increased at the cost of scanning time. For this reason, a trade-off between angular and spatial resolution has to be made at any given scanning time. There is currently no consensus on this trade-off, as it may depend on the application.

Tractography

While the voxelwise orientation distributions may already prove useful, they do not provide information on long-range connections between different brain regions. Tractography fits a (likely) trajectory across multiple voxels based on their individual orientation distributions. It has become the most popular method of reconstructing white matter fibre trajectories in vivo. In this work, we use tractography to reconstruct white matter trajectories in individual patients.

Various tractography methods exist, although they share the same principles. The main differences lie in the underlying orientation modelling, which ranges from diffusion tensor imaging (DTI) to more advanced spherical deconvolution models that account for crossing fibres, and whether tracking is performed in either a deterministic or probabilistic fashion. Classic diffusion tensor imaging (DTI) only models a single fibre within each voxel. Because as much as 90% of WM voxels have been estimated to contain crossing fibres (Jeurissen et al., 2013), crossing fibre models are preferred. Debate on the optimal scanning parameters is still ongoing and may depend on the anatomical structure to be imaged (Vos et al., 2016)

Tractography algorithms reconstruct tracts according to a set of rules, which intend to prevent generation of anatomically non-plausible streamlines. Deterministic tractography generates one solution for each given situation, whereas probabilistic tractography generates a multitude of streamlines with slightly different parameters to account for noise (e.g., in the FSL toolbox) or the dispersion in the diffusion fit (e.g., in the MRtrix toolbox). In this manner, probabilistic tractography provides an estimation of how specific a given tract reconstruction is, given the underlying data. However, due to the qualitative nature of tractography, tract probabilities or streamline counts do not provide information about connectivity strength or likelihood (Jones, 2010).

When conducting tractography research, one has to be careful to avoid some of the well-known pitfalls (Jones & Cercignani, 2010). First, to prevent generation of unrealistic streamlines, tracts have to be constrained to anatomical priors by drawing regions-of-interest (ROI). These ROI masks should ideally be annotated for each

individual patient. Furthermore, connectivity strength cannot be calculated directly. Comparing the spatial relationships between tracts and leads should be done in individual space to retain as much individual variability as possible.

dMRI preprocessing

Some dMRI models are quantitative by nature. It is important that dMRI preprocessing is done carefully as image artifacts may skew these quantitative measures. While a full description of the potential artifacts scans is outside the scope of this work, it should be noted that these artifacts are not equally present in every scan. Distortions, for example, scale with field strength, making distortion correction especially important for scans made at ultra-high field (i.e. 7T) scanners. Additionally, since the magnetic field gradients cause a loss of signal, and decreasing the voxel size also lowers the signal-to-noise ratio (SNR), noise filtering is more important in higher-resolution diffusion-weighted images. Diffusion preprocessing consists of many steps to counteract the different possible artifacts in the image. These include noise filtering, Gibbs' ringing correction, correction for motion between acquisition of subsequent slices and volumes, correction for eddy currents (often done together with motion correction), and distortion correction. As with all MRI scans, however, not all artifacts can be removed.

1.9 Treatment outcome prediction

In addition to improving treatment outcomes through targeting of specific white matter structures, one of the desires of the DBS community was to find a reliable way to select only those patients who are likely to respond to treatment. With reliable patient selection, unhelpful surgeries could potentially be prevented to save on patient burden and costs. As mentioned, a relationship between preoperative symptoms and DBS treatment success was not established. This suggests that preoperative patient symptoms do not provide clinicians with much information on who to indicate for DBS treatment, which is also evident in the response rate of DBS of roughly 50-60% across OCD and TRD (Alonso et al., 2015; Dandekar et al., 2018).

Could neuroimaging provide a suitable biomarker? Most neuroimaging studies to date have performed univariate analyses, focusing on group-level differences of a single parameter. While useful in explaining certain phenomena, group-level differences often do not make good (bio)markers as the variability within groups can be larger than the differences between groups. On top of that, univariate analyses cannot account for dependencies on multiple properties. A simple example of this is when two classes are separated by two variables, with one class being where $A<B$ and another where $A \geq B$. Multivariate analysis could help to bypass these limitations, as it

allows uncovering of complex patterns that consist of multiple features such as clinical symptom scores or MRI voxels. These multivariate patterns can be captured with machine learning.

Machine learning can be used to predict responder status (classification), or a continuous variable such as an estimation of post-treatment symptom severity (regression). Different types of neuroimaging data can be used, in addition to clinical variables. An important matter in machine learning is feature selection. Features are used to generate a predictive model for future unseen cases. Typical machine learning features in MRI could be volumes of brain structures obtained with structural MRI, or quantitative diffusion metrics in diffusion-weighted MRI. It may be advantageous to select only those features which are already suspected to play a part in DBS response to reduce the number of to be learned parameters.

In many experiments different combinations of features are evaluated to see which combination yields the best results, as there is often no way of knowing which (combination of) features will be most suitable for generating an accurate prediction. To prevent overfitting, machine learning experiments will validate the model's performance on out of sample data. When out of sample data (e.g., from a different patient population) are not available, the data can be divided into *n* parts or *folds*, of which *n*-1 will be used for training. The remaining fold – which is unseen during training – will then be used for validation. This procedure will be repeated multiple times with different permutations of training and validation folds in a procedure called cross-validation.

1.10 Overview of research

In this dissertation, several neuroimaging techniques are used to investigate the efficacy of DBS in treatment-resistant OCD and TRD. The research has two distinct objectives. The first is to search for a more optimal strategy for DBS targeting, thereby improving the efficacy of the treatment (Chapters 2-4). The second is to find a potential biomarker which could be used to select only those patients likely to respond for treatment (Chapter 5).

In **Chapter 2** and **Chapter 3** we used a combination of dMRI tractography and structural imaging to retrospectively relate the positioning of the electrodes with respect to individual white matter tracts to outcomes in cohorts of OCD (chapter 2) and TRD (chapter 3) patients. For both OCD and TRD, we suspected that individual differences in the (white matter) anatomy of the brain were related to DBS treatment response. Therefore, we reconstructed relevant tracts in each individual patient and calculated distances from tract to the active DBS contacts. These distances were

related to outcomes to provide information that could be directly relevant to clinical DBS targeting. Thus, in addition to potentially improving our understanding of DBS, both studies could be of high clinical relevance.

In **Chapter 4**, the best trade-off between two important dMRI scanning parameters to reconstruct the relevant tracts to DBS of the vALIC was investigated. In order to further improve specific targeting of individual white matter tracts, the imaging protocol itself should also be optimized. We suspect that within the vALIC, where tracts are mostly organized in an anterior-posterior direction in parallel, it is more beneficial to improve the spatial than the angular resolution. Discernibility of the relevant tracts was evaluated visually and by the calculated amount of overlap. The findings of this study could have implications for clinical targeting, as it is known that small differences in electrode placement could already affect DBS outcomes.

In **Chapter 5**, we used group-level and individual-level analysis to investigate whether pre-operative structural MRI is predictive of treatment outcome at 1-year follow-up in DBS for OCD. It is important to know whether there are any structural volumetric differences between responders and non-responders, as those may be used to guide treatment selection. With a reliable biomarker, unhelpful surgeries may be prevented, decreasing patient burden and improving DBS efficacy.

II. TREATMENT OPTIMIZATION

Chapter 2

Individual white matter bundle trajectories are associated with deep brain stimulation response in obsessive-compulsive disorder

Authors: L.C. Liebrand, M.W.A. Caan, P.R. Schuurman, P. van den Munckhof, M. Figee, D. Denys, G.A. van Wingen

Published in: Brain Stimulation (2019), 353-360, 12(2)
doi: 10.1016/j.brs.2018.11.014

Abstract

Background: The ventral anterior limb of the internal capsule (vALIC) is a target for deep brain stimulation (DBS) in obsessive-compulsive disorder (OCD). Conventional surgical planning is based on anatomical landmarks.

Objective/hypothesis: We hypothesized that treatment response depends on the location of the active DBS contacts with respect to individual white matter bundle trajectories. This study thus aimed to elucidate whether vALIC DBS can benefit from bundle-specific targeting.

Methods: We performed tractography analysis of two fiber bundles, the anterior thalamic radiation (ATR) and medial forebrain bundle (MFB), using diffusion-weighted magnetic resonance imaging (DWI) data. Twelve patients (10 females) who had received bilateral vALIC DBS for at least 12 months were included. We related the change in OCD symptom severity on the Yale-Brown obsessive-compulsive scale (Y-BOCS) between baseline and one-year follow-up with the distances from the active contacts to the ATR and MFB. We further analyzed the relation between treatment response and stimulation sites in standard anatomical space.

Results: We found that active stimulation of the vALIC closer to the MFB than the ATR was associated with better treatment outcome ($p = 0.04$; $r^2 = 0.34$). In standard space, stimulation sites were largely overlapping between treatment (non)responders, suggesting response is independent of the anatomically defined electrode position.

Conclusion: These findings suggest that vALIC DBS for OCD may benefit from MFB-specific implantation and highlight the importance of corticolimbic connections in OCD response to DBS. Prospective investigation is necessary to validate the clinical use of MFB targeting.

2.1 Introduction

Deep brain stimulation (DBS) is an emerging treatment for treatment-refractory obsessive-compulsive disorder (OCD) with an average treatment response rate of around 60% (Alonso et al., 2015). Building on psychosurgical lesioning experience (Tierney et al., 2014), DBS is often targeted at ventral capsule/ventral striatum (VC/VS) areas (Greenberg et al., 2010), and normalizes pathological hyperconnectivity to the prefrontal cortex (PFC) (Figee et al., 2013). At our institute, DBS is applied within the ventral part of the anterior limb of the internal capsule (vALIC) (van den Munckhof et al., 2013), a region which is known for large inter-subject white matter (WM) tracts variability (Makris et al., 2016; Nanda et al., 2017). We hypothesized that treatment response could depend on the location of the active contacts with respect to these tracts, which is currently not accounted for in DBS target planning based on anatomical landmarks.

Earlier work using diffusion-weighted magnetic resonance imaging (DWI) data has shown that the vALIC contains two fiber bundles: the anterior thalamic radiation (ATR) and the medial forebrain bundle (MFB) (Coenen et al., 2012). These bundles connect the PFC to different subcortical structures. The MFB connects the PFC to the ventral tegmental area (VTA) via the nucleus accumbens (NAc), and contains dopaminergic projections from the VTA to the VS (Haber & McFarland, 1999). The supero-lateral branch of the MFB has been described as a DBS target for treatment-resistant depression (TRD) (Schlaepfer et al., 2013) and more recently for OCD (Coenen et al., 2017), where DBS could potentially be effective through improvement of the patient's mood. On the other hand, the ATR connects the PFC to the anterior thalamus and is part of the cortico-striatal-thalamo-cortical (CSTC) network, which is dysregulated in OCD (van den Heuvel et al., 2016).

In this study, we used DWI data to determine whether vALIC DBS for OCD can benefit from specific targeting of the ATR or MFB, which could enable the optimization of DBS targeting and advance our understanding of OCD's pathophysiology. We used tractography to reconstruct the ATR and MFB, and associated the distance between these bundles and the active DBS contacts with treatment response.

2.2 Material and Methods

Patients

The data for this study were collected retrospectively from patients who were routinely treated at the Academic Medical Center (AMC) in Amsterdam, The Netherlands. Data were retrieved from electronic databases and fully anonymized.

Inclusion requirements for this study were the availability of a pre-operative DWI scan suitable for tractography analysis, and a Yale-Brown obsessive-compulsive scale (Y-BOCS) assessment at baseline and after 12 months of DBS. All patients were screened according to regular DBS in- and exclusion criteria for OCD, as described by Denys and colleagues (Denys et al., 2010). In brief, patients between 18-65 years of age, diagnosed with primary OCD for at least 5 years with a minimum baseline Y-BOCS score of 28 were eligible for DBS if the following treatments were unsuccessful: two sessions with a selective serotonin reuptake inhibitor (SSRI) at maximum dosage for 12 weeks, one session of clomipramine for 12 weeks, one augmentation trial with an atypical anti-psychotic and an SSRI for 8 weeks, and at least 16 sessions of cognitive-behavioral therapy (CBT). Exclusion criteria were significant comorbid DSM-IV Axis I disorders (except major depressive disorder (MDD) and mild anxiety disorders), severe DSM-IV Axis II personality disorders, and clinically significant neurological and medical illnesses. An independent psychiatrist from a different hospital verified the screening.

We started DBS for OCD in 2005. From 2009 onwards, DWI scans suitable for tractography were obtained as part of the pre-operative MRI protocol in a subset of patients. Twelve OCD patients (10 female, age = 38.5 ± 12.0 years) out of a total of 30 that underwent DBS in the timeframe 2009-2016 met the inclusion criteria for this study, as 1) they had received DBS for OCD for at least 12 months, and 2) DWI scans suitable for tractography were made before implantation. The group consisted of seven responders (with a Y-BOCS score decrease ≥ 35%) and five non-responders. Demographic data are presented in Table 2.1. In accordance with the Dutch Medical Research Involving Human Subjects Act (WMO), the medical ethics committee of the AMC (Amsterdam, The Netherlands) waived the evaluation of this retrospective study with anonymized data, as well as the requirement to obtain informed consent.

DBS surgery

3T MRI scans were made to assess surgical eligibility at baseline. On the morning of surgery, a stereotactic frame was attached to the patient's head under general anesthesia, before scanning the patient in a 1.5T MRI scanner. Surgical planning was performed according to standard stereotactic procedures described in detail by Van den Munckhof et al. (2013). In short, the 3T scan and stereotactic 1.5T scan were co-registered with SurgiPlan (Elekta AB, Stockholm, Sweden) to enable planning in the stereotactic space. Target planning started with standard stereotactic coordinates relative to intercommissural line: 7 mm lateral of the midline, 3 mm anterior to the anterior border of the anterior commissure, and 4 mm inferior to the intercommissural line. Target planning was subsequently optimized, i.e, direct target planning based on representation of the nucleus accumbens and ALIC, in such way that the deepest

contact of the quadripolar electrode (contact 0) was targeted in the nucleus accumbens and the upper three contacts (contacts 1-3) in the vALIC. Target coordinates were expressed in stereotactic space. Electrodes (model 3389 with 1.5 mm contacts and 0.5 mm interspace, Medtronic, Minneapolis, MN, USA) were implanted bilaterally with a sagittal angle of ±75° to the intercommissural line, and a coronal angle approximately following the ALIC into the NAc.

Table 2.1. Patient demographics with Y-BOCS scores at baseline and follow-up and DBS settings.

Age at inclusion (years)	**Gender**	**Y-BOCS baseline**	**Y-BOCS follow-up**	**Response (% Y-BOCS change)**	**DBS active contacts** 0: *bottom;* 1: *lower mid*; 2: *upper mid*; 3: *top*	**Voltage (V)**	**Frequency (Hz)**	**Pulse duration (µs)**
47	F	36	17	-53%	1,2	5.1	130	90
37	M	28	13	-54%	2,3	5.0	130	90
25	M	29	26	-10%	0,1,2	5.8	130	90
32	F	33	10	-70%	1,2	4.4	130	90
48	F	25	30	20%	1,2	3.5	130	90
33	F	35	13	-63%	1,2	3.5	130	90
52	F	37	22	-41%	1,2	4.0	130	90
35	F	30	20	-33%	1,2	5.5	130	90
31	F	36	11	-69%	1,2	5.0	130	150
64	F	40	12	-70%	1,2	3.5	180	130
23	F	32	23	-28%	1,2	4.7	150	130
35	F	31	25	-19%	1,2	3.8	130	60

DBS treatment

The DBS device was activated two weeks after implantation, with the two middle electrode contact points (contacts 1 and 2) bilaterally activated at 3.5V, 130 Hz, 90 ms, double unipolar stimulation. This marked the start of the optimization phase, during which the voltage was varied and clinically evaluated (bi)weekly. If deemed necessary, other electrode contact points were activated. The optimization phase lasted for 6-12 months. The Y-BOCS score obtained 12 months after surgery was used to evaluate treatment efficacy.

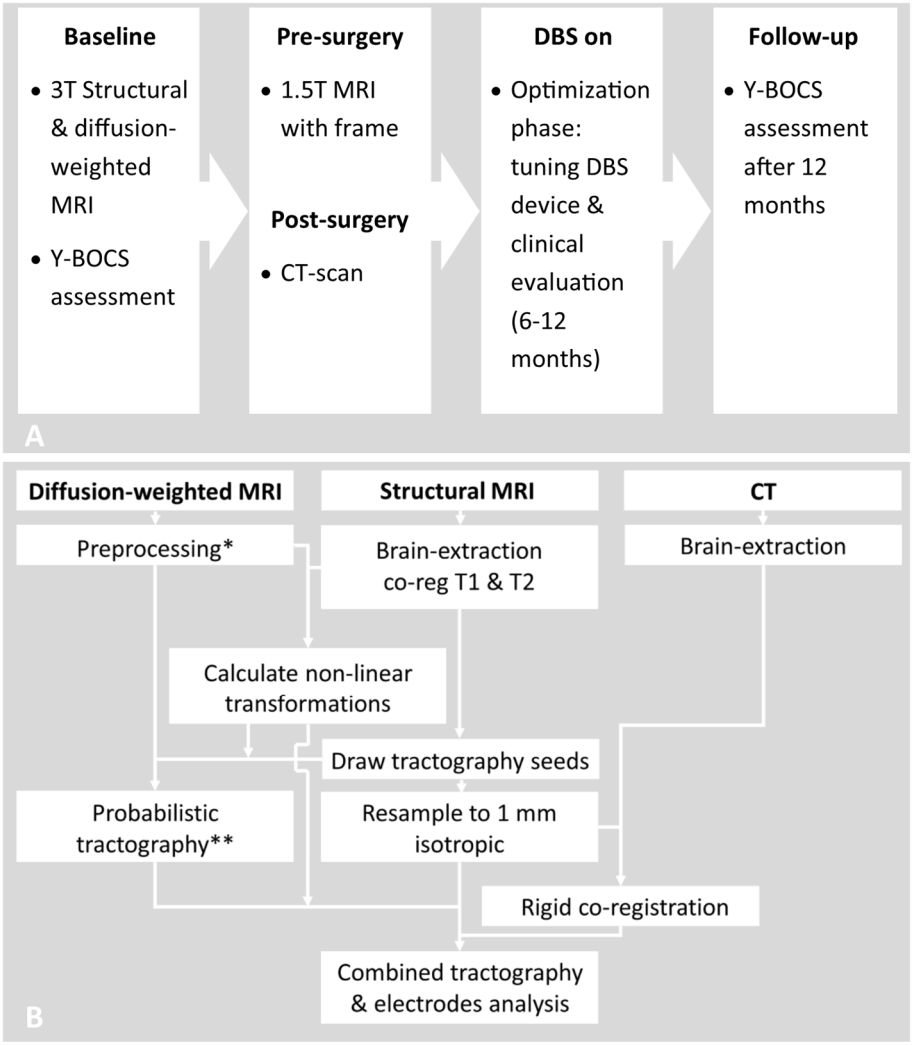

Figure 2.1. Schematic overview of the treatment timeline and analysis pipeline. Panel (A) depicts a timeline showing phases of the DBS treatment that are important to this study. In (B), a schematic overview of image (pre)processing steps is shown. Note that diffusion preprocessing (*) and probabilistic tractography (**) consist of multiple smaller steps that are combined in this schematic for brevity.

Imaging

We used 3T structural MRI and DWI data to reconstruct the ATR and MFB, and merged the results with the post-operative computed tomography scan that visualizes

the DBS electrode position. The distance from the active stimulation site relative to the ATR and the MFB was computed, and associated with the change in the Y-BOCS score due to DBS treatment. We also compared the anatomical locations of stimulation in standard space without DWI to ascertain that treatment response is bundle dependent.

All scans were routinely made according to clinical protocols. The 3T scans were made at baseline (T= -1), 2-3 weeks prior to surgery, and included T_1- and T_2-weighted structural scans, as well as a diffusion-weighted scan. Post-surgery, a low-dose CT scan with a resolution of 0.46 x 0.46 x 2.0 mm^3 was made to confirm electrode placement. For a complete overview, see the timeline in Figure 2.1A.

The 3T scans were made on a Philips Ingenia scanner (Philips Medical Systems, Best, The Netherlands), equipped with a 16-channel phased array head coil. Imaging parameters for the structural scans varied slightly over the inclusion period, and were as follows. The T_1-scans were acquired in 3D with a resolution of 0.5-1.0 mm in-plane and slices of 0.9-1.2 mm thick. The T_2-weighted scans had a slice-wise acquisition with an in-plane resolution of 0.4-0.5 mm and slice thickness of 2.0-3.3 mm. The standard clinical protocol for the acquisition of the diffusion-weighted images was changed after seven patients, which means that there are two slightly differing sets of scanning parameters. Both protocols used a 2D Stejskal-Tanner spin-echo sequence (Stejskal & Tanner, 1965). The scans had a resolution of 1.8 x 1.8 x 3.0 / 2.0 x 2.0 x 2.0 mm^3, TE = 94 / 92 ms, and TR = 6740 / 7861 ms, with 32 / 30 volumes with a diffusion-weighting of b = 1000 s/mm^2 and one b_0-reference volume. To prevent the difference in diffusion acquisitions from having an effect on tractography results, intermediate (pre)processing steps were visually inspected, and the results of statistical analysis were corrected for acquisition type.

Image analysis pipeline

The image analysis pipeline was developed with the goal of identifying the electrode contact point coordinates relative to the MFB and ATR. To reduce the effects of different spatial resolutions, varying levels of anatomical detail and different levels of distortion, special care has been taken to ensure robust co-registrations and resampling of data. A schematic overview of the pipeline is given in Figure 2.1B. After brain extraction with ANTS (Advanced Normalization Toolbox, version 2.1.0, http://stnava.github.io/ANTs/), the T_1- and T_2-weighted scans were linearly co-registered with FSL's (FMRIB Software Library, version 5.0.10, https://fsl.fmrib.ox.ac.uk/) flirt. Subsequently, registration parameters between diffusion and structural space were calculated with ANTS symmetric diffeomorphic image registration (Avants et al., 2008). Since CT scans are not spatially distorted, the

CT scans were co-registered to the structural MRI scans via a rigid transformation (ANTS), after the non-brain parts of the CT scan were removed with a custom Matlab 2014b (The Mathworks, Natick, MA) script. Individual tractography seed ROIs were drawn in the ATR and MFB in the anterior thalamic nucleus and ventral tegmental area respectively, based on Coenen et al. (2012). Additional waypoint seeds were drawn in the vALIC. All seeds were drawn in structural space and transformed to diffusion space prior to tractography.

Diffusion preprocessing and tractography

Diffusion preprocessing consisted of correcting for eddy currents and motion artifacts by affinely co-registering all diffusion-weighted volumes to the b_0 reference volume with FSL. The orientation of the b-vectors was updated accordingly (Leemans & Jones, 2009). Subsequently, the data were noise filtered with an adaptive LMSSE-filter that was implemented in Matlab (Caan et al., 2010a). To ensure data uniformity in the subsequent stages of analysis and because most tracking algorithms perform better with isotropic voxel sizes (Basser et al., 2000; Mukherjee et al., 2008), the data were resampled into an isotropic 2 mm resolution. Finally, voxelwise diffusion orientation estimates were extracted with FSL's Bedpostx (Behrens et al., 2007). Probabilistic tractography was carried out with FSL's probtrackx, with the aforementioned seeds. Tracking parameters were mostly default (5000 samples; curve threshold = 0.2; max. steps = 2500; 0.5 mm step length). The tracking results were visually inspected before and after transformation to structural space to ensure that there were no systematic differences between the two diffusion acquisitions.

Distance calculation and group level analysis

In order to preserve the individual spatial relationship between bundles and electrodes, tractography results were analyzed in subject space. Since all electrodes were identical, we performed group level analyses in a common space centered around the electrode as described below. Using this procedure, we maintained the neuroimaging data in subject space, while the analyses were performed in the common 'electrode-space'. This is schematically depicted in Figure 2.2. All electrodes are oriented approximately along the inferior-superior direction within the brain, so that the axial slices centered around the electrodes can be related to a fixed depth along the electrode (Figure 2.2B). Aligning these slices while preserving the transversal orientations enabled a direct comparison of tractography results between subjects.

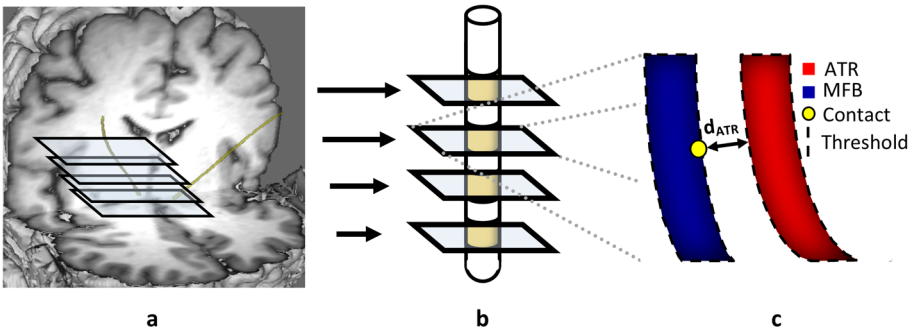

Figure 2.2. Overview of distance calculation from bundles to DBS contacts. A) A 3D reconstruction of the electrodes (yellow) within a patient's brain, along with four example axial slices which are centered around one electrode. B) Since each patient was implanted with the same electrode model, these slices can be compared on a group level by overlaying the electrodes. C) Schematic overview of the distance calculation between the active contact (yellow) and the ATR (red) and MFB (blue) along the electrode axis. Distances are calculated in 3D from the contact to the closest point where the bundle exceeds the threshold. Here, $d_{MFB} = 0$ and $\Delta d < 0$.

We calculated the relative distance from the electrode to the MFB and ATR to determine which bundle was closer to the active stimulation. The relative distance was defined as $\Delta\bar{d} = \bar{d}_{MFB} - \bar{d}_{ATR}$, where $\bar{d}$ signifies the left-right average. The individual distances between the electrode and the bundles $\bar{d}_{MFB}$ and $\bar{d}_{ATR}$ were calculated between the active contact and the closest part of the bundle (Figure 2.2C). All distances were computed based on normalized and thresholded tract probability maps. The threshold level was heuristically set to 18%, at which value the distribution of distances over subjects between contacts and bundles was optimal. Note that the relative distance is relatively invariant to this threshold level. The distances between the active contact points and the thresholded bundles were calculated in 3D with a custom Matlab script using the distance transform from the dip image toolbox (version 2.4.1, http://www.diplib.org/). Since subjects were stimulated at more than one contact, the shortest distance was chosen for the analysis.

Statistical analysis

We calculated Pearson's correlation between the relative distances $\Delta\bar{d}$ and the percentage change in Y-BOCS score to investigate their possible relationship. To

correct for possible effects of using two different DWI acquisition types, we additionally performed linear regression with the sequence type as covariate.

Stimulation site heat map

To assess whether the anatomical positioning of DBS electrodes was different between responders and non-responders, we performed an additional analysis without using the information provided by DWI. We generated a heat map of treatment (non-)responders by combining the previously identified active contact sites of all patients in MNI-space (Montreal Neurological Institute), based on nonlinear transformation parameters that were calculated between each individual's T1-scan and a brain template with ANTS. In this way, it was possible to assess whether differences in treatment outcome depend on stimulation location with respect to anatomical landmarks, or bundle trajectories alone.

2.3 Results

Group level results: distance from bundles to active contacts

We first identified the ATR and MFB in both hemispheres for all subjects and located their positions with respect to the implanted electrodes. According to surgical planning, the electrode tips were located ventrally to the WM bundles in the NAc and the active contacts were located within the vALIC. For most subjects, there was a distinct medial-lateral organization of, respectively, the ATR and MFB within the vALIC. The electrodes were targeted to pass through the lateral part of the vALIC, which for most subjects coincided with a more proximate MFB. Next, we associated the difference in distances from the MFB and ATR to the closest active contact points to the percentage change in Y-BOCS score between baseline and one year follow-up. This analysis showed a significant positive correlation ($p = 0.04$; $r^2 = 0.34$), indicating that treatment response was better when the active contact was closer to the MFB and more distant to the ATR. After correcting for different DWI scanning sequences the result remained significant ($p = 0.02$). The results are illustrated in Figure 2.3. For illustration, axial and coronal views of the tractography around the electrodes' active stimulation depth for a responder and non-responder are shown in Figure 2.4. The responder is stimulated closer to the MFB than the ATR, and vice-versa for the non-responder. A complete overview of axial slices of all patients ordered by treatment response is shown in Figure 2.5.

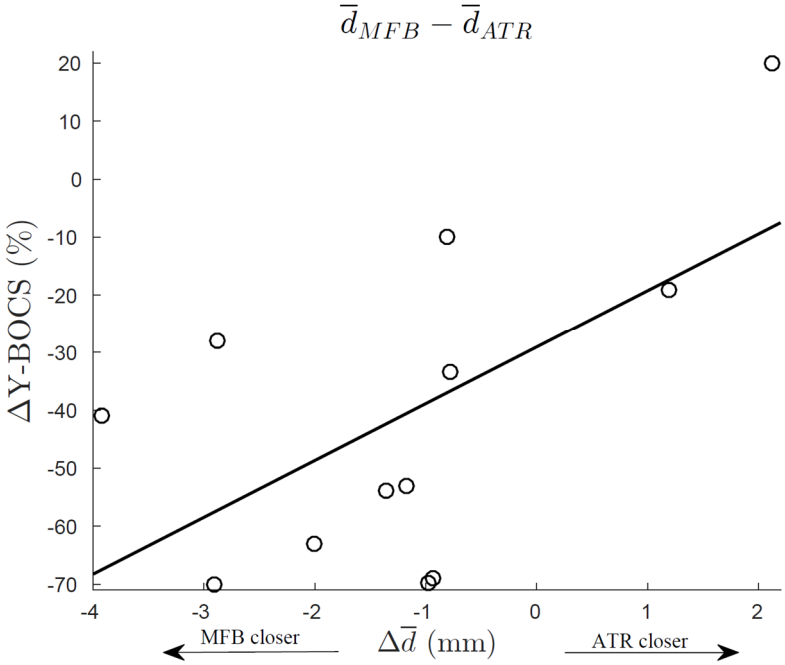

Figure 2.3. Correlation of change in Y-BOCS with difference in distance from DBS contacts to ATR and MFB trajectories. Patient (N=12) treatment response (ΔY-BOCS) plotted vs. the difference in distance in mm from contact to MFB and contact to ATR, $\Delta\bar{d}$. There is a significant correlation ($p = 0.04$, $r^2 = 0.34$; $p = 0.02$ after correcting for different scanning sequences), which is indicated with the line. Stimulation closer to the MFB seems to suggest a better treatment response (larger decrease in Y-BOCS).

Stimulation heat map

To determine whether treatment responders and non-responders could also be distinguished without knowledge of white matter bundle orientations, we created a heat map of active contact point positions in standard anatomical space, which is shown in Figure 2.6. There is a large overlap within and between groups, with all stimulation sites in approximately the same location within the vALIC. This indicates that the anatomical location of the DBS electrodes does not differentiate treatment responders from non-responders.

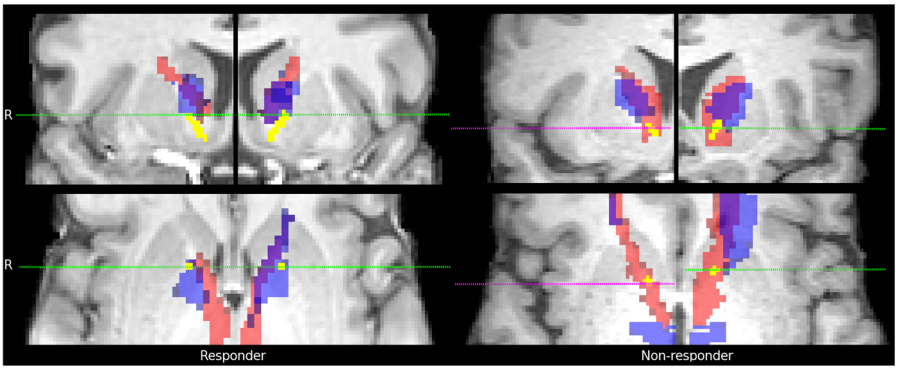

Figure 2.4. Comparison of bundle trajectories around the active DBS contacts between a treatment responder and non-responder. Coronal (top) and axial (bottom) views with tractography results of the MFB (blue) and ATR (red) along with the electrodes (yellow) for a responder and non-responder. The dashed lines indicate the position of the orthogonal slice at the depth of stimulation. Note that the left electrode of the non-responder is anteriorly situated relative to the right electrode, so that the coronal view of the left hemisphere is anterior to the right hemisphere (green vs. magenta dashed lines).

2.4 Discussion

The aim of this study was to determine whether vALIC DBS for OCD could benefit from specific targeting of the MFB or ATR. We performed fiber tractography to investigate the potential relationship between bundle trajectories and stimulation sites. Through comparison of distances from the active contacts to both bundles for all patients, we found that stimulation closer to the MFB is significantly correlated with better treatment response, while there was no apparent relationship between treatment response and location of stimulation with respect to anatomical landmarks. These results may be relevant for future DBS surgical planning and targeting in OCD, but they may also help elucidating underlying mechanisms of DBS for OCD.

Our main finding suggests that targeting the MFB would be beneficial to improve treatment efficacy, even though stimulation may reach beyond the MFB. DBS specifically targeted at the MFB has already gained some interest as therapy for TRD (Bewernick et al., 2017), whereas specific targeting of the MFB for OCD is in its infancy (Coenen et al., 2017). Based on this study it is not possible to determine the optimal location to stimulate the MFB. The patients described in this study received DBS in the vALIC based on anatomical landmarks, and as such are not directly comparable to patients receiving MFB-specific DBS near the VTA. Further research is necessary to determine the efficacy of MFB-targeted DBS in the vALIC as opposed

to near the VTA, although the use of tractography-informed stimulation in both anatomical locations seems warranted.

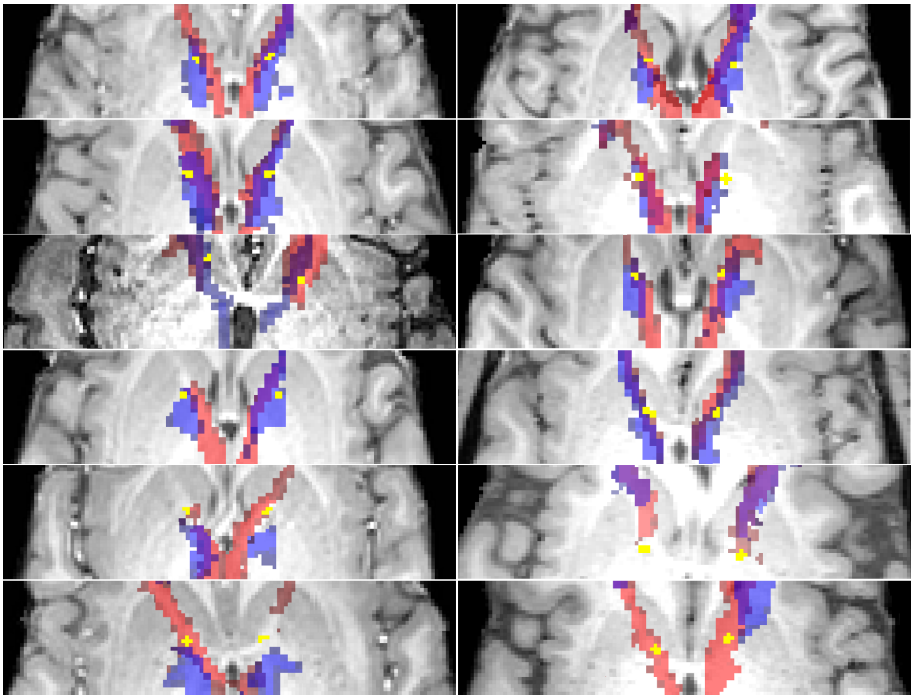

Figure 2.5. Electrode and tractography overview of all patients. Axial slices showing tractography results of the MFB (blue) and ATR (red) around the electrodes (yellow) for all patients included in this study. The slices are ordered (top-bottom) based on treatment response, with the best treatment response at the top. In the top slices the electrodes appear to be more proximate to the MFB, whereas in the lower slices the ATR seems closer.

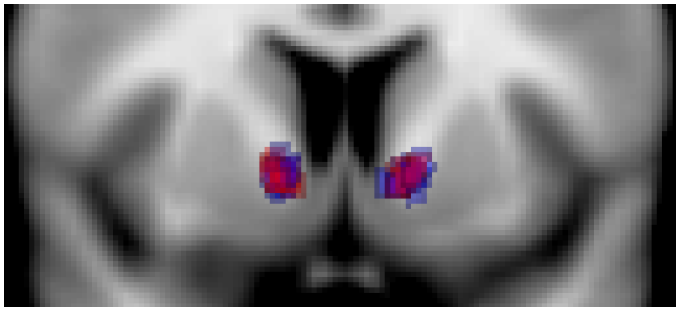

Figure 2.6. Comparison of stimulation sites in standard anatomical space. Coronal slice of a T1-scan in MNI-space overlaid with two heat maps showing active contact sites for all 12 patients, with treatment responders in blue and non-responders in red. All active contacts are situated in the white matter (vALIC), with a large overlap within and between groups.

Considering the prevalence of comorbid depression in treatment-resistant OCD patients (Denys et al., 2010; Greenberg et al., 2006), it is possible that stimulation of the MFB initiates a therapeutic effect in OCD through an improvement in mood similar to MFB DBS for TRD. This is supported by clinical observations that suggest that DBS initially improves mood and anxiety(de Koning et al., 2016), in advance of long-term recovery of compulsive symptoms through CBT (Denys et al., 2010; Mantione et al., 2014). Within OCD pathophysiology, it would seem that the MFB is mainly responsible for the depressed mood and anxiety associated with obsessions, and stimulation of the MFB would indirectly increase the patients' ability to cope with and challenge compulsive behavior. Nonetheless, our results do not provide evidence on whether pathological MFB connectivity is responsible for OCD in the first place, or that the improvement in mood and anxiety due to MFB stimulation merely acts as a catalyst for CBT targeted at compulsivity.

The limited role of the ATR in the efficacy of DBS for OCD could be considered surprising, as the ATR connects different brain structures within the CSTC network that are at the core of the pathophysiological model of OCD (Ahmari et al., 2013). The more prominent role for the MFB supports more recent models of OCD that acknowledge the importance of additional affective networks (Milad & Rauch, 2012; van den Heuvel et al., 2016; Wood & Ahmari, 2015). Nevertheless, these networks may interact at the level of the striatum, as the MFB connects the striatum, PFC and VTA. Therefore, the MFB could influence the CSTC at different locations within the network, which may be necessary to enable normalization of CSTC activity for these otherwise refractory patients (Figee et al., 2013, 2014).

Limitations of this work include the small number of subjects (N=12). Even though statistical power was sufficient to detect associations between white matter trajectories and clinical outcome, small sample sizes limit the generalizability of the results. Nevertheless, our sample was considerable given the limited number of patients that underwent DBS for OCD and completed pre-surgical DWI scanning. Regardless, our results should be replicated in a future study with more subjects. A second limitation is the use of two different diffusion sequences that originated from an update in clinical scanning protocols over the inclusion period. After correction for sequence differences (by including a categorical covariate for the different sequence types) the results remained significant ($p=0.02$), indicating that the results are robust

with respect to sequence type. Another limitation lies within the use of tractography. Tractography is a powerful tool that can be used to optimize existing targeting procedures (Riva-Posse et al., 2018), or provide a rationale for hitherto untested DBS targets (Schlaepfer et al., 2013). However, one must take care when interpreting tracking results, since tractography is not an exact reconstruction of WM pathways and trajectories may vary with the tracking algorithm's parameters. Furthermore, diffusion-weighted scans are susceptible to imaging artifacts and results may be dependent on the quality of data (pre-)processing. To minimize the influence of these factors, we used robust preprocessing strategies and probabilistic tractography (Jones & Cercignani, 2010).

Future work should focus on prospective testing of MFB-targeted stimulation by incorporating tractography information into surgical planning and DBS optimization, which may increase treatment response and shorten the time to optimize stimulation settings.

2.5 Conclusions

In this retrospective study, we have shown that active stimulation of the vALIC closer to the MFB than the ATR is related to a better outcome for treatment-refractory OCD. It is possible that stimulation of the affective circuitry is responsible for this treatment effect, similar to antidepressant effects of MFB DBS for TRD. Tractography-assisted targeting of the MFB inside the vALIC could lead to improved treatment response, which needs to be tested in a prospective study.

2.6 Supplementary information

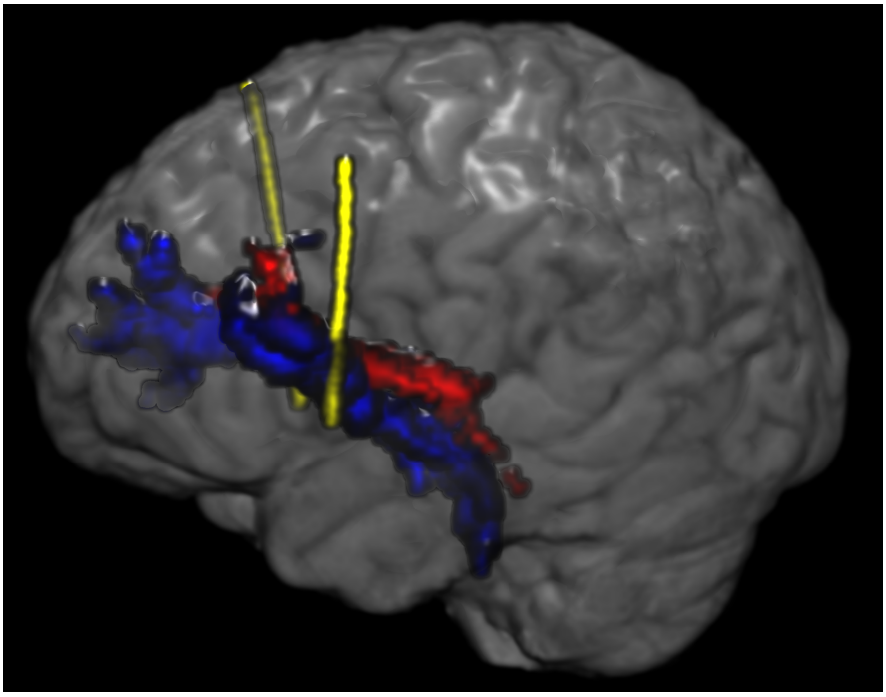

Figure 2.S1. Overview of anterior thalamic radiation (ATR; red) and (supero-lateral branch of the) medial forebrain bundle (MFB; blue) trajectories, along with DBS leads (yellow) for one patient in 3D. The anterior thalamic radiation connects the anterior thalamus to the prefrontal cortex, whereas the supero-lateral branch of the medial forebrain bundle projects to the prefrontal cortex via the ventral tegmental area. Both bundles are in close proximity to each other in the DBS target area, which is the ventral anterior limb of the internal capsule.

Chapter 3

Distance to white matter trajectories is associated with treatment response to internal capsule deep brain stimulation in treatment-refractory depression

Luka C. Liebrand, Samuel J. Natarajan, Matthan W.A. Caan, P. Richard Schuurman, Pepijn van den Munckhof, Bart de Kwaasteniet, Judy Luigjes, Isidoor O. Bergfeld, Damiaan Denys, Guido A. van Wingen

Published in: NeuroImage: Clinical (2020), 102363, 28

doi: 10.1016/j.nicl.2020.102363

Abstract

Background: Deep brain stimulation (DBS) is an innovative treatment for treatment-refractory depression. DBS is usually targeted at specific anatomical landmarks, with patients responding to DBS in approximately 50% of cases. Attention has recently shifted to white matter tracts to explain DBS response, with initial open-label trials targeting white matter tracts yielding much higher response rates (>70%).

Objective/Hypothesis: Our aim was to associate distance to individual white matter tracts around the stimulation target in the ventral anterior limb of the internal capsule to treatment response.

Methods: We performed diffusion magnetic resonance tractography of the superolateral branch of the medial forebrain bundle and the anterior thalamic radiation in fourteen patients that participated in our randomized clinical trial. We combined the tract reconstructions with the postoperative images to identify the DBS leads and estimated the distance between tracts and leads, which we subsequently associated with treatment response.

Results: Stimulation closer to both tracts was significantly correlated to a larger symptom decrease ($r=0.61$, $p=0.02$), suggesting that stimulation more proximal to the tracts was beneficial. Biophysical modelling indicated that 37.5% of tracts were even outside the volume of activated tissue. There was no difference in lead placement with respect to anatomical landmarks, which could mean that differences in treatment response were driven by individual differences in white matter anatomy.

Conclusions: Our results suggest that deep brain stimulation of the ventral anterior limb of the internal capsule could benefit from targeting white matter bundles. We recommend acquiring diffusion magnetic resonance data for each individual patient.

3.1 Introduction

Deep brain stimulation (DBS) is an innovative last-resort treatment for treatment-refractory depression (TRD). Patients in DBS trials usually failed to respond to multiple adequate treatments, including antidepressants and electroconvulsive therapy. Approximately 10-15% percent of patients with depression has a severe level of treatment-refractory depression (Ruhé et al., 2012). DBS studies have shown promising results with half of patients responding to DBS. However, results of randomized controlled trials have been mixed, with some showing large differences between active and sham DBS (Bergfeld et al., 2016; Coenen, Bewernick, et al., 2019; Puigdemont et al., 2015), and others failing to find differences (Dougherty et al., 2015; Holtzheimer et al., 2017).

Different brain regions have been targeted for TRD, including the subcallosal cingulate(Mayberg et al., 2005), anterior limb of the internal capsule (Bergfeld et al., 2016), the ventral capsule/ventral striatum(Malone et al., 2009), and nucleus accumbens (Schlaepfer et al., 2008). The mechanism of action of DBS seems to be that it normalizes pathological network connectivity (Figee et al., 2013), which has motivated specifically targeting white matter tracts that make up these networks (Coenen et al., 2012; Fenoy et al., 2016; Riva-Posse et al., 2014).

The most popular method for in-vivo reconstruction of white matter tracts is tractography in diffusion-weighted magnetic resonance imaging (dMRI) data. Several groups have reported retrospective or prospective open-label studies where they used tractography to refine surgical targets (Coenen, Bewernick, et al., 2019; Fenoy et al., 2016; Hartmann et al., 2016; Lujan et al., 2013; Riva-Posse et al., 2014). In retrospective studies, the goal was often to determine whether proximity to, or activation of, white matter tracts is related to treatment response, whereas prospective studies aimed to exploit this knowledge by selectively targeting or avoiding one or more tracts (Calabrese, 2016). In this retrospective study, we are interested in a relationship between tracts coursing through the ventral anterior limb of the internal capsule (ALIC) and treatment response.

The white matter anatomy of the ALIC has been shown to be well-ordered, but variable along individuals (Coenen et al., 2012; Lehman et al., 2011; Makris et al., 2016; Nanda et al., 2017). It was hypothesized that stimulation of disrupted dopaminergic connections from the ventral tegmental area (VTA) to the nucleus accumbens/striatum might be related to treatment response for TRD (Coenen et al., 2011). Research based on this hypothesis disentangled two important fiber pathways coursing through the ALIC: the anterior thalamic radiation (ATR), and the superolateral medial forebrain bundle (slMFB) (Coenen et al., 2012). The slMFB

makes up the rostral part of the cortico-pontine connection between the VTA and prefrontal cortex, whereas the ATR originates in the anterior and dorsomedial thalamus, also connecting to the prefrontal cortex through the ALIC.

Stimulation of the slMFB, as the dopaminergic connection between the VTA and striatum, proposedly elicits response through normalization of striatal dopamine levels. This idea is in line with the finding that ALIC stimulation induced striatal dopamine release in patients with obsessive-compulsive disorder (OCD) (Figee et al., 2014). Taken together, this theoretical framework has resulted in the investigation of the slMFB as a stimulation target for TRD (Bewernick et al., 2017; Coenen, Bewernick, et al., 2019; Schlaepfer et al., 2013), although closer to the VTA instead of in the ALIC.

Based on the work on sIMFB stimulation and our previous finding that proximity of stimulation to sIMFB was related to treatment response in OCD (Liebrand et al., 2019), we hypothesize that stimulation more proximal to the slMFB within the ALIC is also beneficial for treatment response in TRD. However, a possible role of the ATR and thalamus cannot be ruled out, given reported structural changes within the thalamus (Kempton, 2011), and hyperactivity of the pulvinar nucleus in MDD patients (Hamilton et al., 2012). Therefore, here we use tractography to establish whether there is a relationship between proximity of stimulation to the slMFB and ATR with respect to treatment outcome. The findings could have a direct clinical impact by refining the surgical target in future cases and could lead to reevaluation of DBS lead placement in our current non-responders.

3.2 Material and Methods

3.2.1 Participants

The data for this study were acquired as part of the clinical trial published by Bergfeld et al. (2016). This trial was a collaboration between the Academic Medical Center (AMC) in Amsterdam, and the St. Elizabeth Hospital in Tilburg, both in the Netherlands, and was approved by the medical ethics committees of both hospitals.

Patients (aged 18 to 65 years) had a primary diagnosis of major depressive disorder (MDD), with an illness duration of >2 years, a score of ≥18 on the 17-item Hamilton depression rating scale (HAM-D), and a global assessment of function Score of ≤45. Patients were considered to have TRD if they failed to respond to: two classes of second-generation antidepressants; two single trials of a tricyclic antidepressant (with and without lithium augmentation, respectively); one trial of a monoamine oxidase inhibitor; and bilateral electroconvulsive therapy for ≥6 sessions. Additionally, for inclusion patients had to have an IQ of >80 and be eligible for surgery. Exclusion

criteria were schizophrenia, psychosis unrelated to MDD, bipolar disorder, recent substance abuse (i.e. within the past 6 months), antisocial personality disorder, Parkinson's disease, dementia, epilepsy, tic disorder, and pregnancy. In addition to abovementioned criteria, sufficient quality imaging data – particularly dMRI scans suitable for tractography – were necessary for inclusion into present study.

3.2.2 DBS surgery and treatment

Structural and diffusion-weighted MRI scans were made at 3T at baseline. Imaging details are described in the "*Imaging*" section. A stereotactic frame was attached to the patient on the morning of surgery. The patient was subsequently scanned at 1.5T to express the surgical planning in stereotactic coordinates. The neurosurgeon performed the surgical planning in SurgiPlan (Elekta AB, Stockholm, Sweden) according to standard stereotactic procedures (van den Munckhof et al., 2013). In short, the following coordinates relative to the intercommissural line were the starting point of surgical planning: 3 mm anterior to the anterior border of the anterior commissure, 7 mm lateral to the midline, and 4 mm inferior to the intercommissural line. From there, the bilateral targets were refined with respect to the nucleus accumbens (NAc) and ALIC, so that the deepest of four contacts was placed in the NAc and the remaining contacts were placed in the ventral ALIC. Electrodes (model 3389, Medtronic, Minneapolis, MN, USA) with 1.5 mm contacts and 0.5 mm interspace were placed along a sagittal angle of approximately 75° to the intercommissural line, and a coronal angle following the ALIC into the NAc. Directly after surgery, a computed tomography (CT) or 1.5T structural MRI scan was made to ensure correct lead placements.

Two weeks after implantation, the DBS device was switched on and the (open-label) DBS settings optimization phase started. All patients received voltage-controlled monopolar (cathodic) stimulation from one or more active contacts. We refer to Bergfeld et al. (2016) for details. After optimizing DBS settings for each patient, stimulation parameters remained unchanged during chronic stimulation (until the cross-over period which is not part of this study). We compared HAM-D scores after optimization for each patient had finished (mean time (±SD)= 416 ±154 days from surgery) to ensure that stimulation parameters were stable. Treatment response was measured by the percentage difference in HAM-D scores between baseline and post-optimization follow-up.

3.2.3 Imaging: acquisition

Our aim was to represent individual patients' white matter tracts relative to the electrodes. For this reason, we combined the post-operative CT scans with

tractography results from the pre-operative 3T dMRI scans in each patient's native structural space (i.e. pre-operative 1.5T T1-weighted scans). This approach has the benefit compared to an atlas-based approach that it retained as much individual information as possible, thereby allowing to better assess individual differences. A schematic overview of this procedure is given in figure 3.1.

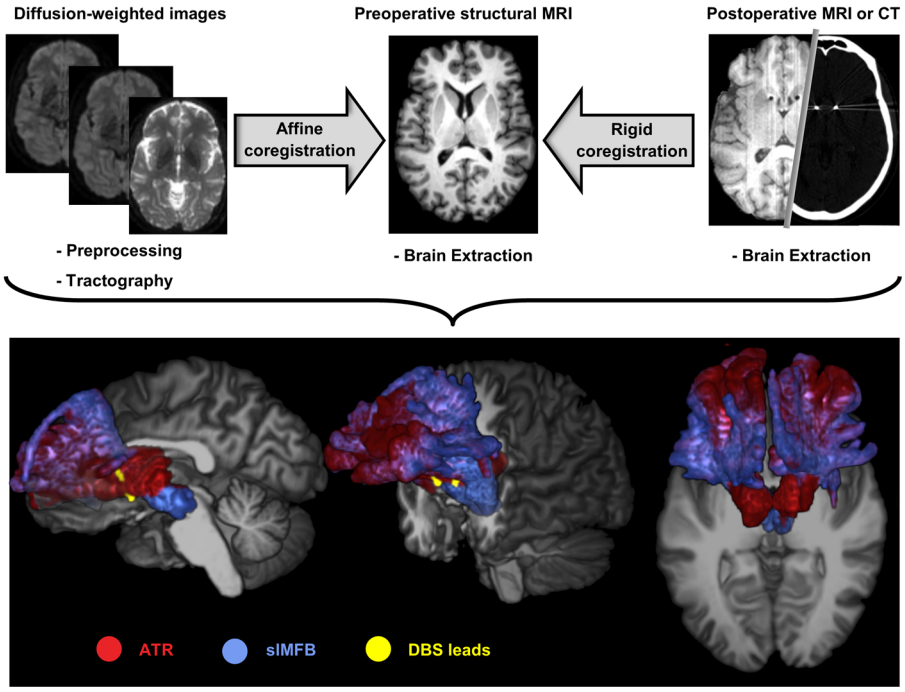

Figure 3.1. Schematic overview of analysis pipeline. (Top row) The preprocessed diffusion data were used to generate tractography results. The tractography results were affinely coregistered to the brain-extracted preoperative structural scan. The postoperative scan was rigidly coregistered to add the lead localization. **(Bottom row)** 3D-rendering of one patient's structural scan, overlaid with the reconstructed anterior thalamic radiation (ATR), superolateral medial forebrain bundle (slMFB), and deep brain stimulation (DBS) leads. Views are as follows: **(left)** sagittal (right hemisphere), **(middle)** side-view(from the left), and **(right)** axial view (top-down). Low visualization thresholds (1-2% of the maximum in the vALIC) for the tracts were chosen here to display the full extent of the forward connectivity.

All 3T scans were made at a Philips Ingenia scanner (Philips Medical Systems, Best, The Netherlands) equipped with a 16-channel phased-array headcoil. The T1-weighted scans were sagittally acquired on a 1.5T Siemens Avanto scanner, with a 3D

inversion-recovery sequence with 0.9 x 0.9 x 1.2 mm^3 voxel size and 256x256 x182 matrix size. The diffusion-weighted scans were acquired according to a 2D Stejskal-Tanner spin-echo sequence, with 2.0^3 mm^3 resolution, 112x112x70 matrix, 32 non-collinear directions with b = 600 s/mm^2 and one b = 0 s/mm^2, TE = 60 ms, TR = 6770 ms. Post-operative MRI scans were made at a 1.5T, at a resolution of 1.0 x 1.0 x 1.0 mm^3, 192x256x256 matrix size, TE = 3 ms, TR = 1900 ms. The CT scans had a resolution of 0.45 x 0.45 x 1.0 mm^3 and 512x512x162 matrix size.

3.2.4 Imaging: (pre)processing

The preprocessing for the structural MRI scans consisted of brain extraction with FSL's *bet* toolbox (FMRIB Software Library, version 5.0.10, https://fsl.fmrib.ox.ac.uk/). The post-operative CT scans were brain extracted with a custom Matlab script (version R2016a, The Mathworks, Natick, MA). The postoperative T1 and CT scans were rigidly coregistered to the preoperative T1 scans with FSL's Flirt tool.

Preprocessing of dMRI data consisted of a (first-order) correction of ringing artefacts with an in-house developed Matlab script, eddy current and movement correction with FSL's eddy correct tool, which coregistered all diffusion-weighted images to the b0 image. The b-vectors were rotated accordingly (Leemans & Jones, 2009). We calculated the affine transformations between structural and diffusion space (i.e. preoperative T1 and b0 image, respectively) with ANTS symmetric diffeomorphic registration (Advanced Normalization Toolbox, version 2.1.0, http://stnava.github.io/ANTs/) (Avants et al., 2008). Voxelwise diffusion orientations were estimated with a model that accounts for crossing fibers (FSL's BedpostX) (Behrens et al., 2007).

3.2.5 Tractography

In this study, we were interested in reconstructing the slMFB and ATR. Tractography seeds were hand-drawn bilaterally on the scan of each individual patient in the VTA for the slMFB, and anterior thalamus for the ATR, with a common waypoint in the ALIC, according to the work by Coenen et al. (2012). Probabilistic tractography was performed with FSL's probtrackx (default parameters). Tracking results were visually inspected and tractography seeds were refined if necessary. Finally, tractography results were transformed to structural space according to the earlier calculated transformations.

3.2.6 Distance from tracts to contacts

First, the location of all contacts was determined through an algorithm that traced a path along the center of the electrode artefact on the CT scan, starting from the tip located in the NAc, spacing contacts according to the lead's specifications (Medtronic 3389). All contacts were labeled and visually checked for accuracy. In subsequent stages, only the active contacts for each patient were used. The shortest distances between the active cathodes and tracts were calculated in 3D in Matlab, with a heuristically determined threshold of 34% that yielded the optimal distribution of distances for statistical analysis. We estimated the average distance d from contact to tract for both tracts, $\bar{d} = (d_{slMFB} + d_{ATR})/2$, and the difference between distances from contact to tract of both tracts, $\Delta d = d_{slMFB} - d_{ATR}$. Here, d_{slMFB} and d_{ATR} represent the (average of left and right) distance to respectively the slMFB and the ATR. If multiple contacts were active, the distance to the closest active contact was chosen, because it most strongly affects the tissue.

3.2.7 Distance to volume of activated tissue (VAT)

Stimulation voltages varied considerably between patients, ranging between 2.5 and 7.3 Volts (see Table 1). To assess whether an association between distance and treatment response could be related to differences in the volume of activated tissue (VAT), we calculated the radius of the VAT according to the simplified model (i.e. model #10) proposed by Mädler & Coenen (2012). This model provides an approximate estimation of the VAT radius (r) based on the measured impedance and stimulation voltage. We calculated the distance of each tract to the VAT ($d - r$) to assess whether the tracts were within the range of electrical stimulation.

3.2.8 Statistical analysis

We correlated the percentage change in HAM-D scores between baseline and follow-up for each patient with the average distance of the active cathodes to both bundles ($\bar{d}$) (i.e. main effect term), and the differential distance to the bundles (Δd) (i.e. interaction term). To assess whether there was a relationship between the distance from active cathodes to tracts and the distance between VAT and tracts, we correlated d to $d - r$. We then assessed whether distances from the tracts to the VATs ($d - r$) were correlated to the change in HAM-D. Because of the apparent non-Gaussian distribution of the data, we calculated the non-parametric Spearman's ranked correlation.

3.3 Results

Out of a cohort of 25 patients, ten patients did not have a complete dataset consisting of preoperative T1 and dMRI scans, and a postoperative T1 or CT scan. One patient's

dMRI scan suffered from large movement artefacts and was excluded. This resulted in a total of 14 subjects of whom we had a complete dataset of sufficient quality for inclusion into this study. The treatment response in this cohort was on average 7.4 points (-33%) on the 17-point HAM-D scale, with seven patients being responders (with at least 50% decrease in symptom scores). An overview of treatment response and stimulation settings is shown in Table 3.1.

Table 3.1. Patient response and DBS settings. Overview of treatment response and stimulation settings of all included patients. All active contacts were cathodes. HAM-D: Hamilton depression rating scale.

Patient	Change in HAM-D (%)	Responder (Yes/No)	Active contacts (Left) Lowest-highest: 0-3	Voltage (Left) (V)	Active contacts (Right) Lowest-highest: 8-11	Voltage (Right) (V)	Stim. frequency (Hz)	Pulse duration (µs)
01	-87.5	Y	2, 3	5.0	10, 11	3.5	180	120
02	+36.8	N	0, 1, 2	3.8	9, 10, 11	3.8	190	90
03	-62.5	Y	2	4.3	10	4.3	180	90
04	-77.8	Y	1, 2	5.5	9, 10	5.5	180	90
05	+54.5	N	0, 1	5.5	9, 10	5.5	130	90
06	-50.0	Y	2, 3	4.3	10, 11	4.3	180	90
07	+6.3	N	1, 2	5.4	9, 10	5.4	180	90
08	-72.7	Y	1, 2, 3	7.3	9, 10, 11	7.3	180	90
09	-53.3	Y	1, 2	3.5	9, 10 ,11	6.0	180	90
10	-8.3	N	1, 2	5.0	9, 10	5.0	130	90
11	+8.3	N	2, 3	6.7	10, 11	6.7	180	90
12	-27.3	N	2, 3	2.5	10, 11	2.5	130	60
13	-83.3	Y	1, 2	5.4	9, 10	5.4	180	90
14	-30.4	N	1	5.2	9	5.2	130	60

For all included subjects, we were able to reconstruct both tracts of interest (slMFB and ATR). As expected, the reconstructions of the slMFB and ATR could be clearly distinguished from their respective starting points in the VTA and anterior thalamus,

up to the ALIC, where they were often laterally-medially organized, and slightly overlapping. Finally, both tracts terminated in different (pre)frontal areas: the orbitofrontal cortex (OFC), the dorsal anterior cingulate cortex (dACC), the ventromedial and ventrolateral prefrontal cortex (vlPFC/vmPFC). The tracts followed roughly the same trajectory and respective organization in each individual, although there were differences in the exact trajectory. In order to give an impression of the variability within the ALIC, an overview of tractography results is shown in figure 3.2. For most subjects, the trajectory of the slMFB and ATR were located dorsally with respect to the DBS contacts. This is reflected in the relatively high average distances from the active contacts to both bundles (mean $\bar{d}$ = 4.9 ± 1.3 mm), as can be seen in figure 3.3.

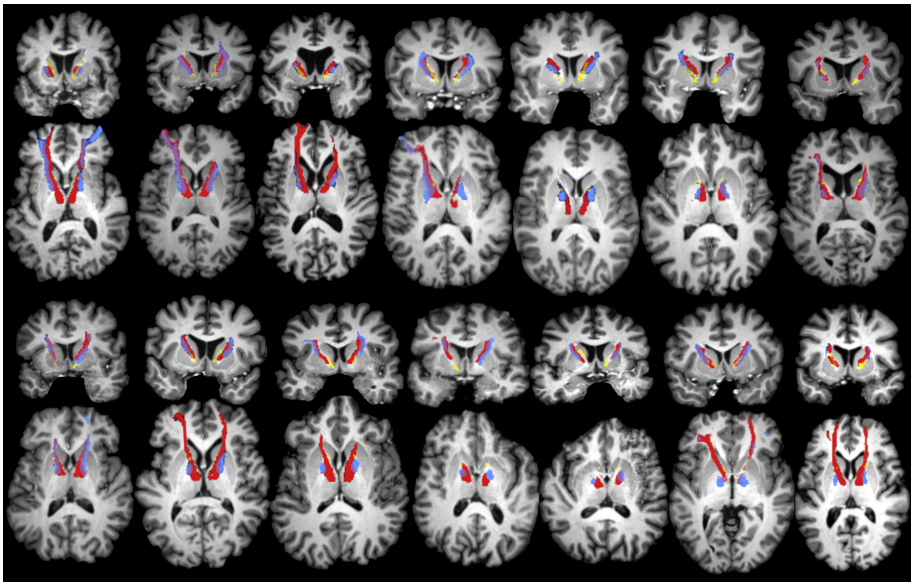

Figure 3.2. Overview of tractography results for all patients. Coronal and axial views of reconstructed anterior thalamic radiation (ATR), superolateral medial forebrain bundle (slMFB), and deep brain stimulation (DBS) leads, for all 14 subjects included in this study. Each coronal view corresponds to the axial view directly below. Color coding is identical to Figure 3.1. It can be seen that the ATR is consistently medial to the slMFB within the anterior limb of the internal capsule (ALIC). For some subjects, the slMFB appears more dorsal in the ALIC than the ATR.

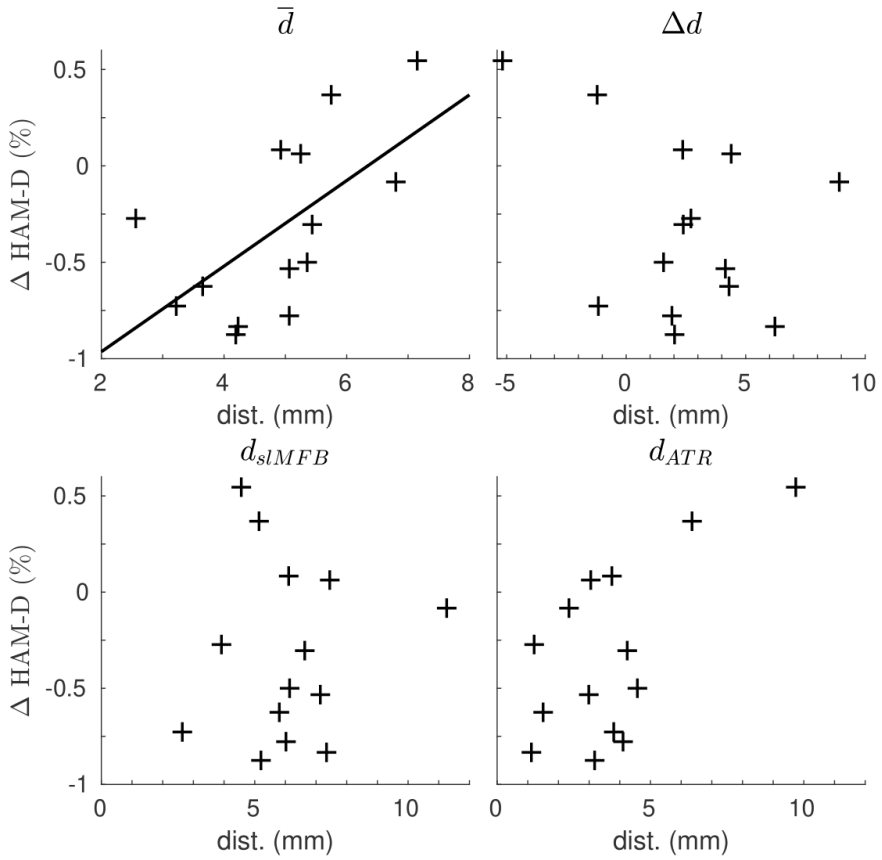

Figure 3.3. Distance from tracts to contacts associated with response. Scatter plots showing the relationship between distance of the anterior thalamic radiation (ATR) or superolateral medial forebrain bundle (slMFB) to the active cathodes, and percentage change on the Hamilton depression rating scale (HAM-D). The different panels include **(top left)** the average distance to both bundles (main effect), **(top right)** the difference between distances (interaction term), **(bottom left)** relationship to slMFB only, and **(bottom right)** relationship to the ATR. Only the relationship between the average distance to both bundles and treatment response **(top left)** was significant (r = 0.61, p = 0.02), which is indicated by the line.

There was a significant relationship between average distance ($\bar{d}$) and percentage response (r = 0.61, p = 0.02). In contrast, there was no significant relationship between the differential distance (Δd) and response (r = -0.20, p = 0.50). Post-hoc, we also related the distances from the active contacts to either the slMFB (r = -0.02, p = 0.96)

or ATR (r = 0.39, p = 0.17), to the change in HAM-D, but these correlations were not significant.

3.3.1 VAT radius

The VAT analysis showed that only 35 out of 56 (62.5%) bundles (2 bundles by 2 hemispheres by 14 patients) were located within the VAT. More specifically, the ATR was in VAT range in both hemispheres for nine patients (11 left, 10 right), whereas the VAT covered the slMFB in both hemispheres in only two patients (5 left, 9 right). In only two patients did the VAT cover both bundles in both hemispheres. The distances of the VAT to tracts were significantly associated with the distances from active contact to tracts (slMFB: $r = 0.91$, $p < 10^{-5}$; ATR: $r = 0.94$, $p < 10^{-6}$). Hence, the average distance of both tracts to the VAT was also significantly associated with the percentage change in HAM-D ($r = 0.69$, $p = 0.01$). The difference in distance from VAT to either slMFB or ATR was not significantly associated with response ($r = 0.20$, $p = 0.50$). Post-hoc, we associated the average distance of the individual tracts to the VAT to the percentage change in HAM-D and found no significant results for the ATR ($r = 0.44$, $p = 0.12$), and slMFB ($r = 0.17$, $p = 0.56$). To find out whether the optimization time was related to white matter proximity, we correlated the average VAT-to-tract distance with the optimization duration and found a significant correlation ($r = 0.74$, $p = 0.004$). Potentially, this was driven by a relationship between treatment outcome and the optimization time, although this relationship only reached trend-level significance ($r = 0.49$, $p = 0.08$).

3.3.2 Stimulation site comparison

In addition to tractography in individual patient space, we show the overlap of individual stimulation sites after nonlinear transformation to MNI-space (figure 3.4). The stimulation sites show a high degree of overlap, suggesting that there was no difference in placement with respect to anatomical landmarks between responders and nonresponders.

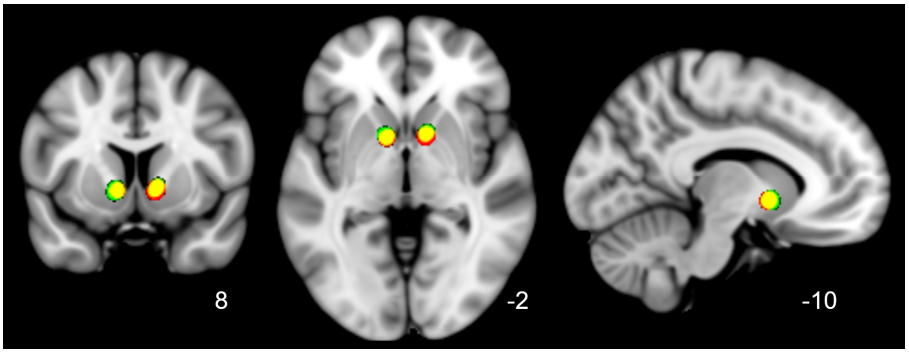

Figure 3.4. Overlap of active stimulation sites of (non)responders in standard (MNI) space. Transformed and smoothed (4 mm full width at half max (FWHM)) stimulation sites of all subjects shown in standard MNI space (1 mm) with respective coronal, axial and sagittal views. Color coding: responders (green), nonresponders (red), overlap (yellow). Stimulation sites of responders and nonresponders were all located in the ventral anterior limb of the internal capsule, directly above the nucleus accumbens, and almost completely overlapped. This suggests that differences in treatment outcome were unrelated to stimulation with respect to anatomical landmarks.

3.4 Discussion

In this work, we set out to determine whether the treatment outcome of DBS of the ventral ALIC for TRD was related to the stimulation's proximity to the slMFB and ATR white matter tracts, using tractography to reconstruct their likely trajectories. The cortical projections of the ATR and slMFB are in agreement with previously published results (Coenen, Schlaepfer, et al., 2020; Safadi et al., 2018), with terminals in the OFC, dACC, vmPFC, and vlPFC. On average, the tracts were located quite dorsally with respect to the stimulation site in the ventral ALIC directly above the nucleus accumbens. By relating the distances of the slMFB and ATR to the active contacts to treatment response, we discovered that stimulation closer to both bundles was associated with better treatment outcome. In addition, optimization times were lower for patients who were stimulated closer to both tracts, suggesting tractography can be used to inform stimulation parameter choices.

This result supports recent studies indicating the potential of tract stimulation in DBS for TRD (Coenen, Bewernick, et al., 2019), and agrees with our finding in obsessive-compulsive disorder suggesting treatment response is related to tract proximity (Liebrand et al., 2019). The large degree of overlap in stimulation sites suggests that treatment outcome does not depend on lead placement with respect to anatomical

landmarks. The results were substantiated by biophysical modeling of VATs, which presumably provide a better estimate of the actual stimulation area than the mere location of the cathode by taking the impedance and stimulation voltage into account. The VAT analysis also showed that closer distance of the VAT to the tract is associated with better treatment outcome. Considering VAT models are often not available in operation software, it is fortunate that distances from tract to contact are also associated with treatment outcome, since they can be directly used in surgical planning. Therefore, the outcome of this study may be of clinical relevance, and prospective studies have to determine whether tractography-assisted surgical targeting in vALIC DBS for TRD is indeed beneficial by placing the leads within the tracts and avoid placement of leads outside of the VAT range of these tracts. In addition, this result suggests that patients with limited clinical response might benefit from repositioning the leads.

Based on earlier work by others and our findings in OCD, we hypothesized that the slMFB would be the preferable target over the ATR in the ALIC. A prominent role for the slMFB is supported by recent promising results of slMFB stimulation close to the VTA, distant from the ATR (Coenen, Bewernick, et al., 2019). Contrary to our expectations, there was no significant relationship to the individual proximity of either bundle and treatment outcome. The large distance between the leads with respect to both tracts might have made it difficult to differentiate each tract's contribution to the treatment outcome, which is reflected in the low number of patients for whom both the ATR and slMFB were inside the VAT radius. Therefore, given present findings, we cannot invalidate the hypothesis that the slMFB is the preferable target. However, we cannot rule out a potential role of the ATR in ALIC DBS for TRD either. Little evidence points to the ATR as the optimal target in ALIC DBS for TRD, although a recent study did find a positive association between stimulation of frontothalamic (presumably ATR) in addition to brainstem (likely slMFB) connections in the ALIC and treatment outcome for OCD (Baldermann et al., 2019), similar to present findings. While structural changes in the thalamus (Kempton, 2011), and hyperactivity in the pulvinar nucleus have been reported in patients with MDD (Hamilton et al., 2012), these are outside the context of DBS for TRD. Nevertheless, disruption of frontothalamic connectivity through stimulation of the ATR might have been (at least partly) responsible for improvement of depressive symptoms (Baldermann et al., 2019).

Possible working mechanisms of slMFB stimulation have been proposed, recently identifying it as an important structural connection within the reward network (Coenen, Schlaepfer, et al., 2020), in which dopaminergic connections from the VTA to the striatum and prefrontal cortex are suggested to play an important role (Coenen et al., 2012). This is supported by work showing ventral ALIC stimulation in OCD

patients was associated with an increase in striatal dopamine (Figee et al., 2014). The supposedly central role of the VTA has motivated stimulation of the slMFB much closer to the VTA, and away from the ALIC (Schlaepfer et al., 2013). Interestingly, there is a possibility that the tract itself is the optimal target, relatively independent of where it is being stimulated, which supports the theory that a common network across different stimulation targets underlies DBS response in TRD. Here, we focused on separating different subcortical projections pathways, in line with the corticopetal approach described in (Coenen, Schlaepfer, et al., 2020). According to their definitions, our stimulation target mostly addresses the reward (slMFB) and affect (ATR) networks. Considering that the target sites within our sample are all positioned ventrally in the ALIC, and the small interspace between electrode contacts used in our patient sample, it is unlikely that we address the more dorsal (pre)frontal targets belonging to the control network (Coenen, Schlaepfer, et al., 2020). While we prefer using electrodes with small contact interspacing to allow more precise tuning, larger interspace electrodes potentially allow switching between different networks.

The large overlap in prefrontal connections from the ventral ALIC causes separation of fibers in the ventral ALIC based on their (pre)frontal terminals to be challenging. Possibly, such an approach requires data acquired at a higher angular resolution, in contrast to the relatively low angular resolution needed to separately track the ATR and slMFB from the subcortex to the ventral ALIC (Liebrand et al., 2019).Since the ALIC is a white matter hub with many different (pre)frontal connections (Coizet et al., 2017; Lehman et al., 2011; Safadi et al., 2018), dissection of adjacent fiber connections with high-resolution individual patient data and studying its relationship to treatment response and side effects in future studies may prove useful. Continued acquisition of high-quality diffusion data in patients is therefore of the utmost importance.

3.4.1 Limitations

This work is primarily limited by the number of subjects (N=14). Sample size is a limitation in most DBS studies for psychiatric indications, and our sample size is comparable to other tractography studies in this field. Nevertheless, care must be taken in interpretation of the results, and future studies should aim to replicate these findings, possibly pooling data of multiple centers using the same target to overcome the limited sample sizes inherent to psychiatric DBS. Even so, we were able to find an association between overall proximity of the slMFB and ATR to the active DBS contacts and treatment outcome. We therefore believe that our sample size was sufficient for this study. Our relatively straight-forward study design further facilitated interpretation of the results, although we realize that a model for antidepressant response depends on more than the distance to tracts alone, and that different subjects

may have different slopes in their distance-to-response relationship (Coenen, Sajonz, et al., 2020). We did not compare treatment effect over multiple contact settings and distances within subjects, which could potentially provide a better insight into variation between subjects, owing to the long time to evaluate response in psychiatric conditions and the retrospective nature of this study.

As mentioned above, the retrospective nature was a limitation in our study. Surgical targeting during this study was based on anatomical landmarks, notably the nucleus accumbens, causing the stimulation site to be quite ventral within the ALIC. Although the resulting variability in distance between the contacts and tracts actually enabled the current study, the large distance made it more difficult to associate treatment response to stimulation of one tract specifically. In prospective studies, there can be much more control over the positioning of the electrodes with respect to the tracts, allowing a direct comparison between slMFB and ATR stimulation.

Finally, we were limited by the qualitative nature of tractography (Jones et al., 2013), which makes it difficult to determine the volume of a tract. As a result, distances from tracts to the active contacts may not be exact, although we believe this does not undermine the validity of our results. Our findings do not dependent on precise distance but the variability in distance between subjects. We specifically avoided quantification of connectivity strength to and from our stimulation target, since for this tractography is unsuited (Jones, 2010). By taking care in assessing our results, and using an easily interpretable method that can also be used for surgical planning, we believe that we have found a middle ground between usability and prudence.

3.4.2 Outlook

Based on our results, we recommend and will incorporate tractography-guided surgical planning in order to target the slMFB and ATR within the internal capsule for TRD. It is probable that within the ALIC, the slMFB is the optimal target, although future studies stimulating closer to both targets should be done to be able to discern the slMFB and ATR. Even for other DBS targets and indications, we recommend collecting dMRI data, in order to perform retrospective studies to elucidate the potential role of white matter tracts in response.

3.5 Conclusions

In this work, we show that stimulation closer to the slMFB and ATR in the ventral ALIC is associated with better treatment outcome in TRD. We were not able to distinguish between individual contributions of slMFB and ATR stimulation, probably due to these bundles being outside the VAT in many patients. There seems to be no relationship between lead placement with respect to anatomical landmarks

and treatment response. Prospective studies should evaluate whether tractography-assisted surgical targeting yields better treatment outcome, and whether one bundle is a superior target compared to the other.

Chapter 4

Spatial versus angular resolution for tractography-assisted planning of deep brain stimulation

Luka C. Liebrand, Guido A. van Wingen, Frans M. Vos, Damiaan Denys, Matthan W.A. Caan

Published in: NeuroImage: Clinical (2020), 25

doi: 10.1016/j.nicl.2019.102116

Abstract

Given the restricted total scanning time for clinical neuroimaging, it is unclear whether clinical diffusion MRI protocols would benefit more from higher spatial resolution or higher angular resolution. In this work, we investigated the relative benefit of improving spatial or angular resolution in diffusion MRI to separate two parallel running white matter tracts that are targets for deep brain stimulation: the anterior thalamic radiation and the supero-lateral branch of the medial forebrain bundle. Both these tracts are situated in the ventral anterior limb of the internal capsule, and recent studies suggest that targeting a specific tract could improve treatment efficacy. Therefore, we scanned 19 healthy volunteers at 3T and 7T according to three diffusion MRI protocols with respectively standard clinical settings, increased spatial resolution of 1.4 mm, and increased angular resolution (64 additional gradient directions at b = 2200s/mm^2). We performed probabilistic tractography for all protocols and quantified the separability of both tracts. The higher spatial resolution protocol improved separability by 41% with respect to the clinical standard, presumably due to decreased partial voluming. The higher angular resolution protocol resulted in increased apparent tract volumes and overlap, which is disadvantageous for application in precise treatment planning. We thus recommend to increase the spatial resolution for deep brain stimulation planning to 1.4 mm while maintaining angular resolution. This recommendation complements the general advice to aim for high angular resolution to resolve crossing fibers, confirming that the specific application and anatomical considerations are leading in clinical diffusion MRI protocol optimization.

4.1 Introduction

Deep brain stimulation (DBS) is an established treatment for movement disorders and is also used for several treatment-refractory psychiatric disorders, such as obsessive-compulsive disorder (OCD) and major depressive disorder (MDD). DBS for these indications has been successful in multiple targeted brain regions (Alonso et al., 2015), although there is a shift towards understanding DBS as a network effect (Figee et al., 2013), with an increased focus on targeting specific white matter bundles visualized with tractography (Noecker et al., 2017).

The (ventral) anterior limb of the internal capsule (ALIC) is a popular DBS target for psychiatric indications (Tierney et al., 2014). Earlier work on the neuroanatomy of the ALIC has shown that there is a large amount of inter-subject variance in the white matter organization (Coenen et al., 2012; Makris et al., 2016; Nanda et al., 2017). This suggests that accurate subject-specific tractography is required for clinical applications. Tractography studies have identified the supero-lateral medial forebrain bundle (slMFB) (Coenen et al., 2012; Liebrand et al., 2019), possibly in combination with frontothalamic fibers – likely belonging to the anterior thalamic radiation (ATR) (Baldermann et al., 2019) – as preferred target structures in ALIC DBS. The ATR connects the anterior thalamus with the prefrontal cortex, while the slMFB constitutes the rostral part of the cortico-pontine connection between the ventral tegmental area and prefrontal cortex (Coenen et al., 2012). When passing through the ALIC, these bundles run in approximately the anterior-posterior direction with, typically, a respective medial-lateral organization (with the slMFB being slightly dorsal to the ATR).

In order to refine tractography-assisted DBS targeting, and evaluate the relative benefits of slMFB versus ATR stimulation in the ALIC, more prospective tractography studies are necessary. DBS targeting requires high precision, and in our experience slight alterations in placement may affect the treatment outcome (Liebrand et al., 2019). Therefore, it is important to optimize diffusion-weighted imaging (DWI) acquisitions and develop robust tractography pipelines for these studies. Current clinical applications of tractography are often based on the diffusion tensor imaging (DTI) model (Petersen et al., 2016), which enables reproducible reconstruction of the major white matter tracts, despite the low spatial and angular resolution of the DWI's (Wakana et al., 2007). However, the DTI model cannot account for more complex fiber configurations, such as fibers crossing or touching, which may occur in up to 90% of white matter voxels (Jeurissen et al., 2013). It is therefore suggested to acquire DWI data at a higher angular resolution and with multiple b-values, in order to use more sophisticated models that can resolve multiple fiber populations within each voxel (Caan et al., 2010).

Here, we focus on optimizing the acquisition for distinguishing the slMFB and ATR in the ALIC with tractography for use in a clinical setting. It can be reasoned that resolving parallel fibers in the ALIC does not require high angular resolution compared to crossing fiber configurations, so that, as long as the angular resolution (i.e. diffusion sensitivity) is sufficient to detect tract orientations, clinical scanning time can be spent on improving spatial resolution (i.e. voxel size). For this reason, we investigate the tradeoff between angular and spatial resolution for reconstructing and distinguishing between both tracts by comparing a standard clinical 3T protocol to respectively high angular (3T) and high spatial (7T) resolution protocols. Tract reconstructions for each protocol will be evaluated based on their capability to resolve the slMFB and ATR, to choose the optimal tradeoff for specific targeting of either bundle.

4.2 Materials and Methods

4.2.1 Participants

Nineteen healthy volunteers (age range: 23-55 years, mean (±SD) = 31.5 (±8) years) were included in this study approved by the Institutional Review Board after giving written informed consent. After screening for MR contraindications, all participants were scanned in 3T and 7T scanners, with both scanning sessions taking place on the same day in the period between August and October, 2017. Structural (T1 -weighted) scans were made at 3T to allow for comparison between the diffusion protocols in individual structural space.

4.2.2 Scan protocols

Data were acquired on Philips Ingenia 3T and Achieva 7T scanners (Philips Medical Systems, Best, Netherlands) equipped with 32-channel phased-array head coils (Nova Medical, Wilmington, MA). A complete overview of the applied diffusion MRI scan parameters is given in Table 1. Three diffusion-weighted scans were made: a standard scan with parameters similar to clinical protocol of around 3 minutes, and two high resolution scans with a duration of approximately 10 minutes, which is a timescale that is usable in the clinic. One high resolution scan included more diffusion orientation measurements (higher angular resolution), and the other had a higher spatial resolution, respectively. We will refer to these as the HARDI and HSRDI scans. Structural T_1 scans were acquired at 3T (MPRAGE sequence; FOV=256x256x225mm^3; voxel size=1x1x1mm^3; TR=8.1ms; TE=3.7ms; TI=900ms; flip angle=9°; SENSE= 1; total scan time= 15:04 min).

The standard scan was made at 3T with an isotropic 2.3 mm voxel size, and contained 32 volumes with non-collinear diffusion directions and a diffusion weighting of

b=1000 s/mm^2 and a single b0-reference volume. The HARDI scan extended the standard scan with an additional shell of 64 directions at a higher diffusion weighting value (b=2200 s/mm^2) to investigate the relative importance of angular resolution. The scanning was further expedited by applying a multiband factor of 2.

The HSRDI scan was made at 7T at a higher spatial resolution of 1.4 mm^3, and contained the same number of diffusion-weighted volumes as the standard scan (i.e., 32x b=1000 s/mm^2, 1x b=0), acquired without multiband acceleration. The field-of-view was slightly reduced in the z-direction (feet-head) to keep scanning time in line with the 3T scans. In order to minimize the distortions that come with longer readout times when scanning at higher spatial resolution, the field-of-view (FOV) was reduced in the phase encoding direction, with

additional outer volume suppression to prevent aliasing (Gallichan, 2018; Heidemann et al., 2012). In order to correct for distortions during preprocessing, b0-reference volumes with opposite phase encoding polarity were also acquired at 3T and 7T.

Table 4.1. Overview of acquisition parameters for the three sequences. (HARDI: high angular resolution diffusion imaging, HSRDI: high spatial resolution diffusion imaging, FOV: field-of-view)

	Standard	**HARDI**	**HSRDI**
Field strength (T)	3		7
Field of view (mm^3)	224 x 224 x 135		140 x 179 x 51
Voxel size (mm^3)	2.3 x 2.3 x 2.3		1.4 x 1.4 x 1.4 (10% slice gap)
Acceleration	SENSE = 1.5 Multiband = 2		SENSE = 2.7 80% FOV in phase encoding direction
Half-scan	0.7		0.7
Repetition time (ms)	5363		3038
Echo time (ms)	99		71
b-values (s/mm^2)	32 x b = 1000	32x b = 1000 64x b = 2200	32 x b = 1000
Signal averages	1		3
Scan time	3:07 min	9:44 min	32 x b = 1000

4.2.3 Diffusion (pre)processing

The raw diffusion data were first converted to nifti before noise filtering with a PCA-based filter (Veraart et al., 2016), as implemented in MRtrix3 (https://mrtrix.readthedocs.io/). Secondly, the data was corrected for Gibbs' ringing artifacts with an in-house developed Matlab (The Mathworks, Natick, MA; version R2017a) script that does a first order correction based on the second spatial derivative. Distortion, motion and eddy current correction was subsequently performed with FSL's (FMRIB's Software Library, version 5.0.10; https://fsl.fmrib.ox.ac.uk/fsl/) TOPUP and *eddy_cuda* (gpu version of *eddy*) tools (Andersson et al., 2016; Andersson & Sotiropoulos, 2015). The preprocessed diffusion data were fit with a diffusion tensor model for visual inspection (see Figure 4.1), and with FSL's Bedpostx, a ball-and-stick model capable of modelling multiple diffusion orientations per voxel (Behrens et al., 2007), for tractography analysis.

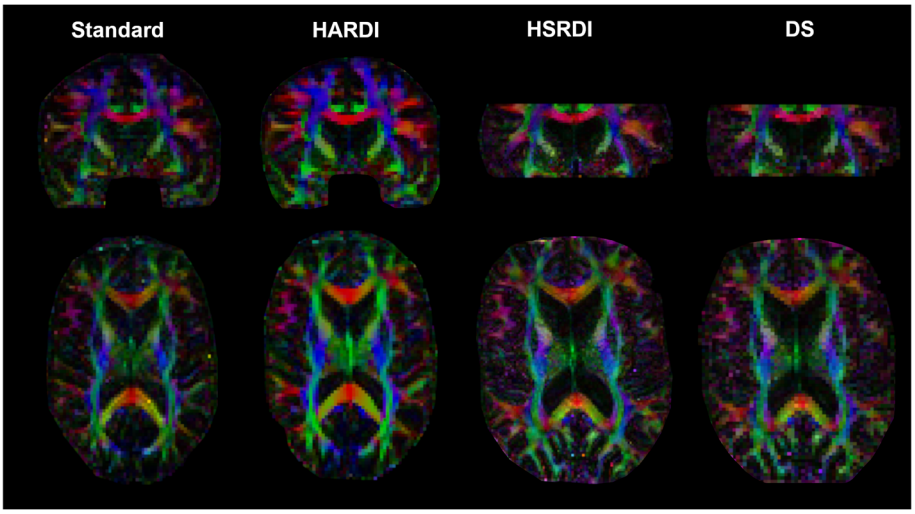

Figure 4.1. Comparison of coloured fractional anisotropy maps between the four datasets (standard, HARDI, HSRDI, and DS, respectively) in native diffusion space for one participant. Note that the slices are not exactly at the same location and orientation because of differences in acquisition parameters and participant position in the scanner.

4.2.4 Down-sampled dataset

To ensure that eventual differences between the HSRDI dataset and standard are not caused by field strength, we additionally performed tractography in a down-sampled 7T dataset (hereafter 'DS'). The HSRDI dataset was down-sampled to match the spatial resolution of the other datasets after denoising and Gibbs ringing correction, since the correction tools recommend not using interpolated data. Further processing was identical for all datasets.

4.2.5 Tractography analysis

Rigid co-registrations between diffusion and structural space were performed with SPM (statistical parametric mapping, version 12; https://www.fil.ion.ucl.ac.uk/spm/) based on the fractional anisotropy (FA) maps and T1-scans, and visually inspected. Tractography seeds for the ATR and slMFB were drawn bilaterally, on the images of each individual participant in the anterior thalamic nucleus and ventral tegmental area, respectively, with an additional waypoint in the anterior limb of the internal capsule, according to (Coenen et al., 2012). The seeds were subsequently transformed to diffusion space. Probabilistic tractography was performed with FSL's Probtrackx between the seed and waypoint for both bundles bilaterally (default parameter settings). The tract reconstructions were transformed to structural space and resliced to 1 mm isotropic resolution, after which they were visually assessed. See Figure 4.2 for a tractography example of the ATR and slMFB.

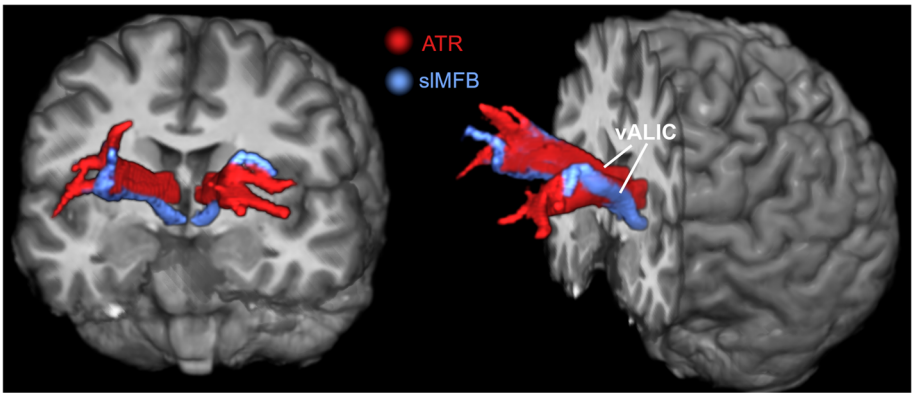

Figure 4.2. Three-dimensional tractography overview of the ATR (red) and slMFB (blue) on top of a structural MR image. In the ventral ALIC (as indicated by the lines), the slMFB runs lateral to the ATR. Towards the prefrontal cortex, the bundles are more intermixed, as they branch out and connect to adjacent prefrontal structures. The diffusion data in this figure were acquired to the HSRDI protocol.

4.2.6 Comparison of tract probability profiles and statistical analysis

We compared the separability of the ATR and slMFB in the anterior limb of the internal capsule per sequence. In order to preserve the spatial information of each individual, we performed the tractography analysis in subject space. To compare tract probability profiles across subjects and DWI sequences, we quantified their separability. This was done in the coronal plane, which is oriented approximately perpendicular to the anterior-posterior axis orientations of the ATR and slMFB (Coenen et al., 2012). For each participant, the target area for DBS was manually identified in the vALIC on the T_1-weighted scan, based on knowledge of the location of active contacts in vALIC DBS (van den Munckhof et al., 2013). Track probability profiles of the ATR and slMFB were computed along an approximately medial-lateral line through our target area, as shown in Figure 4.3. Track probabilities were normalized across each such line to exclude potential effects of differing seed volumes and arbitrary intensity scaling. We calculated the mean standardized difference (MSD) as a measure of bundle separability, which is defined as the distance between the two peaks divided by the average standard deviation (full width at half max, FWHM). Five adjacent lines (in the superior-inferior direction) per hemisphere were averaged to improve robustness of this measure. Finally, we performed a repeated-measures analysis of variance (ANOVA) in Matlab (*fitrm*), with Greenhouse Geisser non-sphericity correction when necessary, to assess possible differences between the three scans (standard, HARDI, and HSRDI). In case of significant differences, we calculated pairwise differences post-hoc with Bonferroni correction for multiple comparisons *(ttest*).

4.3 Results

Data collection of two participants could not be completed at 3T, as a result of technical issues; furthermore, one participant withdrew and was not scanned at 7T. These participants were excluded from the analysis to yield 16 complete datasets. We were able to reconstruct the slMFB and ATR bilaterally for all DWI sequences in every participant except one, for whom the inferior part of the slMFB was outside of the HSRDI scan's field of view. In order to keep the groups balanced, we excluded the other scans from this participant from further analysis. Therefore, the final analysis consisted of 45 DWI scans of fifteen participants (mean age = 32 ±8 years, 5 females). An overview of all tractography results of can be found in Figure 4.S1.

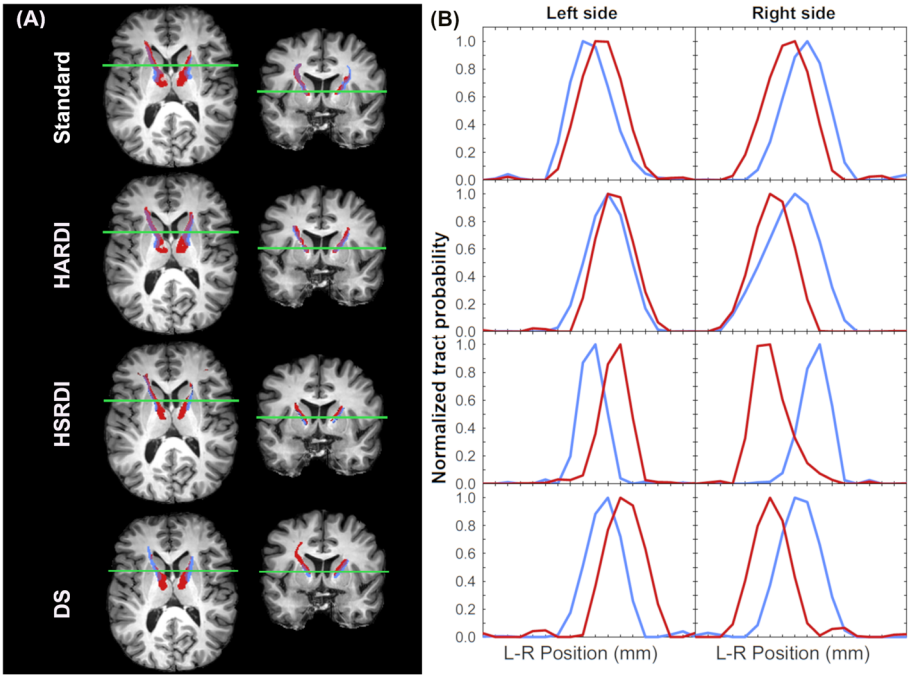

Figure 4.3. Co-registered (not normalized) tractography results of the ATR (red) and slMFB (blue) for the four datasets (rows) (A) and corresponding (normalized) tract probability profiles (B) of a representative subject.

From figure 4.1, the difference between the HSRDI and the HARDI scans is immediately apparent, whereas the differences between the standard and HARDI scans are more subtle. The HSRDI scan shows more anatomical detail and suffers less from partial voluming, resulting in increased distinction between separate directions. The HARDI is less noisy and looks cleaner than the baseline scan due to the additional volumes. The DS dataset appears very similar to the standard acquisition. Tractography results (figure 4.3) for the standard, HARDI, and DS sequences are quite similar in shape and size, with the HARDI tracts being slightly more voluminous than the baseline. In contrast, the HSRDI tracts appear much narrower and seem to fit the white matter anatomy better. This is also reflected in the tract probability profiles, which show that the peak-to-peak distance does not vary by much between the sequences, although there is a visual difference between the bundle widths.

Figure 4.4 shows the distribution of MSD's between the ATR and slMFB stratified by scan protocol. It can be seen that the HSRDI protocol yielded a higher average MSD than the standard protocol (41% average increase), whereas the HARDI protocol yielded a lower average MSD than the standard protocol (29% average

decrease). The DS dataset performed similar to the standard dataset in all aspects. A repeated-measures ANOVA showed that there was a significant difference in MSD between groups ($F(3,42) = 19.4$, $p = 10^{-5}$). Further assessment of pairwise differences (corrected for multiple comparisons) demonstrated that the MSD of the HSRDI sequence was significantly larger than the other datasets (HSRDI-vs-standard $t(14) = 3.6$, $p = 0.01$; HSRDI-vs-HARDI: $t(14) = 6.2$, $p = 10^{-4}$; HSRDI-vs-DS: $t(14) = -8.3$, $p < 10^{-5}$). The MSD was also significantly higher for the standard dataset compared to the HARDI scan (HARDI-vs-standard: $t(14) = 4.2$, p 0.01).

To investigate whether the difference in MSD between sequences was caused by alterations in peak-to-peak distances between the bundles, or by differences in the width of the tract profiles (i.e. the FWHM), these parameters were also plotted in Figure 4.4. Repeated-measures ANOVAs showed significant differences between the FWHM of the ATR ($F(3,42) = 39.2$, $p < 10^{-11}$) and MFB ($F(3,42) = 59.7$, $p < 10^{-14}$), respectively. Post-hoc assessment of pairwise differences (corrected for multiple comparisons) found that the HSRDI sequence produced a significantly lower FWHM compared to the standard and HARDI sequences for the ATR (HSRDI-vs-standard: $t(14) = -9.7$, $p < 10^{-6}$; HSRDI-vs-HARDI: $t(14) = -13.2$, $p < 10^{-8}$) and slMFB (HSRDI-vs-standard: $t(14) = 9.7$, $p < 10^{-6}$; HSRDI-vs-HARDI: $t(14) = 13.2$, $p < 10^{-7}$; HSRDI-vs-DS: $t(14) = 9.1$, $p < 10^{-5}$). There were also smaller, but still significant, differences in the FWHM of the standard and DS datasets on one hand and HARDI on the other for the slMFB (Standard-vs-HARDI: $t(14) = -3.5$, $p = 0.01$; DS-vs-HARDI: $t(14) = 5.3$, $p < 10^{-5}$). In contrast, the peak-to-peak distances were very similar between sequences and did not show any significant differences.

4.4 Discussion

The aim of this study was to optimize separability of the ATR and slMFB in the ALIC for specific targeting of either bundle in prospective DBS studies. We investigated the relative importance of angular and spatial resolution in diffusion MRI with limited scan time, as is common in clinical practice. DWI data were acquired according to one standard and two extended scan protocols with, respectively, increased angular and spatial resolution from a group of healthy volunteers. We performed probabilistic tractography to reconstruct the ATR and slMFB in all four datasets (i.e. three acquisitions and one down-sampled dataset). Finally, the mean standardized difference (MSD) was calculated as a measure of the separability of the ATR and slMFB. The increased spatial resolution (HSRDI) sequence yielded a significantly larger MSD than the other three datasets, suggesting that it was better able to separate the two bundles.

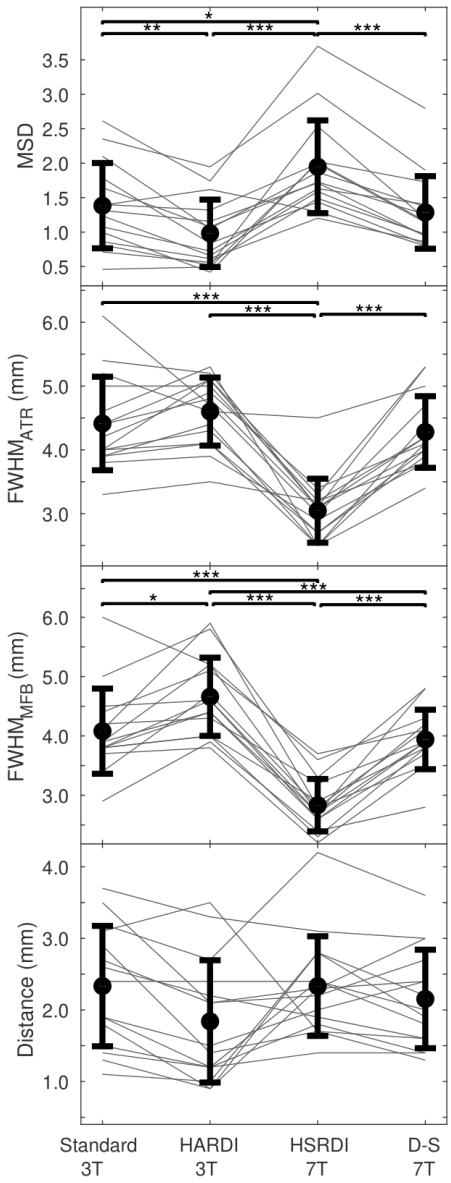

Figure 4.4. Comparison of the mean standardized difference (MSD), full-width-at-half-max (FWHM) and the distance between ATR and slMFB for all datasets. In all four panels, errorbars indicate the mean and standard deviations, with the separate data points for each subject connected by thinner (gray) lines. Bars are only shown for significant differences, with significance levels indicated by the asterisks: * for $p<0.05$; ** for $p<0.01$; *** for $p<0.001$.

The 7T (HRSDI) sequence with increased spatial resolution had better separability due to the smaller apparent cross-sectional area of the bundles, as there was no statistically significant difference in the peak-to-peak distances between the ATR and slMFB of all four datasets. Because of reduced partial voluming at higher spatial resolution at 7T in the plane perpendicular to the bundle trajectory, the overlap between ATR and slMFB could be reduced, thereby improving the separation of the tracts. There were no complex fiber crossings that needed to be resolved in the ATR and slMFB bundles using higher b-values data. It follows that the clinically used b-value of 1000 s/mm^2 was sufficient for accurate tract reconstruction and that increasing spatial resolution benefitted tract reconstruction.

The HARDI sequence actually yielded a small but significant decrease of the MSD compared to the standard sequence. This can be attributed to the significant increase in bundle cross-sectional area of the slMFB in the HARDI protocol. We hypothesize

that the apparent increase in tract cross-sectional area originates from the improved sensitivity to diffusion provided by the additional diffusion-shell. This is supported by our observation (data not shown) that the anisotropic volume fraction of the diffusion model used for tractography increased throughout the white matter, when adding the additional shell with a higher b-value. Effectively, this leads to wider tract outlines. Nevertheless, we have not attempted to quantify the volume of white matter tracts, since quantification of white matter volume and integrity with tractography is inherently limited (Jeurissen et al., 2019; Jones & Cercignani, 2010). Still, it remains possible that the apparent tract cross-sectional area at higher spatial resolutions is more reflective of the actual bundle cross-sectional area than at lower spatial resolutions.

The debate about optimal angular and spatial resolution in DWI acquisitions for tractography is still ongoing. Animal experiments suggest that angular and spatial resolution must be balanced (Calabrese et al., 2014). A later study in the human brain recommended to acquire DWI data at high angular resolution, since scans at a high angular resolution (obtained by applying strong diffusion-weighting gradients along many gradient directions) may help to resolve multiple fiber populations within each voxel (Vos et al., 2016). Conversely, data acquired at a high spatial resolution may increase the uniformity of tissue structures within voxels by decreasing the voxel volume, revealing structure previously unseen (Steele et al., 2017). It is feasible to increase both angular and spatial resolutions simultaneously, but this leads to increasingly longer scan times that may be unsuitable for patient studies and clinical use. Therefore, the choice of angular and spatial resolution may well depend on the white matter bundles being studied (Calabrese et al., 2014).

While high-resolution 7T clinical applications of diffusion MRI exist for DBS (Patriat et al., 2018; Plantinga et al., 2018), 7T hardware availability is limited. Nevertheless, we chose for 7T to push for higher spatial resolutions to better evaluate the tradeoff between angular and spatial resolution. With ongoing developments in acceleration techniques such as multiband, or by using different readouts (Q. Zhang et al., 2019), there is potential for higher spatial resolution acquisitions at 3T. Moreover, data processing packages have become better able to deal with distorted (Andersson & Sotiropoulos, 2015) and noisy data (Veraart et al., 2016), allowing to more readily push for higher spatial resolutions in diffusion acquisitions. Therefore, it should be possible to acquire higher spatial resolution DWI data for clinical use at 3T.

Challenges in establishing the tracts' volumes have the added consequence that absolute distance measurements in tractography suffer from uncertainty (Jones et al., 2013; Jones & Cercignani, 2010). Nevertheless, the relative differences in FWHM and the distance between the probability profiles give an indication of how well we

can distinguish between the ATR and slMFB. The locations of the peak probabilities of both bundles were consistent between sequences, which is supportive to the consistency of the ATR and slMFB tract reconstructions. Since the locations of the peak probabilities were consistent, there were no significant differences in the distances between tracts per sequence.

Current clinical practice in tractography-assisted surgery often relies on deterministic tractography, as opposed to probabilistic tractography (Petersen et al., 2016). In deterministic tractography, there is only one solution for fitting a tractography algorithm to the underlying diffusion MRI data. As a result, it may appear that there is a sharp transition between two bundles, where in reality the bundles are likely to overlap (Coizet et al., 2017). Therefore, we calculated the MSD between two bundles from probabilistic tractography, anticipating that it will provide a more reliable indication of the suitability of the data for tract delineation.

4.4.1 Limitations

There are some limitations to this study. Firstly, the data were acquired at two different field strengths hindering attribution of the results to spatial or angular resolution alone. Tissue properties may differ with field strength, such as decreased T_2-relaxation times at 7T that require shorter echo times. Although other parameters than the echo time also varied between the 3T and 7T sequences, we do not believe that this invalidated our comparison, as it is arguably better to compare sequences with optimized parameters with each other rather than to copy all parameters between sequences. Importantly, the diffusion process can be expected to be unaffected by magnetic field strength. In addition to above arguments, and to fully rule out the effect of field strength on the results, we down-sampled the 7T dataset and compared it to 3T data at the same resolution. This comparison showed a remarkable agreement in tractography results, suggesting that our results did not depend on field strength. Therefore, we believe our findings are also applicable to sites that do not have access to a 7T scanner.

Secondly, the high angular resolution 3T data was not optimized for spatial resolution, since it was our aim to compare data acquired with clinically used parameters to respectively higher angular and spatial resolution alternatives. Higher spatial resolutions in high angular resolution diffusion imaging have been used previously. For instance, data were acquired for the human connectome project (HCP) at a spatial resolution of 1.5 mm isotropic, even for very high b-values up to b = 10,000 s/mm^2 (Setsompop et al., 2013). However, the combination of higher angular and spatial resolutions require specialist scanner hardware (e.g., stronger gradients and coils with a large number of channels), which makes these scan parameters difficult to attain in

a clinical setting. In this light, the use of default clinical parameters and clinically attainable scan times in our study facilitates clinical application.

A third limitation lies in the trade-off between angular and spatial resolution. Many different parameter combinations exist that increase the angular resolution of a diffusion MRI scan. We limited ourselves to investigating only one protocol with improved angular resolution. This protocol's parameters are common in high angular resolution diffusion imaging, albeit with a lower b-value than the reported b = 3000 s/mm^2 for optimal angular resolution (Tournier et al., 2013) to limit the echo time on clinical systems. We expect our diffusion sensitivity at b = 2200 s/mm^2 to be close to the optimum (Caan et al., 2010).

Finally, we have no direct comparison with histological data which could serve as ground truth in determining the bundles' true dimensions, and amount of overlap. Despite this limitation, having to deal with clinically restricted scanning time, and considering the parallel tract orientations within the vALIC, it seems more advantageous to increase the spatial resolution than the angular resolution to solve the overlap issue. Conversely, it is likely that increasing spatial resolution at the cost of angular resolution is detrimental in crossing tract configurations, since these may require a higher angular resolution to be resolved. Thus, we limit our recommendation of focusing on spatial resolution to resolving parallel tracts for DBS planning. Prospective DBS studies are necessary for validation of our findings.

4.4.2 Relevance

This study is relevant to precise delineation of parallel running tracts, such as needed for tractography-assisted targeting in DBS in the ALIC. These (relatively) simple parallel tract configurations have received little attention, while it is our experience that even small differences, on a millimeter scale, in DBS localization can alter treatment efficacy (Liebrand et al., 2019). Additionally, more precise and selective stimulation may potentially decrease side effects and prolong battery life. Especially with the advent of so-called directional, or, steering DBS electrodes (Steigerwald et al., 2019), which are to an extent able to focus the generated electric field to one side, there is an increased potential of delivering stimulation to precisely defined neuroanatomical structures. Therefore, we aim to implement a higher spatial resolution diffusion MRI scan for pre-surgical vALIC DBS planning . We recommend increasing spatial resolution for present application, also to groups without access to a 7T scanner.

4.5 Conclusions

We conclude that, within a limited amount of scanning time, it is more beneficial to increase the spatial than the angular resolution to be able to precisely discern the slMFB and ATR in the vALIC, as is required for tract-specific DBS. This is primarily caused by the smaller cross-sectional area of the tracts found at higher spatial resolution, leading to decreased overlap. Dictated by local anatomy, our protocol advice deviates from general recommendations to aim for high angular resolution to resolve crossing fibers. Our work thereby allows for increased precision of tract-specific DBS targeting in the vALIC by increasing the spatial resolution of the diffusion MRI scans. Furthermore, it encourages researchers and clinicians to optimize the scanning protocol to the specific anatomy and application at hand.

4.6 Supplementary information

Figure 4.S1. Axial and coronal tractography overviews of the complete sample (N=15) included in this study in individual anatomical space, for all four datasets (standard, HARDI, HSRDI, and DS, respectively). All participants, except one, had a T1-scan available. The colour coding corresponds to the other figures in this paper: the anterior thalamic radiation in red, the supero-lateral branch of the medial forebrain bundle in blue. (HARDI: high angular resolution diffusion imaging; HSRDI: high spatial resolution diffusion imaging; DS: down-sampled)

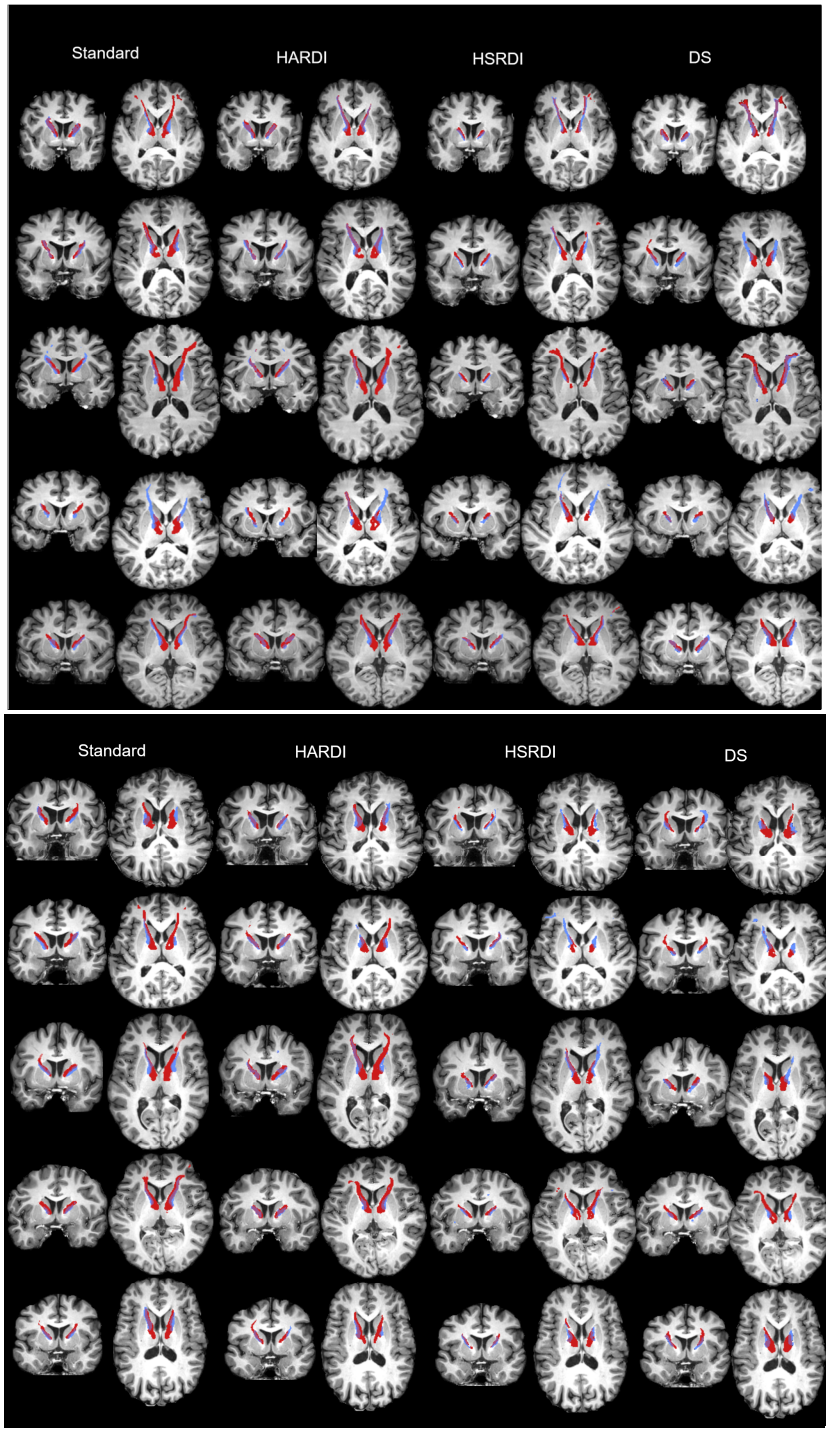
Standard
HARDI
HSRDI
DS
Standard
HARDI
HSRDI
DS

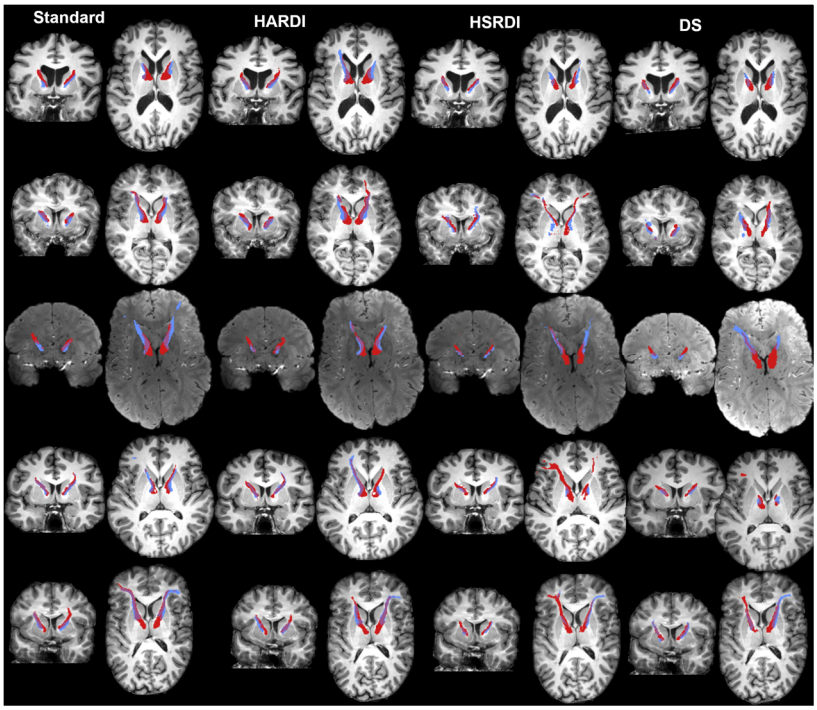
Standard
HARDI
HSRDI
DS

III. PATIENT SELECTION

Chapter 5

Deep brain stimulation response in obsessive-compulsive disorder is associated with preoperative nucleus accumbens volume

Luka C. Liebrand*, Paul Zhutovsky*, Eva K. Tolmeijer, Ilse Graat, Nienke Vulink, Pelle de Koning[1], Martijn Figee, P. Richard Schuurman, Pepijn van den Munckhof, Matthan W.A. Caan, Damiaan Denys, Guido A. van Wingen
*** Both authors contributed equally to this work.**

Published in: NeuroImage: Clinical (2020), 30

doi: 10.1016/j.nicl.2021.102640

Abstract

Background: Deep brain stimulation (DBS) is a new treatment option for patients with therapy-resistant obsessive-compulsive disorder (OCD). Approximately 60% of patients benefit from DBS, which might be improved if a biomarker could identify patients who are likely to respond. Therefore, we evaluated the use of preoperative structural magnetic resonance imaging (MRI) in predicting treatment outcome for OCD patients on the group- and individual-level.

Methods: In this retrospective study, we analyzed preoperative MRI data of a large cohort of patients who received DBS for OCD (n = 57). We used voxel-based morphometry to investigate whether grey matter (GM) or white matter (WM) volume surrounding the DBS electrode (nucleus accumbens (NAc), anterior thalamic radiation), and whole-brain GM/WM volume were associated with OCD severity and response status at 12-month follow-up. In addition, we performed machine learning analyses to predict treatment outcome at an individual-level and evaluated its performance using cross-validation.

Results: Larger preoperative left NAc volume was associated with lower OCD severity at 12-month follow-up ($p_{FWE} < 0.05$). None of the individual-level regression/classification analyses exceeded chance-level performance.

Conclusions: These results provide evidence that patients with larger NAc volumes show a better response to DBS, indicating that DBS success is partly determined by individual differences in brain anatomy. However, the results also indicate that structural MRI data alone does not provide sufficient information to guide clinical decision making at an individual level yet.

5.1 Introduction

Deep brain stimulation (DBS) is a new treatment option for approximately 10% of patients with obsessive-compulsive disorder (OCD) who do not benefit from conventional pharmacological and psychological therapies (Denys et al., 2020). On average, around 60% of these treatment-resistant patients respond to DBS(Alonso et al., 2015). Clinical predictors for DBS outcomes in OCD are scarce, with, e.g., an older age at onset of OCD being associated with better response on the group level (Alonso et al., 2015). However, these predictors cannot yet be used to determine which individual patients may or may not be suitable for DBS. While recent studies showed that treatment response might improve with diffusion magnetic resonance imaging (MRI) guided DBS targeting (Baldermann et al., 2019; Coenen et al., 2018; Liebrand et al., 2019), it is unlikely that all patients will become responders in the future. Since OCD has been associated with various structural brain abnormalities (Boedhoe et al., 2017; Gan et al., 2017; Hashimoto et al., 2014), differences in (individual) brain structure might be used to predict treatment response. Multiple studies used structural MRI data to predict treatment outcome in OCD (e.g., (Hashimoto et al., 2014; Yun et al., 2015)), but few studies examined neural biomarkers for treatment-resistant OCD (Dunlop et al., 2016; Van Laere et al., 2006). Nevertheless, the potential benefits of a reliable biomarker for DBS response are substantial. First, DBS is a long-term invasive treatment which carries several risks (Alonso et al., 2015; de Koning et al., 2011) and presents a possible burden to the patient, which could be avoided if potential non-responders are identified early. Second, DBS is a costly treatment with limited availability. Selecting only those patients who are likely to benefit would increase DBS's cost-effectiveness, since the likelihood of DBS being cost-effective is only 57% over the first two years (Ooms et al., 2017). This could increase the availability of DBS, speeding up patients' and referring clinicians' decision to start treatment. In addition, an effective biomarker could provide valuable information regarding the pathophysiology of (treatment-resistant) OCD.

The nucleus accumbens (NAc) and the neighboring ventral capsule have been the most popular DBS targets for OCD (Alonso et al., 2015). These targets, which were adapted from white matter lesioning sites(Tierney et al., 2014), form a central hub within the cortico-striatal-thalamic-cortical (CSTC) loop (Wood & Ahmari, 2015). Previous findings suggest that DBS reduces OCD symptoms by disrupting pathological hyperconnectivity within the CSTC circuitry (Figee et al., 2013; Schmuckermair et al., 2013), preventing neurons in frontostriatal networks to synchronize (Bahramisharif et al., 2016; Smolders et al., 2013). The NAc is assumed to play an important role in integrating inputs within the CSTC circuitry, receiving

dopaminergic and glutamatergic inputs from the ventral tegmental area and cortico-limbic regions, respectively (Wood & Ahmari, 2015). Successful DBS renormalizes abnormal striatal dopamine levels in OCD patients (Figee et al., 2014), which is in agreement with the assumed working mechanism of the same DBS target for depression (Coenen et al., 2011). Recent tractography studies further support the idea that connections to distal brain regions are important in DBS treatment response, even suggesting that white matter tracts running through the ventral capsule may be the optimal targets. Specifically, these studies have pointed towards the supero-lateral medial forebrain bundle (slMFB) (Coenen et al., 2017; Liebrand et al., 2019), possibly in combination with frontothalamic fibers (likely part of the anterior thalamic radiation (ATR) (Baldermann et al., 2019)). Complementary to their importance as targets, the NAc, slMFB and ATR might contain crucial information regarding treatment response.

In this retrospective study, we perform group- and individual-level analyses on preoperative structural MRI data to infer a potential relationship between voxel-wise grey- and white-matter volume (GM/WM) and DBS treatment response using one of the largest cohorts of OCD patients who received DBS to date. We hypothesized that grey matter (NAc) and white matter (ATR and slMFB) volume surrounding the DBS electrodes would be suitable for predicting improvement in OCD symptoms following DBS treatment. More exploratory, we also investigated DBS treatment effects on the whole-brain level.

5.2 Material and methods

5.2.1 Patients

We retrospectively retrieved and analyzed all available anonymized data of patients who received DBS for treatment-refractory OCD at the Amsterdam UMC (location AMC) in Amsterdam, The Netherlands, between 2005-2017. The first 16 patients participated in a clinical trial(Denys et al., 2010), while all consecutive patients received DBS as part of routine healthcare (Denys et al., 2020). We automatically retrieved preoperative MRI data of 63 patients. Data of six patients were excluded during preprocessing due to suboptimal segmentation or image artifacts (details in the *Imaging* section), so that datasets from 57 patients were used for the final analyses.

Patients aged 18-65 were eligible for treatment if they had a primary diagnosis of severe treatment-resistant OCD according to the DSM-IV (American Psychiatric Association, 2000) for over 5 years, with a minimum symptom score of 28 on the Yale-Brown obsessive compulsive scale (Y-BOCS). Patients were eligible for DBS if they did not previously respond to two 12-week trials with a selective serotonin

reuptake inhibitors (SSRI) at maximum dosage, including augmentation with an atypical antipsychotic for 8 weeks, one 12-week trial of the maximum dosage clomipramine and cognitive behavioral therapy (CBT) at a center specialized in OCD (Denys et al., 2020). Contraindications for DBS were presence of psychotic disorders, recent substance abuse, and unstable neurological or coagulation disorders. Severe comorbid DSM diagnoses such as bipolar disorder or autism spectrum disorder were relative contraindications, outside of the first 16 patients included in our trial for whom these were always exclusion criteria. An independent psychiatrist monitored the inclusion process. More details about the included patients and inclusion and exclusion criteria can be found in Denys et al. (2020).

Since this is a retrospective study with anonymized datasets that does not burden the patient, according to the Dutch Medical Research Involving Human Subjects Act (WMO) this study did not require approval from a medical-ethical committee. The institutional review board of Amsterdam UMC waived the obligation to obtain informed consent.

5.2.2 Treatment

DBS lead implantation

Patients were bilaterally implanted under general anesthesia, according to standard stereotactic procedures. Surgical planning was performed based on anatomical landmarks in SurgiPlan (Elekta AB, Stockholm, Sweden), such that the active DBS contacts (model 3389, Medtronic, Minneapolis, US; 4x 1.5 mm contacts with 0.5 mm interspace) were placed in the ventral anterior limb of the internal capsule (ALIC) (van den Munckhof et al., 2013). The electrodes were coronally angled to follow the ALIC trajectory with an approximate anterior angle of 75°. Correct lead placement was ensured with co-registration of postoperative computed tomography (CT) to preoperative structural MRI.

DBS optimization and CBT

The DBS device was switched on two weeks after surgery, marking the start of the optimization phase. In this phase, stimulation voltage, pulse duration and active contacts were subsequently updated in absence of clinical response. The clinical effect and tolerability of (side) effects of each new parameter combination was evaluated every two weeks, according to published protocols (van Westen et al., 2020). The aim of DBS optimization was to find a clinically effective and tolerable parameter combination. Once achieved, these parameters were kept stable. The length of the optimization phase was not uniform, since the time to find the optimal stimulation

parameters varied between patients. At the end of the optimization phase, patients received CBT during which they had to challenge their symptomatic behavior to augment the clinical effect of DBS (Mantione et al., 2014).

Treatment outcome

Symptom severity was regularly assessed using the Y-BOCS, with a ≥35% symptom reduction with respect to the preoperative baseline determining treatment response. We computed DBS treatment response from baseline and 12-month follow-up Y-BOCS scores, which - outside of the first 16 patients - were obtained as part of routine clinical practice. In our analyses we first focused on the treatment response criterion as it has been used as a typical criterion of treatment success in DBS stimulation (Alonso et al., 2015). In addition, we also predicted the Y-BOCS score at 12-month follow-up directly as this approach should allow for better statistical modelling than prediction of (binarized) percentage change (Altman & Royston, 2006).

5.2.3. Imaging

Data acquisition

The T1-weighted MRI data used in this study were all acquired for surgical planning according to clinical protocol. Given the large timeframe in which patients received DBS, different combinations of scanners/parameters were used in this study (Table 5.S1).

MRI preprocessing

Preoperative MRI data was preprocessed using the standardized pipeline of the CAT12 toolbox (r1450, http://www.neuro.uni-jena.de/cat) for SPM12 (v7487, https://www.fil.ion.ucl.ac.uk/spm/software/spm12) in the MATLAB programming language (R2018b, The Mathworks, Natick, MA). Preprocessing included inhomogeneity correction, partial volume based segmentation and spatial normalization to MNI space via Geodesic Shooting normalization (Ashburner & Friston, 2011) utilizing a template derived from 555 subjects of the IXI-database (http://brain-development.org/) provided by the CAT12 toolbox. The final GM/WM segmentations were modulated by the Jacobian determinant accounting for volume changes during the normalization process. The quality of the segmentations was investigated through the quality control options provided by the CAT12 toolbox and visual inspection. This led to the exclusion of five patients due to suboptimal segmentation quality and one patient due to an artifact in the original MRI scan.

Finally, data were spatially smoothed with an 8mm full-width-at-half-maximum kernel.

For the analyses whole-brain GM and WM masks were created by thresholding individual GM/WM images at 0.15 and only including voxels which survived thresholding across all patients. Bilateral ROI-specific masks for the NAc and the ATR were extracted from the subcortical Harvard-Oxford atlas (25% threshold of the maximum probability maps) and the JHU white-matter tractography atlas (25% threshold of the maximum probability maps), respectively, which are both included in the FSL library (Jenkinson et al., 2012). It is important to note that a large part of the slMFB is included in the atlas definition of the ATR.

We also calculated scalar momenta (Ashburner & Klöppel, 2011) as an additional and more advanced form of MRI data representation since a recent benchmarking study showed them to provide increased performance in pattern recognition tasks (Monté-Rubio et al., 2018). Details on their computation can be found in the Supplementary Methods.

5.2.4 Statistical Analyses

Clinical and Demographic Data

We summarized clinical and demographic data of the entire sample. To investigate whether responders and non-responders differed on demographic variables at baseline and follow-up (symptom severity) we used t-tests and X^2-tests as appropriate. Tests were performed using the SPSS software (version 26).

MRI Group-level analyses

All analyses were performed on ROI- (bilaterally) and whole-brain level. Group-differences between responders (n=31) and non-responders (n=26) were computed using the preprocessed and masked volume maps. Demeaned baseline Y-BOCS scores, age at baseline, sex, total intracranial volume (TIV), and scanner IDs (dummy-coded) were included as covariates in the analysis. The significance level was set at $p<0.05$ family-wise error (FWE) corrected and estimated using the threshold-free cluster enhancement (TFCE) statistic with 10,000 permutations (Smith & Nichols, 2009). FWE corrections were performed using synchronized permutations and included corrections for all voxels within a mask/ROI, and the two-sided tests (Alberton et al., 2020; Winkler et al., 2016). Additional multiple comparison corrections across two masks (NAc-ROI/ATR-ROI or GM/WM) were performed

using Bonferroni-correction. All tests were performed using the PALM toolbox (a117, https://fsl.fmrib.ox.ac.uk/fsl/fslwiki/PALM).

Complementary to this analysis of group-differences, we performed group-level regression analyses between ROI/whole-brain segmentations and post-treatment Y-BOCS scores. We utilized the same covariates and statistical procedures as described above.

MRI Individual-level analyses

In addition to group-level analyses, we also investigated the suitability of structural MRI for making individual-level predictions with machine learning procedures. For that we utilized linear-kernel support vector machine classification/regression (SVC/SVR) (Cortes & Vapnik, 1995; Drucker et al., 1997) and investigated its performance using 10-times-repeated-5-fold cross-validation (10x5 CV). In this procedure, the available data is randomly divided into 5 (approximately) equally sized folds, from which 4 folds are used as training data and the remaining 5th fold is used to estimate the performance of the SVC/SVR. This process is repeated five times, always using a different fold as the test set. The random assignment of data to folds is repeated ten times and performance across all 50 evaluations is averaged. This allows for an unbiased way to estimate generalization performance of machine learning models. Performance was measured as area-under-the-receiver-operator-curve (AUC), balanced accuracy, sensitivity and specificity in the classification case and as mean absolute error (MAE), mean squared error (MSE), root mean squared error (RMSE), Pearson correlation (r) and coefficient-of-determination (R^2) for the regression case. We also applied label permutation tests (Ojala & Garriga, 2010) (n=1000) to statistically determine whether the obtained performances (AUC for classification and MAE for regression) differed from chance-level at alpha=0.05 Bonferroni-corrected for three tests corresponding to the different volumes per data scale (whole-brain or ROI). We corrected for three tests here because the individual-level analyses also considered the combination of each of our data representations (e.g., GM alone, WM alone and a combination of both GM + WM), contrary to the approach on the group-level.

We removed nuisance effects associated with age, sex, TIV, and scanner IDs via linear regression from the MRI data. Importantly, the estimation of the linear regression coefficients was always limited to the training set. In addition, baseline Y-BOCS score was added as a feature in both analyses. Given the high number of voxels in our dataset we implemented a feature selection approach. This corresponded to calculating Fisher scores (Li et al., 2017) in the classification case and Pearson correlations between each voxel and the Y-BOCS follow-up score across patients in

the regression case. These calculations were again only performed on the training set. To determine the optimal percentage of features to select, a nested cross-validation procedure (with 5-fold CV as the inner CV) was implemented. All analyses were run for whole-brain GM/WM and NAc/ATR ROIs and the combination of GM/WM and NAc/ATR data. The combination corresponded to just concatenating the different feature maps. In addition, we also repeated the analysis for scalar momenta as a more advanced form of data representation. All analyses were implemented in the Python programming language (3.7.6) utilizing the scikit-learn toolbox (Pedregosa et al., 2011) (0.22.1).

5.3 Results

5.3.1 Clinical and Demographic Data

A summary of the clinical and demographic data and statistical tests between responders and non-responders are reported in Table 1. Responders and non-responders did not statistically differ at baseline; only Y-BOCS scores at 12-month follow-up differed significantly between these groups ($t(49.571)=-9.986$, $p<0.001$, see Figure 5.S1 for trajectories of Y-BOCS scores per patient).

Table 5.1: Demographic and clinical variables (mean (SD) [range])

	All (n=57)	**Responder (n=31)**	**Non-Responder (n=26)**	
Age [years]	42.65 (11.17) [23 - 69]	43.48 (11.10) [30 - 69]	41.65 (11.40) [23 - 65]	t(55)=0.612, p=0.543[a]
Sex (F/M)	41/16	21/10	20/6	$\chi^2(1)=0.590$, p=0.442[b]
Age at onset of OCD [years]	16.23 (9.13) [4 - 52]	17.45 (8.89) [6 - 52]	14.77 (9.38) [4 - 40]	t(55)=1.107, p=0.273[a]
Duration of illness [years]	26.82 (10.69) [7 - 51]	26.61 (9.65) [12 - 51]	27.08 (12.00) [7 - 50]	t(55)= -0.162, p = 0.872[a]
MRI sequence[c]	6/24/5/15/7	3/14/2/7/5	3/10/3/8/2	$\chi^2(4) = 1.794$, p = 0.774[b]
TIV [ml]	1359.82 (156.65) [1102.17 - 1795.69]	1358.00 (159.13) [1129.47 - 1795.69]	1361.99 (156.76) [1102.17 - 1637.40]	t(55) = -0.095, p = 0.925[a]
Baseline Symptom Severity:				
Y-BOCS	33.85 (3.22) [28 - 40]	33.94 (3.25) [28 - 40]	33.77 (3.24) [28 - 40]	t(55) = 0.193, p = 0.848[a]
HAM-A	26.65 (7.96) [11 - 45]	26.68 (8.22) [11 - 42]	26.62 (7.80) [12 - 45]	t(55) = 0.029, p = 0.977[a]

HAM-D	21.38 (5.89) [8 - 35]	21.30 (6.18) [11 - 31]	21.46 (5.67) [8 - 35]	t(54) = -0.101, p = 0.920[a]
Baseline medication:				$\chi^2(5) = 8.954$, p = 0.111[b]
None	7	4	3	
SSRI	13	5	8	
SSRI + antipsychotic	14	11	3	
Clomipramine	6	1	5	
Clomipramine + antipsychotic	16	9	7	
Other	1	1	0	
Baseline Comorbidities:				
Mood Disorders	30	17	13	$\chi^2(1) = 0.133$, p = 0.716[b]
Anxiety Disorders	6	2	4	$\chi^2(1) = 1.198$, p = 0.274[b]
Addiction	3	2	1	$\chi^2(1) = 0.193$, p = 0.661[b]
Eating Disorders	4	3	1	$\chi^2(1) = 0.795$, p = 0.373[b]
Personality Disorders	11	6	5	$\chi^2(1) < 0.001$, p = 0.991[b]
Other	3	1	2	$\chi^2(1) = 0.566$, p = 0.452[b]
Stimulation settings[d]:				
# Active contacts (1/2/3/4)	1/39/6/4 *3 unknown*	1/23/1/1 *3 unknown*	0/16/5/3	$\chi^2(3) = 4.00$, p = 0.26
Voltage (V)	4.32 (0.90) [2.80-6.30]	4.28 (0.87) [3.00-6.30]	4.35 (0.95) [2.80-6.00]	t(51) = 0.285 p = 0.77
Pulse width (µs) *(60/90/120/150/180)*	3/37/4/4/2 *3 unknown*	3/19/2/2/2 *1 unknown*	0/18/2/2/0 *2 unknown*	$\chi^2(4) = 6.667$, p = 0.15
Frequency (Hz) *(130/180/185)*	37/2/11 *3 unknown*	22/1/5 *1 unknown*	15/1/6 *2 unknown*	$\chi^2(3) = 6.00$, p = 0.20
Post-treatment Symptom Severity:				
Y-BOCS	19.35 (9.40) [0 - 35]	12.61 (6.94) [0 - 24]	27.38 (4.06) [22 - 35]	t(49.571) = -9.986, p < 0.001[e,*]

F: Female; **M**: Male; **MRI**: Magnetic Resonance Imaging; **TIV**: Total Intracranial Volume; **Y-BOCS**: Yale-Brown Obsessive Compulsive Scale; **HAM-A**: Hamilton Anxiety Rating Scale; **HAM-D**: Hamilton Depression Rating Scale; **SSRI**: Selective Serotonin Reuptake Inhibitor

[a] independent samples t-test - equal variances assumed; [b] Chi-square test;
[c] MRI sequence correspond to the five different MRI scanners/sequences described in the supplementary materials; [d] Stimulation settings for n=53, data of 4 patients (2 responders) were not automatically retrievable;
[e] independent samples t-test - equal variances not assumed; * $p < 0.05$

5.3.2 MRI Group-level analyses

The results of the group-level analyses are summarized in Figure 5.1 and Figure 5.2. We found a significant association between Y-BOCS scores at 12-month follow-up and left NAc grey-matter volume (31 voxels, maximum: -7.5, 15, -7.5 [mm], TFCE: 85.91) (Figure 5.1). Lower follow-up Y-BOCS scores were associated with larger preoperative grey-matter volume (Figure 5.2). This result remained significant when an additional covariate encoding time since first DBS operation (mean-centered) in the patient sample was added to the model. We did not find significant associations between clinical outcomes and volumes of the right NAc, or ATR. However, right NAc grey-matter volume did show a comparable association at the uncorrected level, implying a potential lack of power to detect an effect. When comparing groups, larger NAc grey-matter volume in the same voxels was trend-level significant for responders over non-responders. There were no significant associations in the exploratory whole-brain analyses.

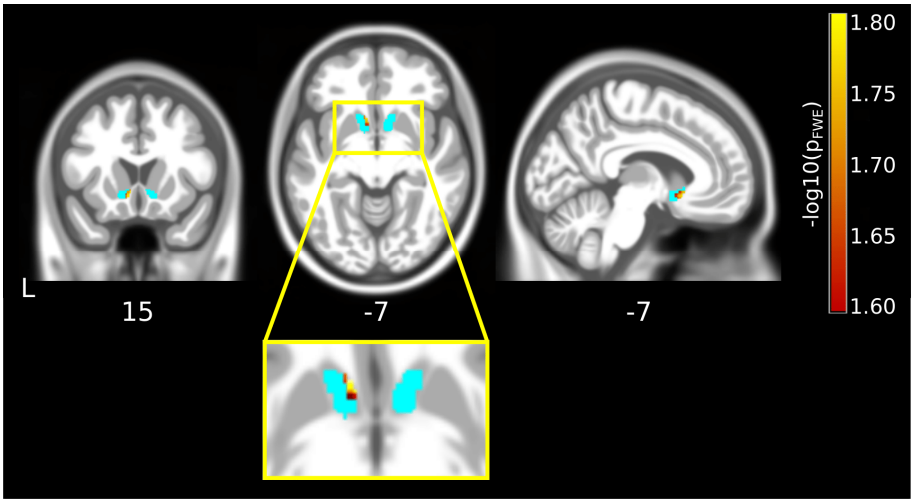

Figure 5.1: Negative group-level association between the post-treatment Y-BOCS score and pre-treatment grey-matter volume of voxels within the nucleus accumbens ROI (in cyan). Results are overlaid over the average T1 image calculated from 555 subjects of the IXI database provided by the CAT12 toolbox. Coordinates are given

in MNI space. Significant associations are shown in hot colors thresholded at $p_{FWE} < 0.025$ (-log10(0.025) = 1.602).

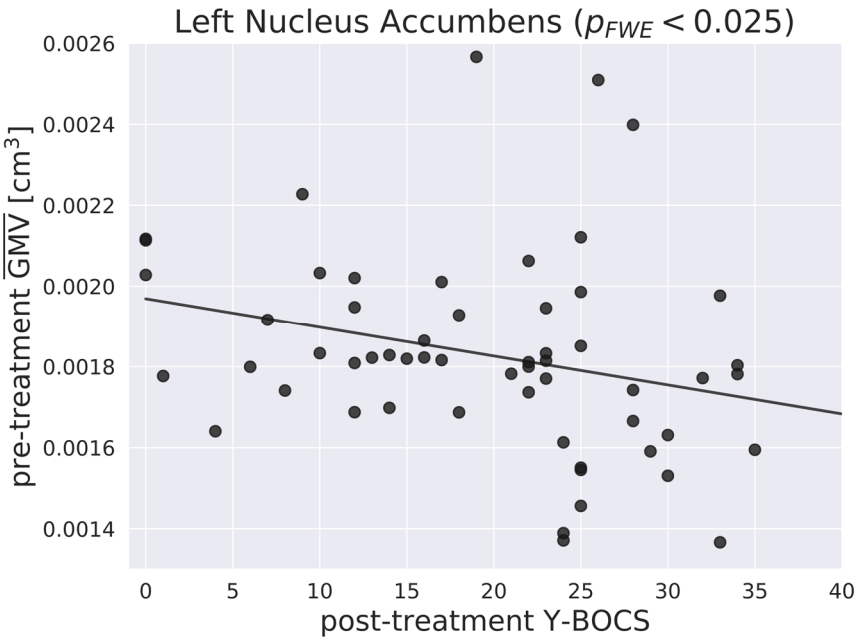

Figure 5.2: Negative group-level association between post-treatment Y-BOCS and the average grey-matter volume of all significant voxels within the left nucleus accumbens ROI.

5.3.3 MRI Individual-level analyses

Results of individual-level regression and classification analyses are reported in Tables 2 and 3. None of the MRI data representations exceeded chance-level performance neither for the regression nor the classification analysis, neither when using whole-brain or ROI data.

Table 5.2: Classification performance for different MRI data representations. Estimated using 10-times repeated 5-fold cross-validation (mean (SD) [range]).

	AUC	Accuracy [%]	Sensitivity [%]	Specificity [%]
GM	0.468 (0.124) [0.167 -0.694]	48.21 (10.25) [26.67 - 72.86]	56.76 (19.96) [16.67 - 100]	39.67 (19.57) [0 - 80]
WM	0.422 (0.173) [0 - 0.80]	44.90 (14.52) [16.67 - 72.86]	57.52 (23.27) [0 - 100]	32.27 (21.58) [0 - 60]
GM + WM	0.433 (0.171) [0 - 0.833]	48.10 (15.56) [0 - 80.00]	60.67 (22.71) [0 - 100]	35.53 (19.40) [0 - 66.67]
NAc	0.543 (0.213) [0.067 - 0.933]	57.30 (13.23) [16.67 - 83.33]	62.19 (19.62) [16.67 - 100]	52.40 (20.00) [0 - 100]
ATR	0.509 (0.201) [0.10 - 0.933]	42.86 (14.86) [16.67 - 73.33]	47.19 (19.16) [0 - 85.71]	38.53 (24.02) [0 - 100]
NAc + ATR	0.481 (0.162) [0.133 - 0.767]	48.57 (14.57) [16.67 - 75.71]	54.14 (17.65) [16.67 - 85.71]	43.00 (22.41) [0 - 80]
Scalar Momentum	0.546 (0.136) [0.233 - 0.857]	51.52 (10.24) [33.33 - 75.71]	56.38 (17.21) [16.67 - 85.71]	46.67 (18.52) [0 - 100]

AUC: Area-under-receiver-operator-curve; **GM**: Grey-matter volume; **WM**: White-matter volume; **NAc**: Grey-matter volume of Nucleus Accumbens; **ATR**: White-matter volume of Anterior Thalamic Radiation

Table 5.3: Regression performance for different MRI data representations. Estimated using 10-times repeated 5-fold cross-validation (mean (SD) [range]).

	MAE	MSE	RMSE	Pearson correlation	R^2
GM	9.23 (2.03) [5.37 - 13.85]	129.44 (47.16) [50.35 - 247.44]	11.19 (2.05) [2.05 - 15.73]	-0.036 (0.012) [-0.496 - 0.156]	-0.684 (0.572) [-2.556 - 0.156]
WM	9.07 (1.64) [5.91 - 13.04]	123.87 (44.80) [51.24 - 278.98]	10.97 (1.90) [7.16 -16.70]	0.012 (0.246) [-0.487 - 0.549]	-0.628 (0.568) [-3.009 - 0.253]
GM + WM	8.80 (1.73) [5.35 - 13.00]	119.17 (40.90) [50.91 - 238.46]	10.77 (1.82) [7.14 - 15.44]	0.055 (0.247) [-0.519 - 0.446]	-0.592 (0.655) [-2.812 - 0.157]
NAc	7.84 (1.46) [4.89 - 11.81]	92.87 (32.02) [38.43 - 178.91]	9.50 (1.61) [6.20 - 13.38]	0.365 (0.272) [-0.208 - 0.738]	-0.253 (0.514) [-1.477 - 0.430]
ATR	9.02 (1.93) [5.44 -16.01]	128.17 (53.35) [54.08 - 329.40]	11.11 (2.20) [7.35 - 18.15]	0.133 (0.279) [-0.662 - 0.583]	-0.694 (0.686) [-2.910 - 0.305]
NAc + ATR	9.17 (1.72) [4.43 - 13.57]	126.27 (43.82) [33.90 - 237.21]	11.07 (1.98) [5.82 -15.40]	0.253 (0.340) [-0.552 - 0.772]	-0.698 (0.672) [-2.443 - 0.471]
Scalar Mo-men-tum	8.96 (1.99) [5.59 - 17.74]	119.07 (58.20) [55.35 - 437.43]	10.69 (2.20) [7.44 - 20.91]	0.161 (0.293) [-0.585 - 0.719]	-0.586 (0.829) [-5.286 - 0.305]

MAE: Mean absolute error; **MSE**: Mean squared error; **RMSE**: Root mean squared error; $\mathbf{R^2}$: Coefficient of determination; **GM**: Grey-matter volume; **WM**: White-matter volume; **NAc**: Grey-matter volume of Nucleus Accumbens; **ATR**: White-matter volume of Anterior Thalamic Radiation

5.4 Discussion

The aim of this study was to investigate the relationship between voxel-wise brain volumetry and DBS treatment response in OCD. We related the 12-month follow-up Y-BOCS score to volumetric differences on group-level, and tested whether brain volumes were predictive of outcomes on an individual-level with SVC/SVR. In our sample we found that larger preoperative volumes of the left NAc corresponded significantly with lower Y-BOCS scores at 12-month follow-up on the group-level. However, our machine learning analyses did not generate models that could predict individual-level outcome above chance-level.

The NAc is involved in the pathophysiology of OCD and is centrally located in the CSTC circuitry. For this reason the NAc was our original DBS target(Denys et al., 2010), although the clinically effective contacts were located in the ventral ALIC white matter just above the NAc (van den Munckhof et al., 2013). Given the suspected disruptive effect of DBS on connectivity (Bahramisharif et al., 2016; Smolders et al., 2013), it may be remarkable that larger NAc volumes are associated with better outcomes. Potentially, the beneficial effect of stimulation is larger in patients with an increased NAc volume, meaning that patients with smaller NAc volumes could be even more treatment-resistant. Previous studies suggest treatment outcome depends on proximity of stimulation to white matter bundles in the vALIC (Baldermann et al., 2019; Liebrand et al., 2019). It is possible that larger NAc volumes led to electrode positioning such that stimulation was closer to the relevant white matter structures. In this case, larger NAc volumes would rather reflect better odds of achieving optimal electrode positioning than directly predict response. Given the respective scales of the white matter variability in the vALIC (Liebrand et al., 2019) and NAc volumetric differences, the chance that these relatively small volumetric differences were responsible for a difference in electrode positioning large enough to affect treatment outcome appears small. Conversely, the surgical methods are unlikely to have played a role in the observed asymmetry. Although the left-sided electrode was usually implanted first, followed by the right-sided electrode since the infra-clavicular stimulator is usually implanted on the right side, the time between the two electrode insertions is short. Measures like glue in the burr-holes prevent the leakage of cerebrospinal fluid and intraoperative brain shift hardly occurs any longer so there is no asymmetry to be expected in the potential targeting inaccuracy. However, due to

the limited availability of diffusion MRI scans in this sample we could not test for a possible correlation.

Research into the role of the NAc in the context of predicting treatment outcome has been scarce, but earlier studies have linked the NAc to pharmacotherapy and psychotherapy resistance. Treatment-resistant OCD patients showed hypo-responsivity of the NAc during the anticipation of rewards (Figee et al., 2011), as well as micro-structural alterations of the NAc as measured with diffusion tensor fractional anisotropy (Li et al., 2014). More recently, a study investigating patients who received treatment with CBT and SSRIs for anxiety disorders found that larger baseline NAc volumes were associated with a larger reduction of anxiety symptoms (Burkhouse et al., 2020). The authors suggested that treatments targeting anxiety-related avoidance behavior were more effective in patients with larger pretreatment deficits in the systems responsible for the avoidance behavior, which was supported by studies showing a relationship between larger baseline NAc volume and more severe anxiety symptoms (Günther et al., 2018; Kühn et al., 2011) as well as between NAc structural alterations and avoidance behaviors in patients with anxiety symptoms (Lago et al., 2017). In our experience, the treatment effect in DBS for OCD is achieved by an initial anxiolytic effect that is further augmented by exposure-based CBT (Denys et al., 2010; Mantione et al., 2014). Taken together, the larger reduction of OCD symptoms in patients with larger NAc volumes may result from a larger effect of DBS on avoidance behaviors, which needs to be tested in future research. Patients with smaller NAc volumes might benefit less from treatment because the NAc's ability to integrate dopaminergic inputs during reward processing may be impaired, which could interfere with resumption of normal functioning within the CSTC circuitry.

While an association between the left NAc volume and follow-up Y-BOCS was found on the group-level, both the SVC/SVR approaches did not yield predictive values significantly above chance-level. One possible explanation is that multivariate analyses typically require larger samples than univariate analyses (Bzdok & Ioannidis, 2019). Our sample, while sizable for psychiatric DBS studies, may not have been large enough to detect the complex patterns needed for individual-level prediction. Given the group-level association between NAc volume and Y-BOCS follow-up score, it is possible that future studies with larger sample sizes may be able to find a structural MRI biomarker. However, another possibility is that NAc volume differences may be obscured by variation in OCD subtypes, or that subcortical alterations in OCD may depend on gender (L. Zhang et al., 2019). Development of models that account for these subgroups requires a further increase in sample size.

Given that structural alterations in OCD patients are small, often finding limited effect sizes in large multicenter group studies (Bruin et al., 2020), inclusion of additional

imaging modalities, such as (resting-state) functional and diffusion MRI, could strengthen the predictive value of our models (van Waarde et al., 2015; Zhutovsky et al., 2019). The availability of functional and diffusion MRI scans for our cohort was limited, since most patients were routinely treated and not enrolled into a neuroimaging study. Conversely, structural MRI scans were readily available due to their necessity in surgical planning. Increased use of tractography in surgical planning for DBS for OCD will improve future availability of diffusion MRI scans (Baldermann et al., 2019; Coenen et al., 2017; Liebrand et al., 2019).

5.4.1 Limitations

The most notable limitation to this study is the sample size. Despite being among the largest studies on patients with DBS for psychiatric conditions, our sample was still modest for state-of-the-art machine learning applications. This could have caused our individual-level prediction to be underpowered. In addition, at these sample sizes it is impossible to stratify for differences in disease history, medication use, and OCD subtypes. Given the long timeframe during which this dataset was acquired, the only possibility of rapidly increasing the number of patients would be pooling data from different sites. However, pooling data across centers comes with its own set of challenges, like variation in diagnosis and inclusion criteria per institute, non-uniformity of stimulation targets and parameters across sites, and restrictions on data sharing due to privacy laws. These challenges might explain the lack of large retrospective multicenter studies in DBS for OCD.

Another limitation lies in the naturalistic follow-up for all patients after the first 16 patients. After the initial trial(Denys et al., 2010) DBS was approved for routine care for treatment-refractory OCD. Combined with the long inclusion period, this caused the treatment follow-up and imaging parameters to vary over time. To address this issue, we corrected for scanner/parameter combinations in our analyses. More importantly, after analysis of our clinical trial cohort showed that active contacts were always located in the vALIC (van den Munckhof et al., 2013), the targeting was altered so that the 3 topmost contacts were always placed in the vALIC white matter for new patients. This heterogeneity in targeting strategies potentially confounded our results, although given the large degree of overlap in anatomical positioning of the active contacts in our previous study on a subsample of this dataset (Liebrand et al., 2019) we expect no systematic differences between (non-)responders. The more important relationship between positioning of the electrodes and individual white matter connections is impossible to ascertain without additional diffusion MRI data. Comparisons over such a long timeframe could have been improved by using a fixed protocol. However, it is debatable whether this would have been beneficial for the patients. Patients should be able to benefit from new insights gained with experience.

We attempted to address this limitation by including a covariate indicating the time since first operation into our model which showed that the association remained significant. However, it is important to note that changes in targeting cannot be assumed to vary linearly across patients and such an adjustment cannot circumvent the need for a fixed protocol.

The current study focused on response to DBS within a 12-month follow-up. This time period enables the identification of most responders, though a small minority only starts responding between one to two years after the application of DBS (van Westen et al., 2020). Therefore, future studies could investigate whether the observed associations also applies to patients with a delayed response.

5.5 Conclusions

We performed the – to our knowledge – largest neuroimaging study on patients who received DBS for treatment-refractory OCD. Our results showed that increased left-side NAc volume was associated with a lower 12-month follow-up Y-BOCS score. Caveated by non-significant predictions at the individual-level, group-level associations between NAc volume and DBS treatment outcomes suggest that patients with a larger NAc are better able to benefit from CBT and regain their functioning after receiving DBS. Although individual-level predictions with SVC/SVR were not accurate, the results could provide a stepping stone for future biomarker studies for DBS for OCD. It is our hope that these studies will contribute to improved informing and supporting of patients and clinicians in their decision-making process, which can help optimize the response rate, reduce potential harm or burden to patients, and improve the allocation of resources.

5.6 Supplementary material

Calculation of Scalar Momenta

In addition to the calculation of the grey- and white-matter volumes (GM/WM) as presented in the main manuscript we also investigated scalar momenta a as an additional structural MRI representation for our individual-level classification/regression analyses. The reason for this was a recent benchmarking study which showed that scalar momenta outperformed many of the other VBM types of data representations for multiple datasets and various different clinical and non-clinical tasks (Monté-Rubio et al., 2018). The calculation of the scalar momenta followed the corresponding description provided in the benchmarking paper and included: 1. Use of SPM12's unified segmentation (Ashburner & Friston, 2005) approach to obtain GM, WM and cerebrospinal fluid tissue types for each individual

MRI scan. The segmentation was set up according to the VBM tutorial by John Ashburner (http://www.fil.ion.ucl.ac.uk/~john/misc/VBMclass10.pdf), 2. Normalization of the GM and WM segmentations to MNI space by using the Geodesic Shooting Toolbox (Ashburner & Friston, 2011) for SPM12, utilizing the same group template derived from 555 subjects of the IXI-database (http://brain-development.org/) as provided by the CAT12 toolbox which was also considered for the main analyses, 3. Calculation of scalar momenta using the Geodesic Shooting Toolbox, 4. Spatial smoothing with a 12 mm^3 full-width at half-maximum kernel as it was shown to provide the best performance in the benchmarking study. Scalar momenta are computed by scaling the difference between the template GM/WM segmentations and their corresponding warped individual segmentations with the Jacobian-determinant. They can therefore be seen as Jacobian-scaled residual-errors of the normalization of the individual segmentations. In accordance with (Monté-Rubio et al., 2018) we considered the scalar momenta for GM and WM together in our analyses.

Table 5.S1. Scanning parameters for the different scans. The order of the labels (A/B/C/D/E) correspond to the labels used in the main text and Table 1.

Sequence Label	Vendor & scanner name	Field Strength (T)	Acquisition matrix	Acquisition resolution (mm^3)	Repetition time (ms)	Echo time (ms)	Flip angle (°)
A	Philips Intera	3	256x256	1x1x1	9	4	8
B	Philips Ingenia	3	284x284	0.9x0.9x0.9	9	4	8
C	Siemens Avanto	1.5	256x256	1x1x1	1900	3	15
D	Genesis Signa	1.5	256x256	1x1x1	13	6	20
E	Philips Intera	3	256x256	0.88x0.88x1.2	10	5	8

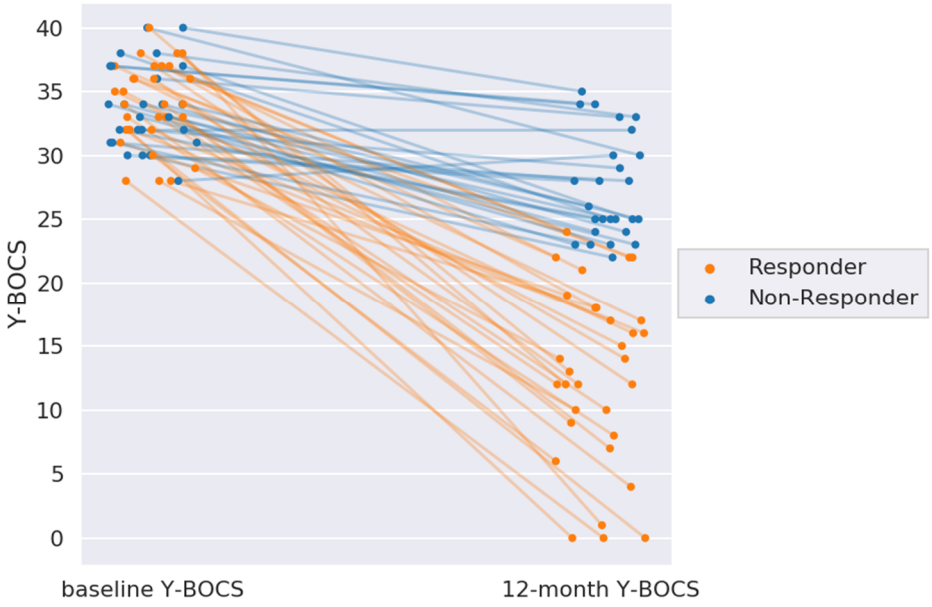

Figure 5.S1: Trajectories of baseline to 12-month follow-up progression of the Yale-Brown obsessive compulsive scale (Y-BOCS) total score for each individual patient included in this study. Each dot represents a patient, color coded for whether the baseline Y-BOCS score decreased by at least 35% from baseline to 12-month follow-up (Responder) or not (Non-Responder). Lines connect data of the same patient.

IV. GENERAL DISCUSSION

Chapter 6

Summary of main findings

In this thesis, we have focused on deep brain stimulation (DBS) treatment of two psychiatric disorders, refractory obsessive-compulsive disorder (OCD) and treatment-resistant depression (TRD). While DBS – due to its nature – cannot be studied separately from neuroimaging and the way the brain interacts with electronic stimulation, quite a few open questions regarding DBS remained that could be potentially answered with neuroimaging. We used advanced acquisition, processing and analysis techniques to evaluate some of the most pressing issues. First, we used tractography to assess how stimulation of certain white matter tracts was related to treatment response. Second, we evaluated advanced diffusion protocols to determine the best way to apply tractography-assisted targeting with the aim of improving stimulation specificity. Finally, we used machine learning to query a multivariate dataset whether we could predict a priori which patients would respond to treatment. This dissertation thus presents applications of advanced techniques to better understand and optimize DBS in psychiatry.

In **chapter 2**, we retrospectively investigated the potential of tractography-assisted targeting in a cohort of twelve patients who received treatment with DBS for OCD. We hypothesized that treatment response depended on the location of the active contacts with respect to individual white matter bundle trajectories. Two tracts within the ventral anterior limb of the internal capsule (vALIC) were visualized with tractography. These tracts were the supero-lateral medial forebrain bundle (slMFB) and the anterior thalamic radiation (ATR). We related the percentage change in OCD symptom severity on the Yale-Brown obsessive-compulsive scale (Y-BOCS) between baseline and one-year follow-up with the distances from the active contacts to the ATR and slMFB. Placement of the active contacts closer to the slMFB than the ATR was associated with better treatment outcome ($p=0.04$; $r^2=0.34$). A comparison in standard space showed that stimulation sites were largely overlapping between treatment (non)responders, suggesting response was independent of the anatomically defined electrode position. These findings suggest that vALIC DBS for OCD may benefit from slMFB-specific implantation and highlight the importance of corticolimbic connections in OCD response to DBS. Prospective investigation remains necessary to validate the clinical use of slMFB targeting.

In **chapter 3**, we used tractography to retrospectively study whether DBS treatment response was related to the placement of the electrodes with respect to white matter

tracts as presented in chapter 2. However, here we investigated a cohort of TRD patients. To this end, we reconstructed the slMFB and the ATR with tractography to determine their distance to the active DBS contacts in fourteen patients who participated in our randomized clinical trial. We associated these distances with the change in depressive symptoms measured with Hamilton's depression rating scale (HAM-D) between baseline and 1-year follow-up as a measure of treatment response. Stimulation closer to both tracts was significantly correlated to a larger symptom decrease ($p=0.02$, $r=0.61$), suggesting that stimulation more proximal to the tracts was beneficial. Biophysical modelling indicated that 38% of tracts were even outside the volume of activated tissue. There was no difference in lead placement with respect to anatomical landmarks, which could mean that differences in treatment response were driven by individual differences in white matter anatomy. Our results suggested that deep brain stimulation of the ventral anterior limb of the internal capsule could benefit from targeting white matter bundles. We recommend acquiring diffusion magnetic resonance data for each individual patient to account for individual variations and to allow for further studies.

In **chapter 4**, we investigated the diffusion MRI scanning protocol and the potential gain of improving the resolution for application in DBS surgical planning. Given the restricted total scanning time for clinical neuroimaging, it was unclear whether clinical diffusion MRI protocols would benefit more from higher spatial resolution or higher angular resolution – a tradeoff that might even be application-dependent. As we were interested in applying diffusion MRI in DBS of the vALIC, we investigated the relative benefit of improving spatial or angular resolution in diffusion MRI to separate the two parallel running white matter tracts studied in chapters 2 and 3: the ATR and the slMFB. As this was a study to evaluate scanning protocols, we scanned 19 healthy volunteers at 3T and 7T according to three diffusion MRI protocols with respectively standard clinical settings, increased spatial resolution of 1.4 mm, and increased angular resolution (64 additional gradient directions at $b=2200 s/mm^2$). We performed probabilistic tractography for all protocols and quantified the separability of both tracts. The higher spatial resolution protocol improved separability by 41% (as measured by Cohen's *d*) with respect to the clinical standard, presumably due to decreased partial voluming. The higher angular resolution protocol resulted in increased apparent tract volumes and overlap, which is disadvantageous for application in precise treatment planning. We thus recommended to increase the spatial resolution for deep brain stimulation planning within the vALIC while maintaining angular resolution. This recommendation complements the general advice to aim for high angular resolution to resolve crossing fibers, confirming that the specific application and anatomical considerations are leading in clinical diffusion MRI protocol optimization.

Chapter 5 focused on treatment outcome prediction in DBS for OCD. As approximately 60% of patients with OCD respond to DBS, biomarkers that could identify patients who are likely to respond a priori could prove beneficial. For this reason, we investigated the potential of predicting treatment outcome in DBS for OCD on the group- and individual-level using structural MRI of 57 patients. Voxel-based morphometry was used to investigate whether grey matter (GM) or white matter (WM) volume surrounding the DBS electrode (nucleus accumbens (NAc), anterior thalamic radiation), and whole-brain GM/WM volume were associated with OCD severity and response status at 12-month follow-up. In addition, we performed machine learning analyses to predict treatment outcome at an individual-level and evaluated its performance using cross-validation. We found that a larger preoperative left NAc volume was associated with lower OCD severity at 12-month follow-up ($p_{FWE} < 0.05$). None of the individual-level regression/classification analyses exceeded chance-level performance. These results provided evidence that patients with larger NAc volumes show a better response to DBS, indicating that DBS success is partly determined by individual differences in brain anatomy. However, the results also indicate that structural MRI data alone does not provide sufficient information to guide clinical decision making at an individual level yet.

Chapter 7

General Discussion

There were two main objectives within this dissertation. The first was centred around the optimisation of DBS targeting with tractography in order to optimise targeting strategies and treatment outcomes, which also included optimising the tractography for this application. The second objective of this dissertation was treatment outcome prediction, in order to better select patients who may respond to treatment. In this chapter, I will position our work towards current developments in the field and identify themes for future research.

7.1 Tractography for DBS

Since the start of this project at the end of 2015, interest in tractography for DBS in psychiatry has drastically increased, going from a handful of papers each year prior to 2015 to 15-20 per year now. Advances in our understanding of the human connectome and imaging methods – spearheaded by the human connectome project (HCP) – have motivated many clinical studies looking into the role of connectivity. In the context of DBS, tractography studies have led to refinement of existing targets (e.g., (Riva-Posse et al., 2018)) and even to use of new ones (Schlaepfer et al., 2013). Nowadays, it is no longer uncommon to use tractography to guide DBS surgeries. However, at the beginning of this project, anatomical landmark based targeting was still the default in DBS for psychiatry.

The main finding of our clinical tractography studies was that the distance of specific tracts within the white matter to the active DBS contacts significantly correlated to treatment outcome – something which is almost universally accepted now. For OCD, our analysis indicated a benefit of stimulating closer to the slMFB than the ATR, whereas for TRD a smaller average distance to both tracts was related to better outcomes. Although a relationship between white matter tracts and treatment outcome was already suspected (e.g., Coenen et al. (2011)) our findings provided some of the first direct evidence that individual white matter connectivity was related to treatment outcomes in DBS for psychiatry. This also meant that treatment response partly depends on anatomical variation within the white matter, since the targeting based on anatomical landmarks ensured that the active contacts were consistently placed within the vALIC across patients (van den Munckhof et al., 2013).

Naturally, our findings raised some additional questions, and, owing to the small sample and retrospective nature of our studies, were in need of validation. There was

also immediate clinical interest, as the first question that came up was: “Can we use these results in the clinic?” This was unsurprising, given that not many treatment options are left for this otherwise intractable patient population. Our results seemed especially applicable considering they indicated that treatment response was related to proximal stimulation of a particular tract, the slMFB.

7.1.1 The slMFB as target for DBS

The working mechanisms of vALIC DBS may be different between OCD and TRD. Even so, parallels between the two disorders can be seen clinically. It has been observed that most OCD patients experience a rapid, almost immediate, improvement of mood and anxiety when switching on the DBS device for the first time (de Koning et al., 2016). This effect precedes a measurable change in OCD symptoms, with improvement in obsessions within weeks and improvement of compulsions often only after combination with CBT (Mantione et al., 2014). A rapid improvement of mood has also been observed in TRD patients for whom the device is switched on (Bergfeld et al., 2016) – at least when both patient groups were implanted in the vALIC, as was the case in our hospital. Such parallels strengthen the idea that the same slMFB might be responsible for treatment response in both patients groups, on top of our largely overlapping findings.

Despite the controversy around the slMFB’s definition and nomenclature (Haber et al., 2021; Haynes & Haber, 2013), it seemed to be a promising DBS target for OCD and TRD. Another group started prospectively targeting the slMFB first for TRD, and later also piloted slMFB targeted stimulation for OCD (Meyer et al., 2022). They achieved some encouraging results, caveated by the small sample sizes and the open-label nature of the initial studies. Here, it has to be noted that the electrodes were implanted much closer to the VTA instead of within the vALIC. It is not yet clear whether stimulation close to the slMFB yields the same effects when implanted near the VTA or in the vALIC, since co-stimulation of other local tissues has to be taken into account. Co-stimulation of unwanted long-range white matter tracts when targeting the slMFB near the VTA seems to be limited (Döbrössy et al., 2021). On the other hand, the ALIC is known to contain multiple connections between different parts of the prefrontal/orbitofrontal cortices (PFC/OFC) which may get co-stimulated. Care has to be taken when aggregating stimulation results for different DBS targets, even when they are the same white matter tract being stimulated at a different location.

As our retrospective results were encouraging, our hospital started tractography-assisted DBS targeting of the slMFB in the vALIC for OCD already in late 2017. The aim was to put the middle two (out of four) contacts of the electrode as close to the slMFB as possible within the vALIC, largely keeping the same approach as before.

For this reason, it could be considered not a change of target, but a target refinement. The main difference is that the tip of the electrode was not always put into the nucleus accumbens anymore, as the slMFB was often too dorsally located compared to it. Incorporation of prospective targeting was done open-label, for a number of reasons. First of all, we did not consider a controlled trial feasible. As can be seen from our first study, landmark based targeting in the vALIC is already likely to cause the electrodes to be placed advantageously with respect to the slMFB in some patients. However, there would be no way of knowing whether the electrodes were placed close to the slMFB in conventional targeting, which would obfuscate our results.

Comparing conventional targeting to tractography-assisted targeting would potentially require large sample sizes to measure any statistically significant effect, especially when considering that the average response rate of landmark based targeting is already about 50-60% (Alonso et al., 2015; Dandekar et al., 2018). Considering our regular inclusion rates, a controlled trial could have taken years to perform. Moreover, explicitly targeting away from the slMFB would not provide a fair comparison, and would potentially cause burden to the patient. We thus chose to prospectively target open-label, and evaluate treatment results with respect to the cohort that was implanted based on anatomical landmarks. Some of our initial findings are detailed in section 7.3.

7.1.2 Tractography approaches for DBS research

The suspected clinical importance of white matter tracts in DBS has increased interest in tractography studies since the start of this project. At the same time, tractography software toolboxes have become more readily available, in addition to toolboxes dedicated to DBS lead placement. With some DBS toolboxes even offering a joint pipeline for lead detection and tractography analysis, it may be unsurprising that the number of studies using tractography in DBS analysis has grown. In this section, different analysis approaches for tractography in DBS will be discussed, after which our approach will be related to others.

The main differences between DBS tractography studies lie in three aspects. These are **I)** the use of individual versus template data; **II)** whether tractography is used to either reconstruct specific bundles or seed from the VATs; and **III)** whether studies relate outcome to lead placement (distances) or estimations of stimulation. While these are fundamental choices in setting up a tractography study for DBS, the benefits and limitations are often not mentioned in the literature. Therefore, I will briefly discuss them below.

I) DBS studies often use a tractography template or to identify white matter connections if dMRI data of individual patients is not available (Baldermann et al., 2019, 2021; Li et al., 2020). In most cases, anatomical scans (including a postoperative scan for electrode locations) of individual patients are registered to a template space, where the electrode locations can be compared to the streamlines of the template. The obvious main benefit of using a template is that individual dMRI data is not required. A secondary benefit is the increased resolution at which the connectivity is represented, which could potentially help elucidating small differences in lead placement. However, use of such a template limits interpretability of the results in the following ways. Some of these critiques have been published by (Coenen, Schlaepfer, et al., 2019).

First of all, these templates are often made from scans of healthy subjects – we do not know for certain whether they are representative of psychiatric patients requiring DBS. Evidence from a number of studies comparing WM in healthy controls to psychiatric patients suggests that there may be differences – see (Koshiyama et al., 2020) for an overview of related findings from the ENIGMA consortium. Second, tractography templates are often available for download just as they were generated – meaning the results were not pruned for false-positives, although research has shown that unaltered tractograms can contain many false-positives (see, e.g., (Maier-Hein et al., 2016)). Conversely, research has shown that tractograms can be highly anatomically accurate when enough prior knowledge is incorporated (Schilling et al., 2020).

Perhaps the most fundamental issue with the use of templates is that it does not account for the large degree of individual variation in white matter tracts, as we encountered in the vALIC (Liebrand et al., 2019, 2020). When using templates, the only variables between patients are the positions of the electrodes and registration errors. Hence, it is virtually impossible to disentangle differences in connectivity to distal areas from differences in electrode positioning. The main recommendation to overcome these problems and to validate findings is to acquire dMRI data suitable for tractography in all DBS patients.

II) The choices for a certain tractography algorithm, regions of interest, and starting and stopping criteria can have large effects in tractography studies. Two different ways of selecting relevant white matter tracts can be distinguished: reconstructing known tracts by seeding from pre-determined regions of interest (i.e. more hypothesis-driven), or seeding from the active contacts / volume of activated tissue (VAT) (i.e. more data-driven). By using pre-determined ROIs, it is more likely that the reconstructed tracts will be anatomically correct, and final results will be influenced less by spurious tracts (e.g. (Maier-Hein et al., 2016; Schilling et al., 2020)). However,

this does limit the research to the tracts that were identified a priori, potentially missing out on other relevant white matter connections that were not included into the analysis.

The more data-driven approach of seeding from the locations of the electrodes or selecting only those streamlines that pass through a VAT from a tractogram is less prone to missing out on potentially relevant tracts. However, the major drawback is that the streamlines being selected in this way are often not checked for anatomical validity, which could potentially lead to spurious results. Spurious results can be somewhat avoided by thresholding based on the total number of streamlines, although even this approach is somewhat limited, as the number of streamlines between two regions does not necessarily correlate with the likelihood of being connected (Jones, 2010). Tractography experts usually recommend using as much prior anatomical knowledge as possible to overcome these kind of limitations (Jeurissen et al., 2019; Schilling et al., 2020).

III) One of the most important choices a DBS researcher faces when performing a tractography study is whether to evaluate lead positioning or stimulation-modulated connectivity – both have their merits. In this work we used distances between active contacts and tracts. The main advantage of this approach is the interpretability: finding an association between stimulating closer to a specific tract is directly translatable to clinical practice, as one has to only aim for the specific tract. The alternative approach models activation from the stimulation site to distal regions as explanation for response, potentially providing more insight into why the treatment works at the cost of clinical utility. When comparing distances it is important to take into account the stimulation parameters, since the distance at which the stimulation affects tissue is dependent on the chosen parameters (Hartmann et al., 2016; Miocinovic et al., 2009). However, the distance of contact-to-tract does not matter beyond the effective range of stimulation: the tract is simply not being stimulated. We encountered this in our study into patients with TRD in Chapter 3.

At the beginning of this project, tractography studies for DBS in psychiatry were still sparse. Diffusion-weighted MRI data was not used in clinical planning and consequently not routinely acquired. Fortunately, we were able to use individually acquired datasets to capture variability between patients. Distances between active contacts and relevant tracts were calculated, to be most directly translatable into a clinical target. We reconstructed known tracts to avoid potential false positives; these tracts were the slMFB and ATR, since they were already hypothesized to play a role in DBS treatment response (Coenen et al., 2012). Interestingly, as already alluded to in the introduction, it is exactly the anatomical validity of the slMFB that has come under debate. Nevertheless, our studies did provide evidence of the clinical relevance

of this tract, showing the importance of reaching consensus regarding the anatomical definition.

7.1.3. Improving tractography for DBS

From the results of ourselves and others it became clear that small variations in stimulation location may affect treatment results. As the placement of the leads with a stereotactic frame is already very precise the main route for improving targeting specificity lies in imaging (Mathiopoulou et al., 2022). With the spatial resolution of the structural scans being higher than dMRI, and dMRI directly providing information about the target structures, we hypothesized that optimizing the diffusion MRI acquisition for resolution may be beneficial for targeting tracts in the vALIC.

We investigated the potential gain of increasing either the angular or spatial resolution for tractography-assisted DBS planning for this reason. The results showed a relative benefit of increasing spatial compared to angular resolution for discerning the slMFB and ATR in the vALIC. Here, it has to be noted that the optimal imaging parameters may be different for each DBS target. For our target within the vALIC, which contains multiple tracts running roughly in parallel, the demands may be different than for targets with more crossing fibers, for example.

In our study, the high spatial resolution scans were acquired at 7T. Availability of these ultra-high field scanners is still limited, but growing. Fortunately, it is possible to acquire similar or even higher spatial resolution dMRI data compared to the data in our study at 3T. An example image that was acquired with a voxel size of 1.28 mm isotropic is shown below in Figure 7.1.

The image shown above was acquired at a much higher resolution than the current clinical standard. Such high-resolution scans may provide additional detail, which may potentially lead to improved targeting accuracy, at the cost of acquisition time. Acquisition of high spatial resolution scans for individual patients brings the level of detail closer to that of tractographic templates, while preserving individual features. However, acquisition and processing of these high-resolution data is more challenging and will require additional steps before entering the clinical workflow.

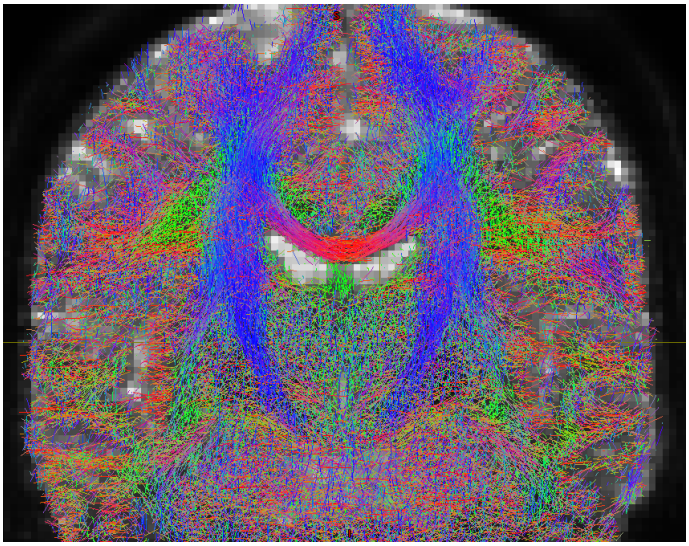

Figure 7.1: Coronal view of tractogram from data acquired at 1.28 mm isotropic spatial resolution at 3T. For more details on these data, see (Keuken et al., 2022).

7.1.4 Tractography in the clinical workflow

Conventionally, DBS leads are placed following a standard stereotactic procedure (van den Munckhof et al., 2013). In this procedure, specialized software is used to define the brain target in stereotactic coordinates which enables precise placement of the DBS leads. Usually, brain scans with different contrasts can be coregistered in order to obtain as much anatomical detail on the target structures and lead trajectory as possible. Developments in the DBS field (both in psychiatry and movement disorders) caused manufacturers of DBS planning software suites to incorporate tractography in their toolboxes.

The software suite currently used in our hospital allows for deterministic tractography based on the DTI model. This model allows visualization of the slMFB and ATR, which are used to update the targeting. Due to the largely parallel orientation of the white matter in the vALIC (Safadi et al., 2018), these tracts are presumably less limited by the DTI model's inability to account for crossing fibers. Visualization of tracts for surgical planning requires some additional time of the neurosurgeons. Typically, this is not a problem as the surgical planning is made prior to the day of surgery.

It is often not possible for users to change the inner workings of the software suite, in order to prevent incorrect usage that could be dangerous to the patient. This essentially

turns it into a black box. To use tractography within the stereotactic DBS planning environment, neurosurgeons have to rely on the software provided by the manufacturer. Regulations require commercially available planning software to have CE marking, which is costly and time-consuming to acquire. For this reason, clinical implementation of new features, such as crossing fiber models, or tools for denoising and distortion correction for high-resolution data, can take a long time. There is an exception for software developed and maintained within the hospital. Still, collaborations between researchers and manufacturers will provide the largest benefit to the DBS community (Mathiopoulou et al., 2022).

7.2 Neuroimaging for individual outcome prediction

The first part of this thesis is focused on optimizing DBS treatment outcome through tractography-assisted targeting. Another way to potentially improve treatment outcome is by selecting only those patients likely to respond to treatment. Finding a neuroimaging biomarker was the second objective of this thesis, since pre-DBS clinical symptoms cannot be used to predict outcome (Graat et al., 2021). A reliable biomarker could not only help clinicians and patients in their decision-making, but could also help to make the decision-making process more transparent and objective.

For the reasons outlined above, we have investigated the potential of structural MRI as a biomarker for DBS response in OCD patients in what is one of the largest single site imaging studies on DBS in psychiatry (**Chapter 5**). Although we did find a group-level association, we did not find a biomarker suitable for predicting outcome in individual patients. Group level associations are not suitable for predicting response on the individual level, which would be required to aid in clinical decision making. To increase our odds of finding a suitable biomarker in the future, two aspects of the dataset could potentially be enhanced: first, the group size could be increased to improve training of our machine learning models, and second, different (imaging) modalities could be combined.

In general, larger datasets allow machine learning to fit models with an increased number of parameters, and could prevent overfitting. Unfortunately, data sizes in psychiatric DBS studies are fairly modest. One of the ways to increase group sizes for outcome prediction studies is to pool data from different hospitals. Sharing data, however, comes with its own difficulties: other than strict privacy regulations, the inclusion criteria may vary between hospitals; the treatment procedure, including the DBS target, is variable; and even the data might be collected in a different manner. In other words, the data might become more heterogeneous, which is detrimental to the predictive capability of machine learning models.

In order to facilitate larger studies with more homogeneous data, which could hopefully provide more conclusive evidence, research groups should try to homogenize data acquisition and streamline (anonymous) data sharing. Moreover, combination of results from patients stimulated at different DBS targets should be further explored, despite the challenges. For example, it is useful to know whether a successful biomarker of vALIC DBS for OCD will generalize to predicting treatment response in STN DBS for OCD.

Another way to potentially improve our models is by incorporating multiple MRI sequences. In our study, we considered structural images only, which allowed us to include most of our patients. However, in studies of other psychiatric populations, structural imaging was generally less predictive than other sequences such as (resting-state) functional MRI or diffusion-weighted MRI (van Waarde et al., 2015; Zhutovsky et al., 2019). These types of data are less routinely collected, leading to smaller overall datasets, thus providing another argument for multi-center collaborations. Of course, this would only be beneficial if data of multiple imaging sequences would be routinely collected.

A fundamental limitation in predicting treatment outcomes in DBS lies in the experimental nature of DBS, which causes treatment strategies to evolve over time. In theory, every change that occurs in how patients are selected or how treatment is provided could lead to a different relationship between a potential biomarker and outcomes. Therefore, each time the treatment is altered, a new machine learning model should be trained to account for these changes. This also applies to our own study: since we have updated our targeting strategy to incorporate tractography-assisted planning (see section 7.3), we should collect new data to evaluate whether the relationship between brain structure and treatment outcomes is unaltered. Until DBS treatment is fully optimized, it remains well imaginable that certain patterns in a patient's brain image will be attributed to treatment non-response, whereas in fact that patient was just not receiving optimal treatment.

Finally, we can wonder what constitutes a suitable biomarker, and, what the minimum requirements for clinical use would be. Any patient that satisfies the inclusion criteria is eligible for DBS, as there is currently no way to predict treatment outcome. If the inclusion criteria remain the same, the main purpose of a biomarker would be to identify those patients who are less likely to respond. The minimum required accuracy of such a biomarker depends on the trade-off between decreased patient burden in correctly identified likely non-responders, and increased patient burden for patients who were incorrectly identified as likely non-responder. Since the patient risks of DBS are low, and the potential gain in quality of life is high, clinicians will want a biomarker that minimizes the odds of falsely identifying patients as likely non-

responder. This is compounded by the fact that DBS is already cost-effective (at least for OCD (Ooms et al., 2017)) and that DBS is one of the last treatment options left for this refractory population. Perhaps models that also provide a certainty estimation with their prediction could prove useful, where the prediction could hypothetically only be consulted in cases where the prediction was made with high certainty, for example with Bayesian methods (Logan et al., 2019).

7.3 Are we on the right track?

Sections 7.1 and 7.2 covered developments in respectively tractography and treatment outcome prediction for DBS for OCD and TRD. These provide two (independent) objectives to improved treatment outcomes. As a result of studies of ourselves and others, tractography-assisted targeting is already implemented into clinical routine in our hospital since 2017. On the other hand, machine learning prediction of individual treatment outcome is not ready yet for clinical implementation. In the following, some preliminary observations from tractography-assisted targeting will be presented along with general recommendations.

7.3.1. Initial experience with tractography-assisted DBS

We decided to implement tractography-assisted DBS for OCD in an open-label setting, mostly for the practical considerations mentioned earlier. To evaluate whether we are on the right track, we performed a preliminary analysis of the relative benefit of tractography-assisted targeting compared to landmark-based targeting *(*Graat et al., *in submission)*. For this analysis, we chose 20 patients who were implanted with tractography-assisted targeting and compared them to 20 propensity-score matched controls who received conventional landmark-based targeting in the period before November 2017. Once again, we primarily focused on the 1-year follow-up clinical symptom severity scores (Y-BOCS). Additionally, we also compared stimulation-associated side effects, adverse events and stimulation parameters.

Using Bayesian analysis, we found no statistically significant difference in the course of symptoms of OCD, depression and anxiety during the 1-year follow-up period. We did find weak evidence for an increased responder rate in the tractography-assisted vs. conventionally-targeted group (65% vs. 45%), as expressed by the Bayes factor BF_{10}=1.44 (increased vs. no increased responder rate). This result was likely exaggerated by partial response in the conventionally-targeted DBS group. The number of stimulation adjustments, time to response, stimulation current, or medication usage did not differ between groups. However, we found very strong evidence that tractography-assisted DBS caused fewer adverse effects than

conventionally-targeted DBS (38 vs. 58 transient; and 1 vs. 17 lasting adverse effects; BF_{10}=40.83).

Likely, our results were influenced by a ceiling effect in response to DBS, as even conventionally-targeted DBS is already effective. Our sample size was possibly too modest to be able to detect anything but large differences. An alternative explanation could be that further individualization in targeting is necessary depending on individual symptom profiles. Perhaps co-stimulation of other tracts than the slMFB in relationship to these symptom profiles is key to understanding treatment response. A retrospective tractography study should be performed to validate this assumption. In spite of no significant differences in the course of OCD symptoms, it seems that tractography-assisted targeting is beneficial in the lower reported number of adverse effects. A more thorough investigation with more patients will have to be performed in the future, although for now it appears in the patient's best interest to continue with tractography-assisted targeting for DBS for OCD due to the reduced number of adverse effects.

7.3.2 Which target to use?

Our tractography studies have identified the slMFB as a promising target within the vALIC, which is why we currently use it as a target for OCD. Others are stimulating the slMFB closer to the VTA, as described in (Coenen et al., 2018). This adds another dimension to the question of which target to use, as it is the same underlying white matter tract that is targeted, although in a different anatomical location with different local surrounding areas.

An opportunity to gain experience with stimulation of the slMFB near the VTA came when a new clinical trial on DBS for TRD using the slMFB-VTA started in our hospital in 2020. Initial clinical observations of switching on the DBS device for the first time have been positive, with a rapid and more pronounced immediate effect compared to stimulation in the vALIC. As reported before by Coenen et al. (2017), stimulation of the slMFB-VTA appears to require lower stimulation currents, although the number of subjects is still too low for a formal comparison. If patient response would otherwise be identical for both targets, it could prove that this target is preferable over our current target of the slMFB in the vALIC because of battery longevity. However, it is too early to evaluate this and the clinical efficacy of stimulating the slMFB-VTA from the new trial.

The decision to choose the slMFB as target, or to switch another target has to be carefully weighed based on available literature and clinical experience. As mentioned before, it is difficult to compare the efficacy of two effective DBS targets. With open-

label tractography-assisted targeting studies reporting similarly good results across targets (Coenen et al., 2018; Meyer et al., 2022; Riva-Posse et al., 2018), the decision may come down to clinical preference. For this reason, the slMFB will likely remain the target within our hospital.

7.3.3 DBS imaging in the future

Neuroimaging has had a large role in DBS with surgical planning based on anatomical landmarks, and it seems that over the course of this project the role of neuroimaging has increased as tractography-assisted surgical planning became the norm. This does not mean that the role of neuroimaging in DBS has crystallized. If anything, the role of neuroimaging is set to increase while the search for a biomarker continues. In the following section, I will discuss some potential future directions of the DBS field regarding neuroimaging.

Diffusion MRI research has suggested that targeting specific white matter structures could lead to improved treatment outcomes. Most groups will therefore use tractography-assisted targeting. It is hard to pinpoint a unified target for the specific disorders, considering that most of the studies have looked at white matter surrounding different stimulation target structures. Reassuringly, some overlap exists between study outcomes. For example, part of the tractogram positively associated with treatment response in (Baldermann et al., 2019) looked very similar to the slMFB in our studies (Liebrand et al., 2019, 2020). However, such evidence is likely not enough to reach consensus on using the same tract target within a disorder. The highest level of clinical evidence comes from randomized controlled trials (RCTs). In an ideal situation, the debate on which DBS target is superior would be settled through an RCT comparing different targets. However, there are many practical considerations (e.g., differences in patient populations, and small differences in target efficacies) that could make such an RCT impractical, if not impossible to carry out. Therefore, I expect that until one target is clearly established as superior to the others, multiple established and proven tract targets will be used.

Maybe asking which target is superior is not even the right question. Perhaps further individualization of tractography-assisted targeting is necessary to obtain the best results, as focusing on one particular bundle might not be the best for every patient. For example, it is conceivable that different subtypes of OCD require stimulation at different targets, reaching treatment response in different ways. In that case the question becomes: ‘Which target is the best for this patient? And how do we find out?’ In this regard, one study is worth noting, comparing two stimulation locations with two sets of electrodes in six OCD patients (Tyagi et al., 2019). Their findings support the idea that stimulation using different targets may lead to alleviation of OCD

symptoms in different ways, even within patients. With large-scale studies with multiple sets of electrodes being out of reach, perhaps neuroimaging and data on treatment response across different targets can be pooled to train a machine learning model that can determine which target is optimal for each patient instead. Such a model could then also be used to advice on which target to use prior to treatment, based on a combination of clinical symptoms and neuroimaging.

Knowing what works in DBS does not always explain how or why. Here, clinical DBS research may benefit from preclinical and basic research. Examples for which preclinical research might be indispensable include anatomical validation of tracts reconstructed with neuroimaging (Jbabdi et al., 2013), invasive stimulation experiments (Pinhal et al., 2018), and combination of both imaging and stimulation (Klink et al., 2021) to identify the relevant tracts and understand stimulation. Translating preclinical knowledge to humans can be done if we understand similarities in structure and function across species (Keuken et al., 2021). In the end, our understanding of DBS is crucial even if machine learning could accurately select patients and optimal targets, as it is doubtful that clinicians base their treatment decisions on a machine learning model alone.

When envisioning models capable of accurately predicting the optimal target and stimulation settings for each patient, we could look beyond a static solution of unaltered stimulation settings. A dynamic system, where stimulation would be based on neuronal signatures detected by and autonomously responded to by the DBS device has long been considered the holy grail by the DBS community. Known as closed-loop DBS, such a system would require combining our knowledge in order to understand which information is relevant to the state of the patient. As every patient is different, each device needs to be specifically tuned to each patient. Possibly, patients themselves can teach the DBS device to recognize the neuronal patterns associated with symptom changes by providing feedback. A recent study that claimed successful application of a rudimentary form of closed-loop stimulation by switching the stimulation on or off when required has generated wide interest (Scangos et al., 2021). While this effort may encourage further efforts on the topic of closed-loop stimulation, it does not carry much weight as it is only describing a single patient. Large-scale application of closed-loop DBS may be some time away.

New options in terms of image acquisition, image reconstruction, and data processing are continuously becoming available. Compared to a decade ago, acceleration techniques such as multiband (also known as simultaneous multi-slice) imaging and variable density undersampling acquisitions with compressed sensing reconstructions have become much more common. The time gain could be reinvested in higher resolution acquisitions, acquisition of different (functional or diffusion) sequences, or

even quantitative MRI. At this moment, such advanced acquisitions are not used clinically. It is impossible to know the potential benefit of newer acquisitions without gathering data and training models, and many unforeseen neuroimaging applications for DBS may present themselves.

Taken together, many challenges in the field of DBS imaging still lie ahead. Routinely collecting and sharing data where possible will be important to overcome them.

V. REFERENCES

References

Ahmari, S. E., Spellman, T., Douglass, N. L., Kheirbek, M. A., Simpson, H. B., Deisseroth, K., Gordon, J. A., & Hen, R. (2013). Repeated Cortico-Striatal Stimulation Generates Persistent OCD-Like Behavior. *Science*, *340*(6137), 1234–1239. https://doi.org/10.1126/science.1234733

Alberton, B. A. V., Nichols, T. E., Gamba, H. R., & Winkler, A. M. (2020). Multiple testing correction over contrasts for brain imaging. *NeuroImage*, 116760. https://doi.org/10.1016/j.neuroimage.2020.116760

Alonso, P., Cuadras, D., Gabriëls, L., Denys, D., Goodman, W., Greenberg, B. D., Jimenez-Ponce, F., Kuhn, J., Lenartz, D., Mallet, L., Nuttin, B., Real, E., Segalas, C., Schuurman, R., du Montcel, S. T., Menchon, J. M., Tezenas du Montcel, S., & Menchon, J. M. (2015). Deep Brain Stimulation for Obsessive-Compulsive Disorder: A Meta-Analysis of Treatment Outcome and Predictors of Response. *PLOS ONE*, *10*(7), e0133591. https://doi.org/10.1371/journal.pone.0133591

Altman, D. G., & Royston, P. (2006). The cost of dichotomising continuous variables. *BMJ*, *332*(7549), 1080.1. https://doi.org/10.1136/bmj.332.7549.1080

American Psychiatric Association. (2000). *Diagnostic and Statistical Manual of Mental Disorders* (4th ed. Te). American Psychiatric Association. https://doi.org/10.1176/appi.books.9780890423349

Andersson, J. L. R., Graham, M. S., Zsoldos, E., & Sotiropoulos, S. N. (2016). Incorporating outlier detection and replacement into a non-parametric framework for movement and distortion correction of diffusion MR images. *NeuroImage*, *141*, 556–572. https://doi.org/10.1016/j.neuroimage.2016.06.058

Andersson, J. L. R., & Sotiropoulos, S. N. (2015). An integrated approach to correction for off-resonance effects and subject movement in diffusion MR imaging. *NeuroImage*, *125*, 1063–1078. https://doi.org/10.1016/j.neuroimage.2015.10.019

Ashburner, J., & Friston, K. J. (2005). Unified segmentation. *NeuroImage*, *26*(3), 839–851. https://doi.org/https://doi.org/10.1016/j.neuroimage.2005.02.018

Ashburner, J., & Friston, K. J. (2011). Diffeomorphic registration using geodesic shooting and Gauss–Newton optimisation. *NeuroImage*, *55*(3), 954–967. https://doi.org/10.1016/j.neuroimage.2010.12.049

Ashburner, J., & Klöppel, S. (2011). Multivariate models of inter-subject anatomical variability. *NeuroImage*, *56*(2), 422–439. https://doi.org/10.1016/j.neuroimage.2010.03.059

Avants, B. B., Epstein, C. L., Grossman, M., & Gee, J. C. (2008). Symmetric diffeomorphic image registration with cross-correlation: Evaluating automated labeling of elderly and neurodegenerative brain. *Medical Image Analysis*, *12*(1), 26–41. https://doi.org/10.1016/j.media.2007.06.004

Bahramisharif, A., Mazaheri, A., Levar, N., Richard Schuurman, P., Figee, M., & Denys, D. (2016). Deep Brain Stimulation Diminishes Cross-Frequency Coupling in Obsessive-Compulsive Disorder. *Biological Psychiatry*, *80*(7), e57–e58. https://doi.org/10.1016/j.biopsych.2015.05.021

Baldermann, J. C., Melzer, C., Zapf, A., Kohl, S., Timmermann, L., Tittgemeyer, M., Huys, D., Visser-Vandewalle, V., Kühn, A. A., Horn, A., & Kuhn, J. (2019). Connectivity Profile Predictive of Effective Deep Brain Stimulation in Obsessive-Compulsive Disorder. *Biological Psychiatry*, *85*(9), 735–743. https://doi.org/10.1016/j.biopsych.2018.12.019

Baldermann, J. C., Schüller, T., Kohl, S., Voon, V., Li, N., Hollunder, B., Figee, M., Haber, S. N., Sheth, S. A., Mosley, P. E., Huys, D., Johnson, K. A., Butson, C., Ackermans, L., Bouwens van der Vlis, T., Leentjens, A. F. G., Barbe, M., Visser-Vandewalle, V., Kuhn, J., … Horn, A. (2021). Connectomic Deep Brain Stimulation for Obsessive-Compulsive Disorder. *Biological Psychiatry*, *90*(10), 678–688. https://doi.org/10.1016/j.biopsych.2021.07.010

Basser, P. J., Pajevic, S., Pierpaoli, C., Duda, J., & Aldroubi, A. (2000). In vivo fiber tractography using DT-MRI data. *Magnetic Resonance in Medicine*, *44*(4), 625–632. https://doi.org/10.1002/1522-2594(200010)44:4<625::AID-MRM17>3.0.CO;2-O

Behrens, T. E. J., Berg, H. J., Jbabdi, S., Rushworth, M. F. S., & Woolrich, M. W. (2007). Probabilistic diffusion tractography with multiple fibre orientations: What can we gain? *NeuroImage*, *34*(1), 144–155. https://doi.org/10.1016/j.neuroimage.2006.09.018

Bergfeld, I. O., Mantione, M., Hoogendoorn, M. L. C., Ruhé, H. G., Notten, P., van Laarhoven, J., Visser, I., Figee, M., de Kwaasteniet, B. P., Horst, F., Schene, A. H., van den Munckhof, P., Beute, G., Schuurman, R., & Denys, D. (2016). Deep Brain Stimulation of the Ventral Anterior Limb of the Internal Capsule for Treatment-Resistant Depression. *JAMA Psychiatry*, *73*(5), 456. https://doi.org/10.1001/jamapsychiatry.2016.0152

Bewernick, B. H., Kayser, S., Gippert, S. M., Switala, C., Coenen, V. A., & Schlaepfer, T. E. (2017). Deep brain stimulation to the medial forebrain bundle for depression- long-

term outcomes and a novel data analysis strategy. *Brain Stimulation*, *10*(3), 664–671. https://doi.org/10.1016/j.brs.2017.01.581

Boedhoe, P. S. W., Schmaal, L., Abe, Y., Ameis, S. H., Arnold, P. D., Batistuzzo, M. C., Benedetti, F., Beucke, J. C., Bollettini, I., Bose, A., Brem, S., Calvo, A., Cheng, Y., Cho, K. I. K., Dallaspezia, S., Denys, D., Fitzgerald, K. D., Fouche, J.-P., Giménez, M., … Zhao, Q. (2017). Distinct Subcortical Volume Alterations in Pediatric and Adult OCD: A Worldwide Meta- and Mega-Analysis. *American Journal of Psychiatry*, *174*(1), 60–69. https://doi.org/10.1176/appi.ajp.2016.16020201

Bruin, W. B., Taylor, L., Thomas, R. M., Shock, J. P., Zhutovsky, P., Abe, Y., Alonso, P., Ameis, S. H., Anticevic, A., Arnold, P. D., Assogna, F., Benedetti, F., Beucke, J. C., Boedhoe, P. S. W., Bollettini, I., Bose, A., Brem, S., Brennan, B. P., Buitelaar, J. K., … van Wingen, G. A. (2020). Structural neuroimaging biomarkers for obsessive-compulsive disorder in the ENIGMA-OCD consortium: medication matters. *Translational Psychiatry*, *10*(1), 342. https://doi.org/10.1038/s41398-020-01013-y

Burkhouse, K. L., Jimmy, J., Defelice, N., Klumpp, H., Ajilore, O., Hosseini, B., Fitzgerald, K. D., Monk, C. S., & Phan, K. L. (2020). Nucleus accumbens volume as a predictor of anxiety symptom improvement following CBT and SSRI treatment in two independent samples. *Neuropsychopharmacology*, *45*(3), 561–569. https://doi.org/10.1038/s41386-019-0575-5

Bzdok, D., & Ioannidis, J. P. A. (2019). Exploration, Inference, and Prediction in Neuroscience and Biomedicine. *Trends in Neurosciences*, *42*(4), 251–262. https://doi.org/10.1016/j.tins.2019.02.001

Caan, M. W. A., Khedoe, G., Poot, D., den Dekker, A., Olabarriaga, S., Grimbergen, K., van Vliet, L., & Vos, F. (2010a). Adaptive noise filtering for accurate and precise diffusion estimation in fiber crossings. *Lecture Notes in Computer Science (Including Subseries Lecture Notes in Artificial Intelligence and Lecture Notes in Bioinformatics), 6361 LNCS*(PART 1), 167–174. https://doi.org/10.1007/978-3-642-15705-9_21

Caan, M. W. A., Khedoe, H. G., Poot, D. H. J., den Dekker, A. J., Olabarriaga, S. D., Grimbergen, K. A., van Vliet, L. J., & Vos, F. M. (2010b). Estimation of diffusion properties in crossing fiber bundles. *IEEE Transactions on Medical Imaging*, *29*(8), 1504–1515. https://doi.org/10.1109/TMI.2010.2049577

Calabrese, E. (2016). Diffusion tractography in deep brain stimulation surgery: A review. *Frontiers in Neuroanatomy*, *10*(MAY), 1–11. https://doi.org/10.3389/fnana.2016.00045

Calabrese, E., Badea, A., Coe, C. L., Lubach, G. R., Styner, M. A., & Johnson, G. A. (2014). Investigating the tradeoffs between spatial resolution and diffusion sampling for brain

mapping with diffusion tractography: Time well spent? *Human Brain Mapping*, *35*(11), 5667–5685. https://doi.org/10.1002/hbm.22578

Coenen, V. A., Bewernick, B. H., Kayser, S., Kilian, H., Boström, J., Greschus, S., Hurlemann, R., Klein, M. E., Spanier, S., Sajonz, B., Urbach, H., & Schlaepfer, T. E. (2019). Superolateral medial forebrain bundle deep brain stimulation in major depression: a gateway trial. *Neuropsychopharmacology*, *44*(7), 1224–1232. https://doi.org/10.1038/s41386-019-0369-9

Coenen, V. A., Döbrössy, M. D., Teo, S. J., Wessolleck, J., Sajonz, B. E. A., Reinacher, P. C., Thierauf-Emberger, A., Spittau, B., Leupold, J., von Elverfeldt, D., Schlaepfer, T. E., & Reisert, M. (2022). Diverging prefrontal cortex fiber connection routes to the subthalamic nucleus and the mesencephalic ventral tegmentum investigated with long range (normative) and short range (ex-vivo high resolution) 7T DTI. *Brain Structure and Function*, *227*(1), 23–47. https://doi.org/10.1007/s00429-021-02373-x

Coenen, V. A., Panksepp, J., Hurwitz, T. A., Urbach, H., & Mädler, B. (2012). Human Medial Forebrain Bundle (MFB) and Anterior Thalamic Radiation (ATR): Imaging of Two Major Subcortical Pathways and the Dynamic Balance of Opposite Affects in Understanding Depression. *The Journal of Neuropsychiatry and Clinical Neurosciences*, *24*(2), 223–236. https://doi.org/10.1176/appi.neuropsych.11080180

Coenen, V. A., Sajonz, B., Prokop, T., Reisert, M., Piroth, T., Urbach, H., Jenkner, C., & Reinacher, P. C. (2020). The dentato-rubro-thalamic tract as the potential common deep brain stimulation target for tremor of various origin: an observational case series. *Acta Neurochirurgica*, *162*(5), 1053–1066. https://doi.org/10.1007/s00701-020-04248-2

Coenen, V. A., Sajonz, B., Reisert, M., Bostroem, J., Bewernick, B., Urbach, H., Jenkner, C., Reinacher, P. C., Schlaepfer, T. E., & Mädler, B. (2018). Tractography-assisted deep brain stimulation of the superolateral branch of the medial forebrain bundle (slMFB DBS) in major depression. *NeuroImage: Clinical*, *20*(June), 580–593. https://doi.org/10.1016/j.nicl.2018.08.020

Coenen, V. A., Schlaepfer, T. E., Goll, P., Reinacher, P. C., Voderholzer, U., Tebartz Van Elst, L., Urbach, H., & Freyer, T. (2017). The medial forebrain bundle as a target for deep brain stimulation for obsessive-compulsive disorder. *CNS Spectrums*, *22*(3), 282–289. https://doi.org/10.1017/S1092852916000286

Coenen, V. A., Schlaepfer, T. E., Maedler, B., & Panksepp, J. (2011). Cross-species affective functions of the medial forebrain bundle—Implications for the treatment of affective pain and depression in humans. *Neuroscience & Biobehavioral Reviews*, *35*(9), 1971–1981. https://doi.org/10.1016/j.neubiorev.2010.12.009

Coenen, V. A., Schlaepfer, T. E., Sajonz, B., Döbrössy, M., Kaller, C. P., Urbach, H., & Reisert, M. (2020). Tractographic description of major subcortical projection pathways passing the anterior limb of the internal capsule. Corticopetal organization of networks relevant for psychiatric disorders. *NeuroImage: Clinical*, *25*(October 2019), 102165. https://doi.org/10.1016/j.nicl.2020.102165

Coenen, V. A., Schlaepfer, T. E., Varkuti, B., Schuurman, P. R., Reinacher, P. C., Voges, J., Zrinzo, L., Blomstedt, P., Fenoy, A. J., & Hariz, M. (2019). Surgical decision making for deep brain stimulation should not be based on aggregated normative data mining. In *Brain Stimulation* (Vol. 12, Issue 6, pp. 1345–1348). Elsevier Inc. https://doi.org/10.1016/j.brs.2019.07.014

Coizet, V., Heilbronner, S. R., Carcenac, C., Mailly, P., Lehman, J. F., Savasta, M., David, O., Deniau, J.-M., Groenewegen, H. J., & Haber, S. N. (2017). Organization of the Anterior Limb of the Internal Capsule in the Rat. *The Journal of Neuroscience*, *37*(10), 2539–2554. https://doi.org/10.1523/JNEUROSCI.3304-16.2017

Corripio, I., Roldán, A., Sarró, S., McKenna, P. J., Alonso-Solís, A., Rabella, M., Díaz, A., Puigdemont, D., Pérez-Solà, V., Álvarez, E., Arévalo, A., Padilla, P. P., Ruiz-Idiago, J. M., Rodríguez, R., Molet, J., Pomarol-Clotet, E., & Portella, M. J. (2020). Deep brain stimulation in treatment resistant schizophrenia: A pilot randomized cross-over clinical trial. *EBioMedicine*, *51*. https://doi.org/10.1016/j.ebiom.2019.11.029

Cortes, C., & Vapnik, V. (1995). Support-vector networks. *Machine Learning*, *20*(3), 273–297. https://doi.org/10.1007/BF00994018

Dandekar, M. P., Fenoy, A. J., Carvalho, A. F., Soares, J. C., & Quevedo, J. (2018). Deep brain stimulation for treatment-resistant depression: An integrative review of preclinical and clinical findings and translational implications. *Molecular Psychiatry*, *23*(5), 1094–1112. https://doi.org/10.1038/mp.2018.2

de Koning, P. P., Figee, M., Endert, E., van den Munckhof, P., Schuurman, P. R., Storosum, J. G., Denys, D., & Fliers, E. (2016). Rapid effects of deep brain stimulation reactivation on symptoms and neuroendocrine parameters in obsessive-compulsive disorder. *Translational Psychiatry*, *6*(1), e722. https://doi.org/10.1038/tp.2015.222

de Koning, P. P., Figee, M., van den Munckhof, P., Schuurman, P. R., & Denys, D. (2011). Current Status of Deep Brain Stimulation for Obsessive-Compulsive Disorder: A Clinical Review of Different Targets. *Current Psychiatry Reports*, *13*(4), 274–282. https://doi.org/10.1007/s11920-011-0200-8

Denys, D., Graat, I., Mocking, R., de Koning, P., Vulink, N., Figee, M., Ooms, P., Mantione, M., van den Munckhof, P., & Schuurman, R. (2020). Efficacy of Deep Brain Stimulation of the Ventral Anterior Limb of the Internal Capsule for Refractory Obsessive-Compulsive

Disorder: A Clinical Cohort of 70 Patients. *American Journal of Psychiatry*, *177*(3), 265–271. https://doi.org/10.1176/appi.ajp.2019.19060656

Denys, D., Mantione, M., Figee, M., van den Munckhof, P., Koerselman, F., Westenberg, H., Bosch, A., & Schuurman, R. (2010). Deep Brain Stimulation of the Nucleus Accumbens for Treatment-Refractory Obsessive-Compulsive Disorder. *Archives of General Psychiatry*, *67*(10), 1061. https://doi.org/10.1001/archgenpsychiatry.2010.122

Diefenbach, G. J., & Tolin, D. F. (2013). The cost of illness associated with stepped care for obsessive-compulsive disorder. *Journal of Obsessive-Compulsive and Related Disorders*, *2*(2), 144–148. https://doi.org/10.1016/j.jocrd.2012.12.005

Döbrössy, M. D., Ramanathan, C., Ashouri Vajari, D., Tong, Y., Schlaepfer, T., & Coenen, V. A. (2021). Neuromodulation in Psychiatric disorders: Experimental and Clinical evidence for reward and motivation network Deep Brain Stimulation: Focus on the medial forebrain bundle. In *European Journal of Neuroscience* (Vol. 53, Issue 1). https://doi.org/10.1111/ejn.14975

Dougherty, D. D., Rezai, A. R., Carpenter, L. L., Howland, R. H., Bhati, M. T., O'Reardon, J. P., Eskandar, E. N., Baltuch, G. H., Machado, A. D., Kondziolka, D., Cusin, C., Evans, K. C., Price, L. H., Jacobs, K., Pandya, M., Denko, T., Tyrka, A. R., Brelje, T., Deckersbach, T., … Malone, D. A. (2015). A Randomized Sham-Controlled Trial of Deep Brain Stimulation of the Ventral Capsule/Ventral Striatum for Chronic Treatment-Resistant Depression. *Biological Psychiatry*, *78*(4), 240–248. https://doi.org/10.1016/j.biopsych.2014.11.023

Drucker, H., Burges, C. J. C., Kaufman, L., Smola, A. J., & Vapnik, V. (1997). Support Vector Regression Machines. In M. C. Mozer, M. I. Jordan, & T. Petsche (Eds.), *Advances in Neural Information Processing Systems 9* (pp. 155–161). MIT Press.

Dunlop, K., Woodside, B., Olmsted, M., Colton, P., Giacobbe, P., & Downar, J. (2016). Reductions in Cortico-Striatal Hyperconnectivity Accompany Successful Treatment of Obsessive-Compulsive Disorder with Dorsomedial Prefrontal rTMS. *Neuropsychopharmacology*, *41*(5), 1395–1403. https://doi.org/10.1038/npp.2015.292

Fenoy, A. J., Schulz, P., Selvaraj, S., Burrows, C., Spiker, D., Cao, B., Zunta-Soares, G., Gajwani, P., Quevedo, J., & Soares, J. (2016). Deep brain stimulation of the medial forebrain bundle: Distinctive responses in resistant depression. *Journal of Affective Disorders*, *203*, 143–151. https://doi.org/10.1016/j.jad.2016.05.064

Figee, M., de Koning, P., Klaassen, S., Vulink, N., Mantione, M., van den Munckhof, P., Schuurman, R., van Wingen, G., van Amelsvoort, T., Booij, J., & Denys, D. (2014). Deep Brain Stimulation Induces Striatal Dopamine Release in Obsessive-Compulsive Disorder. *Biological Psychiatry*, *75*(8), 647–652. https://doi.org/10.1016/j.biopsych.2013.06.021

Figee, M., Luigjes, J., Smolders, R., Valencia-Alfonso, C.-E., van Wingen, G., de Kwaasteniet, B., Mantione, M., Ooms, P., de Koning, P., Vulink, N., Levar, N., Droge, L., van den Munckhof, P., Schuurman, P. R., Nederveen, A., van den Brink, W., Mazaheri, A., Vink, M., & Denys, D. (2013). Deep brain stimulation restores frontostriatal network activity in obsessive-compulsive disorder. *Nature Neuroscience*, *16*(4), 386–387. https://doi.org/10.1038/nn.3344

Figee, M., Vink, M., de Geus, F., Vulink, N., Veltman, D. J., Westenberg, H., & Denys, D. (2011). Dysfunctional Reward Circuitry in Obsessive-Compulsive Disorder. *Biological Psychiatry*, *69*(9), 867–874. https://doi.org/10.1016/j.biopsych.2010.12.003

Gallichan, D. (2018). Diffusion MRI of the human brain at ultra-high field (UHF): A review. *NeuroImage*, *168*, 172–180. https://doi.org/10.1016/j.neuroimage.2017.04.037

Gan, J., Zhong, M., Fan, J., Liu, W., Niu, C., Cai, S., Zou, L., Wang, Y., Wang, Y., Tan, C., Chan, R. C. K., & Zhu, X. (2017). Abnormal white matter structural connectivity in adults with obsessive-compulsive disorder. *Translational Psychiatry*, *7*(3), e1062–e1062. https://doi.org/10.1038/tp.2017.22

Graat, I., Mocking, R. J. T., de Koning, P., Vulink, N., Figee, M., van den Munckhof, P., Schuurman, R., & Denys, D. (2021). Predicting Response to vALIC Deep Brain Stimulation for Refractory Obsessive-Compulsive Disorder. *The Journal of Clinical Psychiatry*, *82*(6), 37759. https://doi.org/10.4088/jcp.20m13754

Greenberg, B. D., Gabriels, L. A., Malone, D. A., Rezai, A. R., Friehs, G. M., Okun, M. S., Shapira, N. A., Foote, K. D., Cosyns, P. R., Kubu, C. S., Malloy, P. F., Salloway, S. P., Giftakis, J. E., Rise, M. T., Machado, A. G., Baker, K. B., Stypulkowski, P. H., Goodman, W. K., Rasmussen, S. A., & Nuttin, B. J. (2010). Deep brain stimulation of the ventral internal capsule/ventral striatum for obsessive-compulsive disorder: worldwide experience. *Molecular Psychiatry*, *15*(1), 64–79. https://doi.org/10.1038/mp.2008.55

Greenberg, B. D., Malone, D. A., Friehs, G. M., Rezai, A. R., Kubu, C. S., Malloy, P. F., Salloway, S. P., Okun, M. S., Goodman, W. K., & Rasmussen, S. A. (2006). Three-year outcomes in deep brain stimulation for highly resistant obsessive-compulsive disorder. *Neuropsychopharmacology*, *31*(11), 2384–2393. https://doi.org/1301165 [pii]\r10.1038/sj.npp.1301165

Günther, V., Ihme, K., Kersting, A., Hoffmann, K.-T., Lobsien, D., & Suslow, T. (2018). Volumetric Associations Between Amygdala, Nucleus Accumbens, and Socially Anxious Tendencies in Healthy Women. *Neuroscience*, *374*, 25–32. https://doi.org/10.1016/j.neuroscience.2018.01.034

Haber, S. N., & McFarland, N. R. (1999). The Concept of the Ventral Striatum in Nonhuman Primates. *Annals of the New York Academy of Sciences*, *877*(1 ADVANCING FRO), 33–48. https://doi.org/10.1111/j.1749-6632.1999.tb09259.x

Haber, S. N., Yendiki, A., & Jbabdi, S. (2021). Four Deep Brain Stimulation Targets for Obsessive-Compulsive Disorder: Are They Different? In *Biological Psychiatry* (Vol. 90, Issue 10, pp. 667–677). Elsevier Inc. https://doi.org/10.1016/j.biopsych.2020.06.031

Hamilton, J. P., Etkin, A., Furman, D. J., Lemus, M. G., Johnson, R. F., & Gotlib, I. H. (2012). Functional neuroimaging of major depressive disorder: A meta-analysis and new integration of baseline activation and neural response data. *American Journal of Psychiatry*, *169*(7), 693–703. https://doi.org/10.1176/appi.ajp.2012.11071105

Hartmann, C. J., Lujan, J. L., Chaturvedi, A., Goodman, W. K., Okun, M. S., McIntyre, C. C., & Haq, I. U. (2016). Tractography activation patterns in dorsolateral prefrontal cortex suggest better clinical responses in OCD DBS. *Frontiers in Neuroscience*, *9*(JAN), 1–10. https://doi.org/10.3389/fnins.2015.00519

Hashimoto, N., Nakaaki, S., Kawaguchi, A., Sato, J., Kasai, H., Nakamae, T., Narumoto, J., Miyata, J., Furukawa, T. A., & Mimura, M. (2014). Brain structural abnormalities in behavior therapy-resistant obsessive-compulsive disorder revealed by voxel-based morphometry. *Neuropsychiatric Disease and Treatment*, *10*, 1987–1996. https://doi.org/10.2147/NDT.S69652

Haynes, W. I. A., & Haber, S. N. (2013). The organization of prefrontal-subthalamic inputs in primates provides an anatomical substrate for both functional specificity and integration: Implications for basal ganglia models and deep brain stimulation. *Journal of Neuroscience*, *33*(11), 4804–4814. https://doi.org/10.1523/JNEUROSCI.4674-12.2013

Heidemann, R. M., Anwander, A., Feiweier, T., Knösche, T. R., & Turner, R. (2012). k-space and q-space: combining ultra-high spatial and angular resolution in diffusion imaging using ZOOPPA at 7 T. *NeuroImage*, *60*(2), 967–978. https://doi.org/10.1016/j.neuroimage.2011.12.081

Holtzheimer, P. E., Husain, M. M., Lisanby, S. H., Taylor, S. F., Whitworth, L. A., McClintock, S., Slavin, K. V., Berman, J., McKhann, G. M., Patil, P. G., Rittberg, B. R., Abosch, A., Pandurangi, A. K., Holloway, K. L., Lam, R. W., Honey, C. R., Neimat, J. S., Henderson, J. M., DeBattista, C., … Mayberg, H. S. (2017). Subcallosal cingulate deep brain stimulation for treatment-resistant depression: a multisite, randomised, sham-controlled trial. *The Lancet Psychiatry*, *4*(11), 839–849. https://doi.org/10.1016/S2215-0366(17)30371-1

Hosp, J. A., Coenen, V. A., Rijntjes, M., Egger, K., Urbach, H., Weiller, C., & Reisert, M. (2019). Ventral tegmental area connections to motor and sensory cortical fields in humans. *Brain Structure and Function*, *0123456789*. https://doi.org/10.1007/s00429-019-01939-0

Howes, O. D., Thase, M. E., & Pillinger, T. (2022). Treatment resistance in psychiatry: state of the art and new directions. In *Molecular Psychiatry* (Vol. 27, Issue 1, pp. 58–72). Springer Nature. https://doi.org/10.1038/s41380-021-01200-3

Jbabdi, S., Lehman, J. F., Haber, S. N., & Behrens, T. E. (2013). Human and Monkey Ventral Prefrontal Fibers Use the Same Organizational Principles to Reach Their Targets: Tracing versus Tractography. *Journal of Neuroscience*, *33*(7), 3190–3201. https://doi.org/10.1523/JNEUROSCI.2457-12.2013

Jenkinson, M., Beckmann, C. F., Behrens, T. E. J., Woolrich, M. W., & Smith, S. M. (2012). FSL. *NeuroImage*, *62*(2), 782–790. https://doi.org/10.1016/j.neuroimage.2011.09.015

Jeurissen, B., Descoteaux, M., Mori, S., & Leemans, A. (2019). Diffusion MRI fiber tractography of the brain. *NMR in Biomedicine*, *32*(4), e3785. https://doi.org/10.1002/nbm.3785

Jeurissen, B., Leemans, A., Tournier, J. D., Jones, D. K., & Sijbers, J. (2013). Investigating the prevalence of complex fiber configurations in white matter tissue with diffusion magnetic resonance imaging. *Human Brain Mapping*, *34*(11), 2747–2766. https://doi.org/10.1002/hbm.22099

Johansen-Berg, H., Gutman, D. A., Behrens, T. E. J., Matthews, P. M., Rushworth, M. F. S., Katz, E., Lozano, A. M., & Mayberg, H. S. (2008). Anatomical connectivity of the subgenual cingulate region targeted with deep brain stimulation for treatment-resistant depression. *Cerebral Cortex*, *18*(6), 1374–1383. https://doi.org/10.1093/cercor/bhm167

Jones, D. K. (2010). Challenges and limitations of quantifying brain connectivity in vivo with diffusion MRI. *Imaging in Medicine*, *2*(3), 341–355. https://doi.org/10.2217/iim.10.21

Jones, D. K., & Cercignani, M. (2010). Twenty-five pitfalls in the analysis of diffusion MRI data. *NMR in Biomedicine*, *23*(7), 803–820. https://doi.org/10.1002/nbm.1543

Jones, D. K., Knösche, T. R., & Turner, R. (2013). White matter integrity, fiber count, and other fallacies: the do's and don'ts of diffusion MRI. *NeuroImage*, *73*, 239–254. https://doi.org/10.1016/j.neuroimage.2012.06.081

Kempton, M. J. (2011). Structural Neuroimaging Studies in Major Depressive Disorder. *Archives of General Psychiatry*, *68*(7), 675. https://doi.org/10.1001/archgenpsychiatry.2011.60

Keuken, M. C., Alkemade, A., Stevenson, N., Innes, R. J., & Forstmann, B. U. (2021). Structure-function similarities in deep brain stimulation targets cross-species. In *Neuroscience and Biobehavioral Reviews* (Vol. 131, pp. 1127–1135). Elsevier Ltd. https://doi.org/10.1016/j.neubiorev.2021.10.029

Keuken, M. C., Liebrand, L. C., Bazin, P.-L., Alkemade, A., van Berendonk, N., Groot, J. M., Isherwood, S. J. S., Kemp, S., Lute, N., Mulder, M. J., Trutti, A. C., Caan, M. W. A., & Forstmann, B. U. (2022). A high-resolution multi-shell 3T diffusion magnetic resonance imaging dataset as part of the Amsterdam Ultra-high field adult lifespan database (AHEAD). *Data in Brief*, *42*, 108086. https://doi.org/10.1016/j.dib.2022.108086

Klink, P. C., Aubry, J. F., Ferrera, V. P., Fox, A. S., Froudist-Walsh, S., Jarraya, B., Konofagou, E. E., Krauzlis, R. J., Messinger, A., Mitchell, A. S., Ortiz-Rios, M., Oya, H., Roberts, A. C., Roe, A. W., Rushworth, M. F. S., Sallet, J., Schmid, M. C., Schroeder, C. E., Tasserie, J., … Petkov, C. I. (2021). Combining brain perturbation and neuroimaging in non-human primates. *NeuroImage*, *235*, 118017. https://doi.org/10.1016/j.neuroimage.2021.118017

Koshiyama, D., Fukunaga, M., Okada, N., Morita, K., Nemoto, K., Usui, K., Yamamori, H., Yasuda, Y., Fujimoto, M., Kudo, N., Azechi, H., Watanabe, Y., Hashimoto, N., Narita, H., Kusumi, I., Ohi, K., Shimada, T., Kataoka, Y., Yamamoto, M., … Hashimoto, R. (2020). White matter microstructural alterations across four major psychiatric disorders: mega-analysis study in 2937 individuals. *Molecular Psychiatry*, *25*(4), 883–895. https://doi.org/10.1038/s41380-019-0553-7

Krack, P., Volkmann, J., Tinkhauser, G., & Deuschl, G. (2019). Deep Brain Stimulation in Movement Disorders: From Experimental Surgery to Evidence-Based Therapy. *Movement Disorders*, *34*(12), 1795–1810. https://doi.org/10.1002/mds.27860

Kühn, S., Schubert, F., & Gallinat, J. (2011). Structural correlates of trait anxiety: Reduced thickness in medial orbitofrontal cortex accompanied by volume increase in nucleus accumbens. *Journal of Affective Disorders*, *134*(1–3), 315–319. https://doi.org/10.1016/j.jad.2011.06.003

Lago, T., Davis, A., Grillon, C., & Ernst, M. (2017). Striatum on the anxiety map: Small detours into adolescence. *Brain Research*, *1654*, 177–184. https://doi.org/10.1016/j.brainres.2016.06.006

Leemans, A., & Jones, D. K. (2009). The B-matrix must be rotated when correcting for subject motion in DTI data. *Magnetic Resonance in Medicine*, *61*(6), 1336–1349. https://doi.org/10.1002/mrm.21890

Lehman, J. F., Greenberg, B. D., McIntyre, C. C., Rasmussen, S. A., & Haber, S. N. (2011). Rules Ventral Prefrontal Cortical Axons Use to Reach Their Targets: Implications for Diffusion Tensor Imaging Tractography and Deep Brain Stimulation for Psychiatric Illness. *Journal of Neuroscience*, *31*(28), 10392–10402. https://doi.org/10.1523/JNEUROSCI.0595-11.2011

Li, J., Cheng, K., Wang, S., Morstatter, F., Trevino, R. P., Tang, J., & Liu, H. (2017). Feature Selection: A Data Perspective. *ACM Comput. Surv.*, *50*(6). https://doi.org/10.1145/3136625

Li, N., Baldermann, J. C., Kibleur, A., Treu, S., Akram, H., Elias, G. J. B., Boutet, A., Lozano, A. M., Al-Fatly, B., Strange, B., Barcia, J. A., Zrinzo, L., Joyce, E., Chabardes, S., Visser-Vandewalle, V., Polosan, M., Kuhn, J., Kühn, A. A., & Horn, A. (2020). A unified connectomic target for deep brain stimulation in obsessive-compulsive disorder. *Nature Communications*, *11*(1). https://doi.org/10.1038/s41467-020-16734-3

Li, Z., Ji, W., Li, D., Li, X., & Feng, W. (2014). Microstructural Abnormality in Left Nucleus Accumbens Predicts Dysfunctional Beliefs in Treatment-Resistant Obsessive-Compulsive Disorder. *Medical Science Monitor*, *20*, 2275–2282. https://doi.org/https://dx.doi.org/10.12659/MSM.891102

Liebrand, L. C., Caan, M. W. A., Schuurman, P. R., van den Munckhof, P., Figee, M., Denys, D., & van Wingen, G. A. (2019). Individual white matter bundle trajectories are associated with deep brain stimulation response in obsessive-compulsive disorder. *Brain Stimulation*, *12*(2), 353–360. https://doi.org/10.1016/j.brs.2018.11.014

Liebrand, L. C., Natarajan, S. J., Caan, M. W. A., Schuurman, P. R., van den Munckhof, P., de Kwaasteniet, B., Luigjes, J., Bergfeld, I. O., Denys, D., & van Wingen, G. A. (2020). Distance to white matter trajectories is associated with treatment response to internal capsule deep brain stimulation in treatment-refractory depression. *NeuroImage: Clinical*, *28*, 102363. https://doi.org/10.1016/j.nicl.2020.102363

Logan, B. R., Sparapani, R., McCulloch, R. E., & Laud, P. W. (2019). Decision making and uncertainty quantification for individualized treatments using Bayesian Additive Regression Trees. *Statistical Methods in Medical Research*, *28*(4), 1079–1093. https://doi.org/10.1177/0962280217746191

Lozano, A. M., Mayberg, H. S., Giacobbe, P., Hamani, C., Craddock, R. C., & Kennedy, S. H. (2008). Subcallosal cingulate gyrus deep brain stimulation for treatment-resistant

depression. *Biol Psychiatry*, *64*(6), 461–467. https://doi.org/10.1016/j.biopsych.2008.05.034

Lujan, J. L., Chaturvedi, A., Choi, K. S., Holtzheimer, P. E., Gross, R. E., Mayberg, H. S., & McIntyre, C. C. (2013). Tractography-activation models applied to subcallosal cingulate deep brain stimulation. *Brain Stimulation*, *6*(5), 737–739. https://doi.org/10.1016/j.brs.2013.03.008

Mädler, B., & Coenen, V. A. (2012). Explaining clinical effects of deep brain stimulation through simplified target-specific modeling of the volume of activated tissue. *American Journal of Neuroradiology*, *33*(6), 1072–1080. https://doi.org/10.3174/ajnr.A2906

Maier-Hein, K. H., Neher, P., Christophe, J., & Alexandre, M. (2016). *Tractography - based connectomes are dominated by false - positive connections*. 1–23. https://doi.org/http://dx.doi.org/10.1101/084137

Makris, N., Rathi, Y., Mouradian, P., Bonmassar, G., Papadimitriou, G., Ing, W. I., Yeterian, E. H., Kubicki, M., Eskandar, E. N., Wald, L. L., Fan, Q., Nummenmaa, A., Widge, A. S., & Dougherty, D. D. (2016). Variability and anatomical specificity of the orbitofrontothalamic fibers of passage in the ventral capsule/ventral striatum (VC/VS): precision care for patient-specific tractography-guided targeting of deep brain stimulation (DBS) in obsessive compulsive. *Brain Imaging and Behavior*, *10*(4), 1054–1067. https://doi.org/10.1007/s11682-015-9462-9

Mallet, L., Mesnage, V., Houeto, J. L., Pelissolo, A., Yelnik, J., Behar, C., Gargiulo, M., Welter, M. L., Bonnet, A. M., Pillon, B., Cornu, P., Dormont, D., Pidoux, B., Allilaire, J. F., & Agid, Y. (2002). Compulsions, Parkinson's disease, and stimulation. *Lancet*, *360*(9342), 1302–1304. https://doi.org/10.1016/S0140-6736(02)11339-0

Malone, D. A., Dougherty, D. D., Rezai, A. R., Carpenter, L. L., Friehs, G. M., Eskandar, E. N., Rauch, S. L., Rasmussen, S. A., Machado, A. G., Kubu, C. S., Tyrka, A. R., Price, L. H., Stypulkowski, P. H., Giftakis, J. E., Rise, M. T., Malloy, P. F., Salloway, S. P., & Greenberg, B. D. (2009). Deep Brain Stimulation of the Ventral Capsule/Ventral Striatum for Treatment-Resistant Depression. *Biological Psychiatry*, *65*(4), 267–275. https://doi.org/10.1016/j.biopsych.2008.08.029

Mantione, M., Nieman, D. D. H., Figee, M., & Denys, D. (2014). Cognitive–behavioural therapy augments the effects of deep brain stimulation in obsessive–compulsive disorder. *Psychological Medicine*, *44*(16), 3515–3522. https://doi.org/10.1017/S0033291714000956

Mathiopoulou, V., Rijks, N., Caan, M. W. A., Liebrand, L. C., Ferreira, F., de Bie, R. M. A., van den Munckhof, P., Schuurman, P. R., & Bot, M. (2022). Utilizing 7-Tesla Subthalamic

Nucleus Connectivity in Deep Brain Stimulation for Parkinson Disease. *Neuromodulation*, *0*(0). https://doi.org/10.1016/j.neurom.2022.01.003

Mayberg, H. S., Lozano, A. M., Voon, V., McNeely, H. E., Seminowicz, D., Hamani, C., Schwalb, J. M., & Kennedy, S. H. (2005). Deep Brain Stimulation for Treatment-Resistant Depression. *Neuron*, *45*(5), 651–660. https://doi.org/10.1016/j.neuron.2005.02.014

Meyer, D. M., Spanier, S., Kilian, H. M., Reisert, M., Urbach, H., Sajonz, B. E., Reinacher, P. C., Normann, C., Domschke, K., Coenen, V. A., & Schlaepfer, T. E. (2022). Efficacy of superolateral medial forebrain bundle deep brain stimulation in obsessive-compulsive disorder. In *Brain Stimulation* (Vol. 15, Issue 3, pp. 582–585). Elsevier Inc. https://doi.org/10.1016/j.brs.2022.03.004

Milad, M. R., & Rauch, S. L. (2012). Obsessive-compulsive disorder: Beyond segregated cortico-striatal pathways. *Trends in Cognitive Sciences*, *16*(1), 43–51. https://doi.org/10.1016/j.tics.2011.11.003

Miocinovic, S., Lempka, S. F., Russo, G. S., Maks, C. B., Butson, C. R., Sakaie, K. E., Vitek, J. L., & McIntyre, C. C. (2009). Experimental and theoretical characterization of the voltage distribution generated by deep brain stimulation. *Experimental Neurology*, *216*(1), 166–176. https://doi.org/10.1016/j.expneurol.2008.11.024

Monté-Rubio, G. C., Falcón, C., Pomarol-Clotet, E., & Ashburner, J. (2018). A comparison of various MRI feature types for characterizing whole brain anatomical differences using linear pattern recognition methods. *NeuroImage*, *178*, 753–768. https://doi.org/10.1016/j.neuroimage.2018.05.065

Mukherjee, P., Chung, S. W., Berman, J. I., Hess, C. P., & Henry, R. G. (2008). Diffusion Tensor MR Imaging and Fiber Tractography: Technical Considerations. *American Journal of Neuroradiology*, *29*(5), 843–852. https://doi.org/10.3174/ajnr.A1052

Müller, U., Sturm, V., Voges, J., Heinze, H.-J., Galazky, I., Büntjen, L., Heldmann, M., Frodl, T., Steiner, J., & Bogerts, B. (2016). Nucleus Accumbens Deep Brain Stimulation for Alcohol Addiction – Safety and Clinical Long-term Results of a Pilot Trial. *Pharmacopsychiatry*, *90*(EFirst), 3–6. https://doi.org/10.1055/s-0042-104507

Nanda, P., Banks, G. P., Pathak, Y. J., & Sheth, S. A. (2017). Connectivity-based parcellation of the anterior limb of the internal capsule. *Human Brain Mapping*, *00*. https://doi.org/10.1002/hbm.23815

Nieuwenhuys, R., Geeraedts, L. M. G., & Veening, J. G. (1982). The medial forebrain bundle of the rat. I. General introduction. *The Journal of Comparative Neurology*, *206*(1), 49–81. https://doi.org/10.1002/cne.902060106

Noecker, A. M., Choi, K. S., Riva-Posse, P., Gross, R. E., Mayberg, H. S., & Mcintyre, C. C. (2017). StimVision Software: Examples and Applications in Subcallosal Cingulate Deep Brain Stimulation for Depression. *Neuromodulation*, *2017*. https://doi.org/10.1111/ner.12625

Nuttin, B., Cosyns, P., Demeulemeester, H., Gybels, J., & Meyerson, B. (1999). Electrical stimulation in anterior limbs of internal capsules in patients with obsessive-compulsive disorder. *Lancet*, *354*(9189), 1526. https://doi.org/10.1016/S0140-6736(99)02376-4

Ojala, M., & Garriga, G. C. (2010). Permutation Tests for Studying Classifier Performance. *Journal of Machine Learning Research*, *11*(62), 1833–1863. https://doi.org/10.1109/ICDM.2009.108

Ooms, P., Blankers, M., Figee, M., Bergfeld, I. O., van den Munckhof, P., Schuurman, P. R., & Denys, D. (2017). Cost-effectiveness of deep brain stimulation versus treatment as usual for obsessive-compulsive disorder. *Brain Stimulation*, *10*(4), 836–842. https://doi.org/10.1016/j.brs.2017.04.120

Patriat, R., Cooper, S. E., Duchin, Y., Niederer, J., Lenglet, C., Aman, J., Park, M. C., Vitek, J. L., & Harel, N. (2018). Individualized tractography-based parcellation of the globus pallidus pars interna using 7T MRI in movement disorder patients prior to DBS surgery. *NeuroImage*, *178*(February), 198–209. https://doi.org/10.1016/j.neuroimage.2018.05.048

Pedregosa, F., Varoquaux, G., Gramfort, A., Michel, V., Thirion, B., Grisel, O., Blondel, M., Prettenhofer, P., Weiss, R., Dubourg, V., Vanderplas, J., Passon, A., Cournapeau, D., Brucher, M., Perrot, M., & Duchesnay, E. (2011). Scikit-learn: Machine Learning in Python. *Journal of Machine Learning Research*, *12*(85), 2825–2830. https://doi.org/10.1007/s13398-014-0173-7.2

Petersen, M. V., Lund, T. E., Sunde, N., Frandsen, J., Rosendal, F., Juul, N., & Østergaard, K. (2016). Probabilistic versus deterministic tractography for delineation of the cortico-subthalamic hyperdirect pathway in patients with Parkinson disease selected for deep brain stimulation. *Journal of Neurosurgery*, 1–12. https://doi.org/10.3171/2016.4.JNS1624

Pinhal, C. M., van den Boom, B. J. G., Santana-Kragelund, F., Fellinger, L., Bech, P., Hamelink, R., Feng, G., Willuhn, I., Feenstra, M. G. P., & Denys, D. (2018). Differential Effects of Deep Brain Stimulation of the Internal Capsule and the Striatum on Excessive Grooming in Sapap3 Mutant Mice. *Biological Psychiatry*, *84*(12), 917–925. https://doi.org/10.1016/j.biopsych.2018.05.011

Plantinga, B. R., Temel, Y., Duchin, Y., Uludağ, K., Patriat, R., Roebroeck, A., Kuijf, M., Jahanshahi, A., ter Haar Romenij, B., Vitek, J., & Harel, N. (2018). Individualized parcellation of the subthalamic nucleus in patients with Parkinson's disease with 7T MRI. *NeuroImage*, *168*(September 2016), 403–411. https://doi.org/10.1016/j.neuroimage.2016.09.023

Puigdemont, D., Portella, M. J., Pérez-Egea, R., Molet, J., Gironell, A., de Diego-Adeliño, J., Martín, A., Rodríguez, R., Àlvarez, E., Artigas, F., & Pérez, V. (2015). A randomized double-blind crossover trial of deep brain stimulation of the subcallosal cingulate gyrus in patients with treatment-resistant depression: A pilot study of relapse prevention. *Journal of Psychiatry and Neuroscience*, *40*(4), 224–231. https://doi.org/10.1503/jpn.130295

Riva-Posse, P., Choi, K. S., Holtzheimer, P. E., Crowell, A. L., Garlow, S. J., Rajendra, J. K., McIntyre, C. C., Gross, R. E., & Mayberg, H. S. (2018). A connectomic approach for subcallosal cingulate deep brain stimulation surgery: prospective targeting in treatment-resistant depression. *Molecular Psychiatry*, *23*(4), 843–849. https://doi.org/10.1038/mp.2017.59

Riva-Posse, P., Choi, K. S., Holtzheimer, P. E., McIntyre, C. C., Gross, R. E., Chaturvedi, A., Crowell, A. L., Garlow, S. J., Rajendra, J. K., & Mayberg, H. S. (2014). Defining Critical White Matter Pathways Mediating Successful Subcallosal Cingulate Deep Brain Stimulation for Treatment-Resistant Depression. *Biological Psychiatry*, *76*(12), 963–969. https://doi.org/10.1016/j.biopsych.2014.03.029

Ruhé, H. G., Van Rooijen, G., Spijker, J., Peeters, F. P. M. L., & Schene, A. H. (2012). Staging methods for treatment resistant depression. A systematic review. *Journal of Affective Disorders*, *137*(1–3), 35–45. https://doi.org/10.1016/j.jad.2011.02.020

Rush, A. J., Trivedi, M. H., Wisniewski, S. R., Nierenberg, A. A., Stewart, J. W., Warden, D., George Niederehe, M., Thase, M. E., Lavori, P. W., Lebowitz, B. D., McGrath, P. J., Rosenbaum, J. F., Sackeim, H. A., Kupfer, D. J., Luther, J., & Maurizio Fava, M. (2006). Acute and Longer-Term Outcomes in Depressed Outpatients Requiring One or Several Treatment Steps: A STAR*D Report. In *Am J Psychiatry* (Vol. 163, Issue 11). www.star-d.org

Safadi, Z., Grisot, G., Jbabdi, S., Behrens, T. E., Heilbronner, S. R., McLaughlin, N. C. R., Mandeville, J., Versace, A., Phillips, M. L., Lehman, J. F., Yendiki, A., & Haber, S. N. (2018). Functional segmentation of the anterior limb of the internal capsule: Linking white matter abnormalities to specific connections. *Journal of Neuroscience*, *38*(8), 2106–2117. https://doi.org/10.1523/JNEUROSCI.2335-17.2017

Scangos, K. W., Khambhati, A. N., Daly, P. M., Makhoul, G. S., Sugrue, L. P., Zamanian, H., Liu, T. X., Rao, V. R., Sellers, K. K., Dawes, H. E., Starr, P. A., Krystal, A. D., & Chang, E. F.

(2021). Closed-loop neuromodulation in an individual with treatment-resistant depression. *Nature Medicine*, *27*(10), 1696–1700. https://doi.org/10.1038/s41591-021-01480-w

Schilling, K. G., Petit, L., Rheault, F., Remedios, S., Pierpaoli, C., Anderson, A. W., Landman, B. A., & Descoteaux, M. (2020). Brain connections derived from diffusion MRI tractography can be highly anatomically accurate—if we know where white matter pathways start, where they end, and where they do not go. *Brain Structure and Function*, *225*(8), 2387–2402. https://doi.org/10.1007/s00429-020-02129-z

Schlaepfer, T. E., Bewernick, B. H., Kayser, S., Mädler, B., & Coenen, V. A. (2013). Rapid effects of deep brain stimulation for treatment-resistant major depression. *Biological Psychiatry*, *73*(12), 1204–1212. https://doi.org/10.1016/j.biopsych.2013.01.034

Schlaepfer, T. E., Cohen, M. X., Frick, C., Kosel, M., Brodesser, D., Axmacher, N., Joe, A. Y., Kreft, M., Lenartz, D., & Sturm, V. (2008). Deep Brain Stimulation to Reward Circuitry Alleviates Anhedonia in Refractory Major Depression. *Neuropsychopharmacology*, *33*(2), 368–377. https://doi.org/10.1038/sj.npp.1301408

Schmuckermair, C., Gaburro, S., Sah, A., Landgraf, R., Sartori, S. B., & Singewald, N. (2013). Behavioral and Neurobiological Effects of Deep Brain Stimulation in a Mouse Model of High Anxiety- and Depression-Like Behavior. *Neuropsychopharmacology*, *38*(7), 1234–1244. https://doi.org/10.1038/npp.2013.21

Setsompop, K., Kimmlingen, R., Eberlein, E., Witzel, T., Cohen-Adad, J., McNab, J. A., Keil, B., Tisdall, M. D., Hoecht, P., Dietz, P., Cauley, S. F., Tountcheva, V., Matschl, V., Lenz, V. H., Heberlein, K., Potthast, A., Thein, H., Van Horn, J., Toga, A., … Wald, L. L. (2013). Pushing the limits of in vivo diffusion MRI for the Human Connectome Project. *NeuroImage*, *80*, 220–233. https://doi.org/10.1016/j.neuroimage.2013.05.078

Smith, S. M., & Nichols, T. E. (2009). Threshold-free cluster enhancement: Addressing problems of smoothing, threshold dependence and localisation in cluster inference. *NeuroImage*, *44*(1), 83–98. https://doi.org/10.1016/j.neuroimage.2008.03.061

Smolders, R., Mazaheri, A., van Wingen, G., Figee, M., de Koning, P. P., & Denys, D. (2013). Deep Brain Stimulation Targeted at the Nucleus Accumbens Decreases the Potential for Pathologic Network Communication. *Biological Psychiatry*, *74*(10), e27–e28. https://doi.org/10.1016/j.biopsych.2013.03.012

Steele, C. J., Anwander, A., Bazin, P. L., Trampel, R., Schaefer, A., Turner, R., Ramnani, N., & Villringer, A. (2017). Human cerebellar sub-millimeter diffusion imaging reveals the motor and non-motor topography of the dentate nucleus. *Cerebral Cortex*, *27*(9), 4537–4548. https://doi.org/10.1093/cercor/bhw258

Steigerwald, F., Matthies, C., & Volkmann, J. (2019). Directional Deep Brain Stimulation. *Neurotherapeutics*, *16*(1), 100–104. https://doi.org/10.1007/s13311-018-0667-7

Stejskal, E. O., & Tanner, J. E. (1965). Spin Diffusion Measurements: Spin Echoes in the Presence of a Time-Dependent Field Gradient. *The Journal of Chemical Physics*, *42*(1), 288–292. https://doi.org/10.1063/1.1695690

Sturm, V., Lenartz, D., Koulousakis, A., Treuer, H., Herholz, K., Klein, J. C., & Klosterkötter, J. (2003). The nucleus accumbens: a target for deep brain stimulation in obsessive–compulsive- and anxiety-disorders. *Journal of Chemical Neuroanatomy*, *26*(4), 293–299. https://doi.org/10.1016/j.jchemneu.2003.09.003

Tierney, T. S., Abd-El-Barr, M. M., Stanford, A. D., Foote, K. D., & Okun, M. S. (2014). Deep brain stimulation and ablation for obsessive compulsive disorder: evolution of contemporary indications, targets and techniques. *International Journal of Neuroscience*, *124*(6), 394–402. https://doi.org/10.3109/00207454.2013.852086

Tournier, J. D., Calamante, F., & Connelly, A. (2013). Determination of the appropriate b value and number of gradient directions for high-angular-resolution diffusion-weighted imaging. *NMR in Biomedicine*, *26*(12), 1775–1786. https://doi.org/10.1002/nbm.3017

Tyagi, H., Apergis-Schoute, A. M., Akram, H., Foltynie, T., Limousin, P., Drummond, L. M., Fineberg, N. A., Matthews, K., Jahanshahi, M., Robbins, T. W., Sahakian, B. J., Zrinzo, L., Hariz, M., & Joyce, E. M. (2019). A Randomized Trial Directly Comparing Ventral Capsule and Anteromedial Subthalamic Nucleus Stimulation in Obsessive-Compulsive Disorder: Clinical and Imaging Evidence for Dissociable Effects. *Biological Psychiatry*, *85*(9), 726–734. https://doi.org/10.1016/j.biopsych.2019.01.017

van den Heuvel, O. A., van Wingen, G., Soriano-Mas, C., Alonso, P., Chamberlain, S. R., Nakamae, T., Denys, D., Goudriaan, A. E., & Veltman, D. J. (2016). Brain circuitry of compulsivity. *European Neuropsychopharmacology*, *26*(5), 810–827. https://doi.org/10.1016/j.euroneuro.2015.12.005

van den Munckhof, P., Bosch, D. A., Mantione, M. H. M., Figee, M., Denys, D. A. J. P., & Schuurman, P. R. (2013). Active Stimulation Site of Nucleus Accumbens Deep Brain Stimulation in Obsessive–Compulsive Disorder Is Localized in the Ventral Internal Capsule. In G. Nikkhah & M. Pinsker (Eds.), *Stereotactic and Functional Neurosurgery* (Vol. 117, pp. 53–59). Springer Vienna. https://doi.org/10.1007/978-3-7091-1482-7_9

Van Laere, K., Nuttin, B., Gabriels, L., Dupont, P., Rasmussen, S., Greenberg, B. D., & Cosyns, P. (2006). Metabolic Imaging of Anterior Capsular Stimulation in Refractory Obsessive-Compulsive Disorder: A Key Role for the Subgenual Anterior Cingulate and Ventral Striatum. *Journal of Nuclear Medicine* , *47*(5), 740–747.

van Waarde, J. A., Scholte, H. S., van Oudheusden, L. J. B. B., Verwey, B., Denys, D., & van Wingen, G. A. (2015). A functional MRI marker may predict the outcome of electroconvulsive therapy in severe and treatment-resistant depression. *Molecular Psychiatry*, *20*(5), 609–614. https://doi.org/10.1038/mp.2014.78

van Westen, M., Rietveld, E., Bergfeld, I. O., de Koning, P., Vullink, N., Ooms, P., Graat, I., Liebrand, L., van den Munckhof, P., Schuurman, R., & Denys, D. (2020). Optimizing Deep Brain Stimulation Parameters in Obsessive–Compulsive Disorder. *Neuromodulation*, *2020*. https://doi.org/10.1111/ner.13243

Veraart, J., Novikov, D. S., Christiaens, D., Ades-aron, B., Sijbers, J., & Fieremans, E. (2016). Denoising of diffusion MRI using random matrix theory. *NeuroImage*, *142*, 394–406. https://doi.org/10.1016/j.neuroimage.2016.08.016

Vos, S. B., Aksoy, M., Han, Z., Holdsworth, S. J., Maclaren, J., Viergever, M. A., Leemans, A., & Bammer, R. (2016). Trade-off between angular and spatial resolutions in in vivo fiber tractography. *NeuroImage*, *129*, 117–132. https://doi.org/10.1016/j.neuroimage.2016.01.011

Wakana, S., Caprihan, A., Panzenboeck, M. M., Fallon, J. H., Perry, M., Gollub, R. L., Hua, K., Zhang, J., Jiang, H., Dubey, P., Blitz, A., van Zijl, P., & Mori, S. (2007). Reproducibility of quantitative tractography methods applied to cerebral white matter. *NeuroImage*, *36*(3), 630–644. https://doi.org/10.1016/j.neuroimage.2007.02.049

Whiting, A. C., Oh, M. Y., & Whiting, D. M. (2018). Deep brain stimulation for appetite disorders: A review. *Neurosurgical Focus*, *45*(2). https://doi.org/10.3171/2018.4.FOCUS18141

Winkler, A. M., Webster, M. A., Brooks, J. C., Tracey, I., Smith, S. M., & Nichols, T. E. (2016). Non-parametric combination and related permutation tests for neuroimaging. *Human Brain Mapping*, *37*(4), 1486–1511. https://doi.org/10.1002/hbm.23115

Wood, J., & Ahmari, S. E. (2015). A Framework for Understanding the Emerging Role of Corticolimbic-Ventral Striatal Networks in OCD-Associated Repetitive Behaviors. *Frontiers in Systems Neuroscience*, *9*(December), 171. https://doi.org/10.3389/fnsys.2015.00171

Wu, H., Hariz, M., Visser-Vandewalle, V., Zrinzo, L., Coenen, V. A., Sheth, S. A., Bervoets, C., Naesström, M., Blomstedt, P., Coyne, T., Hamani, C., Slavin, K., Krauss, J. K., Kahl, K. G., Taira, T., Zhang, C., Sun, B., Toda, H., Schlaepfer, T., … Nuttin, B. (2021). Deep brain stimulation for refractory obsessive-compulsive disorder (OCD): emerging or established therapy? *Molecular Psychiatry*, *26*(1), 60–65. https://doi.org/10.1038/s41380-020-00933-x

Yun, J.-Y., Jang, J. H., Kim, S. N., Jung, W. H., & Kwon, J. S. (2015). Neural Correlates of Response to Pharmacotherapy in Obsessive-Compulsive Disorder: Individualized Cortical Morphology-Based Structural Covariance. *Progress in Neuro-Psychopharmacology and Biological Psychiatry*, *63*, 126–133. https://doi.org/https://doi.org/10.1016/j.pnpbp.2015.06.009

Zhang, L., Hu, X., Li, H., Lu, L., Li, B., Hu, X., Bu, X., Tang, S., Tang, W., Liu, N., Yang, Y., Gong, Q., & Huang, X. (2019). Characteristic alteration of subcortical nuclei shape in medication-free patients with obsessive-compulsive disorder. *NeuroImage: Clinical*, *24*, 102040. https://doi.org/10.1016/j.nicl.2019.102040

Zhang, Q., Coolen, B. F., Nederveen, A. J., & Strijkers, G. J. (2019). Three-dimensional diffusion imaging with spiral encoded navigators from stimulated echoes (3D-DISPENSE). *Magnetic Resonance in Medicine*, *81*(2), 1052–1065. https://doi.org/10.1002/mrm.27470

Zhutovsky, P., Thomas, R. M., Olff, M., van Rooij, S. J. H., Kennis, M., van Wingen, G. A., & Geuze, E. (2019). Individual prediction of psychotherapy outcome in posttraumatic stress disorder using neuroimaging data. *Translational Psychiatry*, *9*(1). https://doi.org/10.1038/s41398-019-0663-7

VI. APPENDICES

Nederlandse samenvatting

Dit proefschrift behandelt diepe hersenstimulatie (Engels: *deep brain stimulation*, DBS) bij twee psychiatrische stoornissen: refractaire obsessieve-compulsieve stoornis (OCS) en behandelingsresistente depressie (Engels: TRD). DBS vereist chirurgische implantatie van elektroden in het brein en is daarom afhankelijk van medische beeldvorming van de hersenen (neuroimaging). Er zijn meerdere open vragen rond het optimale gebruik van DBS die mogelijk beantwoord kunnen worden met neuroimaging. Dit proefschrift presenteert toepassingen van geavanceerde neuroimaging-technieken om DBS in de psychiatrie beter te begrijpen en te optimaliseren.

Als eerste hebben we tractografie gebruikt om na te gaan of stimulatie van bepaalde witte-stofbanen gerelateerd was aan een betere behandelrespons. Ten tweede hebben we geavanceerde diffusie-MRI protocollen geëvalueerd op hun geschiktheid voor tractografie-ondersteunde targeting om de specificiteit van stimulatie te verbeteren. Tenslotte gebruikten we *machine learning*, een vorm van kunstmatige intelligentie, om in een multivariate dataset te onderzoeken of we van tevoren konden voorspellen welke patiënten zouden reageren op de behandeling.

In **hoofdstuk 2** onderzochten we retrospectief het potentieel van tractografie-geassisteerde *targeting* in een cohort van twaalf patiënten die behandeld werden met DBS voor OCD. We veronderstelden dat de respons op de behandeling afhing van de locatie van de actieve contacten ten opzichte van individuele witte-stofbanen (ook wel "tracts"). Twee tracts binnen het ventrale deel van het voorste been van de capsula interna (vALIC) werden gevisualiseerd met tractografie. Deze tracts waren de superolaterale mediale voorhersenen bundel (sl medial forebrain bundle; slMFB) en de anterieure thalamische radiatie (ATR). We relateerden de procentuele verandering in de ernst van de OCS-symptomen op de Yale-Brown obsessief-compulsieve schaal (Y-BOCS) tussen baseline en één jaar follow-up aan de afstanden van de actieve contacten tot de ATR en slMFB. Plaatsing van de actieve contacten dichter bij de slMFB dan bij de ATR was geassocieerd met een beter behandelresultaat ($p=0,04$; $r^2=0,34$). Een vergelijking waarbij de scans werden gecoregistreerd in een standaardruimte toonde aan dat de locaties van stimulatie grotendeels overlapten tussen patiënten die wel en geen behandelrespons hadden. Dit suggereert dat de respons onafhankelijk was van de anatomisch bepaalde elektrodepositie. Deze bevindingen suggereren dat vALIC DBS voor OCS baat kan hebben bij slMFB-specifieke implantatie en ze benadrukken het belang van corticolimbische

verbindingen in OCS respons op DBS. Prospectief onderzoek blijft nodig om het klinisch gebruik van slMFB targeting te valideren.

In **hoofdstuk 3** gebruikten we tractografie om retrospectief te bestuderen of de respons op DBS behandeling gerelateerd was aan de plaatsing van de elektroden ten opzichte van witte-stofbanen zoals in hoofdstuk 2. Echter, deze keer onderzochten we een cohort van TRD-patiënten. Daartoe reconstrueerden we de slMFB en de ATR met tractografie om hun respectieve afstand tot de actieve DBS contacten te bepalen in veertien patiënten die deelnamen aan onze gerandomiseerde klinische trial. We associeerden deze afstanden met de verandering in depressieve symptomen gemeten met de Hamilton's depression rating scale (HAM-D) tussen baseline en 1 jaar follow-up als een maat voor de respons op de behandeling. Stimulatie dichter bij beide banen was significant gecorreleerd met een grotere afname van de symptomen (r=0,61, p=0,02), wat suggereert dat stimulatie dichter bij beide banen gunstig was. Biofysische modellering gaf aan dat 38% van de witte-stofbanen zich zelfs buiten het volume van geactiveerd weefsel bevonden. Er was geen verschil in elektrodeplaatsing ten opzichte van anatomische herkenningspunten, wat zou kunnen betekenen dat verschillen in behandelingsrespons werden veroorzaakt door individuele verschillen in witte stof anatomie. Onze resultaten suggereren dat diepe hersenstimulatie van de vALIC voor TRD baat zou kunnen hebben bij het richten op witte-stofbanen. Wij doen de aanbeveling om diffusie-MRI data te verkrijgen voor elke individuele patiënt om zo rekening te kunnen houden met individuele variaties en om verdere studies mogelijk te maken.

In **hoofdstuk 4** hebben we diffusie-MRI scanprotocollen en de potentiële winst van het verbeteren van de resolutie voor toepassing in DBS chirurgische planning onderzocht. Gezien de beperkte totale scantijd voor klinische neuroimaging, was het onduidelijk of klinische diffusie-MRI protocollen meer baat zouden hebben bij een hogere ruimtelijke resolutie of hogere angulaire resolutie – het zou zelfs kunnen dat deze afweging afhangt van de specifieke toepassing. Omdat we geïnteresseerd waren in de toepassing van diffusie MRI in DBS van de vALIC, onderzochten we het relatieve voordeel van het verbeteren van de ruimtelijke of angulaire resolutie in diffusie MRI om de twee parallel lopende witte-stofbanen bestudeerd in hoofdstuk 2 en 3 te scheiden: de ATR en de slMFB. Aangezien dit een studie was om scanprotocollen te evalueren, scanden we 19 gezonde vrijwilligers op 3T en 7T volgens drie diffusie MRI-protocollen met respectievelijk standaard klinische instellingen, verhoogde spatiale resolutie van 1,4 mm, en verhoogde hoekresolutie (64 extra gradiëntrichtingen bij b=2200 s/mm^2). We voerden probabilistische tractografie uit voor alle protocollen en kwantificeerden de onderscheidbaarheid van beide tracts. Het protocol met hogere ruimtelijke resolutie verbeterde de onderscheidbaarheid met 41% (zoals uitgedrukt in Cohen's *d*) ten opzichte van de klinische standaard. Dit is

vermoedelijk als gevolg van een verminderd middelen van verschillende weefsels per voxel. Het hogere angulaire resolutie protocol resulteerde in verhoogde schijnbare tract volumes en overlap, wat nadelig is voor toepassing in tract-specifieke chirurgische planning. We bevelen dus aan om de ruimtelijke resolutie te verhogen voor DBS chirurgische planning binnen de vALIC, met behoud van angulaire resolutie. Deze aanbeveling is een aanvulling op het algemene advies om te streven naar een hoge hoekresolutie om kruisende vezels op te lossen, en bevestigt dat de specifieke toepassing en anatomische overwegingen leidend zijn in klinische diffusie-MRI protocol optimalisatie.

Hoofdstuk 5 richtte zich op de voorspelling van behandelingsresultaten bij DBS voor OCS. Aangezien ongeveer 60% van de patiënten met OCS reageert op DBS, zouden biomarkers die patiënten die baat hebben bij de behandeling al vóór de operatie kunnen identificeren waardevol kunnen blijken. Daarom onderzochten we de mogelijkheid om het resultaat van een behandeling met DBS voor OCS op groeps- en individueel niveau te voorspellen met behulp van preoperatieve structurele MRI van 57 patiënten. Voxel-gebaseerde morfometrie werd gebruikt om te onderzoeken of grijze stof (GM) of witte stof (WM) volumes rondom de DBS elektrode (nucleus accumbens (NAc), anterieure thalamus uitstraling), en GM/WM volumes (in het gehele brein) geassocieerd waren met de ernst van OCS en responsstatus bij 12-maanden follow-up. Daarnaast voerden we machine learning-analyses uit om het resultaat van de behandeling op individueel niveau te voorspellen en evalueerden we de prestaties met behulp van kruisvalidatie. Wij vonden dat een groter preoperatief linker NAc volume geassocieerd was met een lagere OCS-ernst bij 12-maanden follow-up ($pFWE < 0,05$). Geen van de regressie/classificatie analyses op individueel niveau overtrof het toevalsniveau. Deze resultaten leverden bewijs dat patiënten met grotere NAc volumes een betere respons vertonen op DBS, wat aangeeft dat het succes van DBS deels bepaald wordt door individuele verschillen in hersenanatomie. De resultaten geven echter ook aan dat structurele MRI-gegevens alleen nog niet voldoende informatie bieden om klinische besluitvorming op individueel niveau te sturen.

Portfolio

PhD student: PhD period: PhD supervisors & co-supervisor:	Luka Charlie Liebrand November 2015 until November 2019 prof. dr. Damiaan Denys prof. dr. Guido A. van Wingen dr. ir. Matthan W.A. Caan

1. PhD training

	Year	ECTs
General Courses		
Basiscursus Regelgeving en Organisatie voor Klinisch Onderzoekers (BROK)	2016	1.5
AMC PhD Business Course	2016	0.3
Specific courses		
Bootcamp: Workshop Diffusion MRI, International Society for Magnetic Resonance in Medicine (ISMRM), Lisbon	2016	0.4
Seminars, workshops and master classes		
Workshop in Diffusion MRI, Organization for Human Brain Mapping, Geneva	2016	0.4
Workshop Diffusion MRI, International Society for Magnetic Resonance in Medicine (ISMRM), Lisbon	2016	1.0
Deep Learning in Medical Imaging Symposium, UvA, Amsterdam	2016	0.4
Computational Psychiatry symposium, Donders Institute, Nijmegen	2016	0.4
Presentations		
Poster		
'*Which bundles to target with Deep Brain Stimulation for psychiatric disorders?'*, Diffusion Workshop, ISMRM, Lisbon	2016	0.3
'Which white matter bundles are associated with treatment efficacy in deep brain stimulation of the ventral internal capsule for OCD and MDD?', Amsterdam Neuroscience kickoff meeting, Amsterdam	2016	0.3
'Which white matter bundles are associated with treatment efficacy in deep brain stimulation of the ventral internal capsule for OCD and MDD?', ISMRM Benelux Chapter meeting, Tilburg	2017	0.3

'Which white matter bundles are associated with treatment efficacy in deep brain stimulation of the ventral internal capsule for OCD and MDD?', Institute QuantiVision meeting, Amsterdam	2017	0.3
'Which white matter bundles are associated with treatment efficacy in deep brain stimulation of the ventral internal capsule for OCD and MDD?', Brain Stimulation Conference, Barcelona	2017	0.3
'Stimulating closer to the medial forebrain bundle is related to better response in OCD', OptoDBS Conference, Geneva	2017	0.3
'Stimulating closer to the medial forebrain bundle is related to better response in OCD', ECNP Conference, Paris	2017	0.3
'Stimulating closer to the medial forebrain bundle is related to better response in OCD', Amsterdam Neuroscience annual meeting, Amsterdam	2017	0.3
'Angular (3T) versus spatial (7T) resolution in tractography for deep brain stimulation in psychiatry', ISMRM Benelux Chapter meeting, Antwerpen	2018	0.3
'Angular (3T) versus spatial (7T) resolution in tractography for deep brain stimulation in psychiatry', ISMRM Annual meeting, Paris	2018	0.3
'Angular (3T) versus spatial (7T) resolution in tractography for deep brain stimulation in psychiatry', TN2 Conference, Amsterdam	2018	0.3
'Angular (3T) versus spatial (7T) resolution in tractography for deep brain stimulation in psychiatry', Amsterdam Neuroscience annual meeting, Amsterdam	2018	0.3
<u>Oral</u>		
'Tract-specific Deep Brain Stimulation for OCD', ABC Networking Day, power pitch, Amsterdam	2018	0.3
'Tractography in DBS for Psychiatry', invited lecture, group prof. H. Mayberg, New York	2019	0.3
'Personalized prediction of response to Deep Brain Stimulation for Obsessive-Compulsive Disorder', Brain Stimulation Conference, member initiated symposium, Vancouver	2019	0.3
(Inter)national conferences		
ISMRM Benelux Chapter meeting, Eindhoven	2016	0.4
Organization for Human Brain Mapping, Geneva	2016	1.3
Diffusion Workshop, ISMRM, Lisbon	2016	1.3
Amsterdam Neuroscience kickoff meeting, Amsterdam	2016	0.4
ISMRM Benelux Chapter meeting, Tilburg	2017	0.4

Institute QuantiVision meeting, Amsterdam	2017	0.4
Brain Stimulation Conference, Barcelona	2017	1.3
OptoDBS Conference, Geneva	2017	1.3
ECNP Conference, Paris	2017	1.3
Amsterdam Neuroscience annual meeting, Amsterdam	2017	0.4
ISMRM Benelux Chapter meeting, Antwerpen	2018	0.4
ISMRM Annual meeting, Paris	2018	1.3
ABC Networking Day, Amsterdam	2018	0.4
TN2 Conference, Amsterdam	2018	0.4
Amsterdam Neuroscience annual meeting, Amsterdam	2018	0.4
Brain Stimulation Conference, Vancouver	2019	1.3
Other		
Research group meetings Neuroimaging in Psychiatry (weekly), AMC, Amsterdam	2015 - 2019	4.0
Research group meetings MR Physics (weekly), AMC, Amsterdam	2015 - 2019	4.0
Spinoza Centre User Meetings (weekly), Spinoza Centre for Neuroimaging, Amsterdam	2015 - 2019	4.0
2. Teaching		
	Year	**ECTs**
Lecturing		
Lecture & Practical Diffusion MRI, Advanced Cognitive Neurobiology & Clinical Neurophysiology, Master's Course in Biomedical Sciences	2016 - 2019	2.0
Supervising		
Chaira Serrarens, *Default mode network functional connectivity associated with response to deep brain stimulation in treatment-resistant depression patients*, Research Thesis for Master in Biomedical Sciences, UvA	2017	1.0
Samuel Natarajan, *Deep Brain Stimulation of the Ventral Anterior Limb of the Internal Capsule for Treatment Resistant Depression: The role of relative proximity of the MFB and ATR to the electrode contacts in clinical outcomes*, Research Thesis for Master in Biomedical Sciences, UvA	2018	1.0
Eva Tolmeijer, *Personalized prediction of response to deep brain stimulation in obsessive-compulsive disorder*, Research Thesis for Master in Clinical Psychology, Leiden University	2018	1.0
Isaac Acheampong, Targeting specific white matter bundles with deep brain stimulation for TRD and OCD: a systematic review, Thesis for Bachelor in Medicine, AMC	2018	1.0

Other		
Lecture on diffusion MRI, (f)MRI for Dummies course, AMC/Spinoza Centre for Neuroimaging, Amsterdam	2016	0.2

3. Parameters of Esteem	
	Year
Grants	
Personalized Deep Brain Stimulation, ZonMW Grant – Mental Healthcare Program (Programma GGZ), €500.000, co-applicant	2018

4. Publications	
	Year
Peer reviewed – in this thesis	
Liebrand LC, Caan MWA, Schuurman PR, van den Munckhof P, Figee M, Denys D, van Wingen GA. Individual white matter bundle trajectories are associated with deep brain stimulation response in obsessive-compulsive disorder. Brain Stimul. 2019 Mar-Apr;12(2):353-360. doi: 10.1016/j.brs.2018.11.014.	2019
Liebrand LC, Natarajan SJ, Caan MWA, Schuurman PR, van den Munckhof P, de Kwaasteniet B, Luigjes J, Bergfeld IO, Denys D, van Wingen GA. Distance to white matter trajectories is associated with treatment response to internal capsule deep brain stimulation in treatment-refractory depression. Neuroimage Clin. 2020;28:102363. doi: 10.1016/j.nicl.2020.102363.	2020
Liebrand LC, van Wingen GA, Vos FM, Denys D, Caan MWA. Spatial versus angular resolution for tractography-assisted planning of deep brain stimulation. Neuroimage Clin. 2020;25:102116. doi: 10.1016/j.nicl.2019.102116.	2020
Liebrand LC, Zhutovsky P*, Tolmeijer EK, Graat I, Vulink N, de Koning P, Figee M, Schuurman PR, van den Munckhof P, Caan MWA, Denys D, van Wingen GA. Deep brain stimulation response in obsessive-compulsive disorder is associated with preoperative nucleus accumbens volume. Neuroimage Clin. 2021;30:102640. doi: 10.1016/j.nicl.2021.102640 **Contributed equally*	2021
Peer reviewed – not in this thesis	
Vos BE, **Liebrand LC**, Vahabi M, Biebricher A, Wuite GJL, Peterman EJG, Kurniawan NA, MacKintosh FC, Koenderink GH. Programming the mechanics of cohesive fiber networks by compression. Soft Matter. 2017 Dec 6;13(47):8886-8893. doi: 10.1039/c7sm01393k	2017
Eijsker N, Schröder A, **Liebrand LC**, Smit DJA, van Wingen G, Denys D. White matter abnormalities in misophonia. Neuroimage Clin. 2021;32:102787. doi:10.1016/j.nicl.2021.102787	2021

van Westen M, Rietveld E, Bergfeld IO, de Koning P, Vullink N, Ooms P, Graat I, **Liebrand L**, van den Munckhof P, Schuurman R, Denys D. Optimizing Deep Brain Stimulation Parameters in Obsessive-Compulsive Disorder. Neuromodulation. 2021 Feb;24(2):307-315. doi: 10.1111/ner.13243	2021
Mathiopoulou V, Rijks N, Caan MWA, **Liebrand LC**, Ferreira F, de Bie RMA, van den Munckhof P, Schuurman PR, Bot M. Utilizing 7-Tesla Subthalamic Nucleus Connectivity in Deep Brain Stimulation for Parkinson Disease. Neuromodulation. 2022 Feb 22:S1094-7159(22)00023-X. doi: 10.1016/j.neurom.2022.01.003.	2022
Keuken MC, **Liebrand LC**, Bazin PL, Alkemade A, van Berendonk N, Groot JM, Isherwood SJS, Kemp S, Lute N, Mulder MJ, Trutti AC, Caan MWA, Forstmann BU. A high-resolution multi-shell 3T diffusion magnetic resonance imaging dataset as part of the Amsterdam Ultra-high field adult lifespan database (AHEAD). Data Brief. 2022 Mar 23;42:108086. doi: 10.1016/j.dib.2022.108086	2022

Curriculum Vitae

Luka Charlie Liebrand was born in Amsterdam on the 17th of May 1991. He grew up in Hoorn, where he attended the OSG West-Friesland to obtain his prepratory scientific level diploma (Dutch: gymnasium) in 2008. Luka enrolled into the Bachelor of Science in Physics and Astronomy at the University of Amsterdam, during which he began to take an interest in optics and biomedical imaging. Luka was first introduced to the fascinating topic of magnetic resonance imaging (MRI) during his Bachelor's thesis project, which he conducted at the Spinoza Centre for Neuroimaging under the supervision of Dr. Pieter Buur. After completing his thesis, titled '*Improving the Orbitofrontal Cortex BOLD signal in EPI fMRI by comparing slice tilts and 2D, 2D-DE and 3D GE EPI scan sequences'*, he graduated in January of 2014.

Luka enrolled into the joint Master of Science in Physics program of the University of Amsterdam and VU University Amsterdam in February 2014. He chose the track '*Physics of Life and Health*', which focused on biomedical physics and biophysics. Inspired by a course on Statistical Mechanics of Soft Matter, Luka applied for an internship in the lab of Prof. Fred MacKintosh at the VU to work on his Master thesis in the field of theoretical biophysics. The topic of his project was the mechanical properties of fiber networks, specifically of fibrin, which is an important protein in blood clotting. During this project, he collaborated with the experimental research group of Prof. Gijsje Koenderink at AMOLF. The collaboration proved fruitful. It culminated in Luka's Master thesis called '*Remodeling-induced stiffening of fibrous networks under deformation*' and, later, a scientific publication. Luka graduated from his Master's in October 2015.

During his research projects, Luka got enthused about the idea of pursuing a PhD. He considered topics from different research fields, yet in the end his interest for MRI won. Luka started his PhD project on advanced MRI in Deep Brain Stimulation for Psychiatry under supervision of Prof. Guido van Wingen, Dr. Matthan Caan, and Prof. Damiaan Denys at the Academic Medical Center (AMC) in November 2015. Besides the scientific output presented in this thesis, Luka helped to update the neurosurgical targeting strategy in DBS and aided in setting up new imaging protocols.

After conducting his PhD research, Luka extended his collaboration with Dr. Caan in a new MRI project on acute ischemic stroke. Here, he endeavours to speed up MRI acquisition, reconstruction, and subsequent diagnosis for acute ischemic stroke with the help of deep learning.

Dankwoord

Hoewel alleen míjn naam aan de voorkant van dit proefschrift prijkt, heb ik het zeker niet zonder hulp kunnen schrijven. Hierbij mijn dank aan iedereen die heeft bijgedragen aan het onderzoek en de totstandkoming van dit proefschrift. Als eerst hartelijk dank aan alle patiënten en vrijwilligers van wie de data in dit proefschrift zijn beschreven, zonder jullie geen (data-driven) onderzoek.

Dankjewel aan mijn collega's, te beginnen bij mijn promotieteam. Guido, Matthan en Damiaan, ik mag van geluk spreken dat ik zo'n fijne en complete set begeleiders heb gehad. Wie anders heeft er een team bestaande uit een neurowetenschapper, fysicus en psychiater-filosoof? Samen hebben jullie mij wegwijs gemaakt in het doen van neuroimaging-onderzoek naar DBS voor psychiatrie. Guido, dank voor je dagelijkse begeleiding. Fijn dat je altijd voor me klaarstond om te sparren en koffie te drinken (ik weet niet wat belangrijker was). Je hebt me veel geleerd en mij aangemoedigd om mijn onderzoek niet te *undersellen*. Matthan, dank voor je dagelijkse begeleiding en jouw kritisch-fysische blik. In veel opzichten ben je een voorbeeld en ik ben je erg dankbaar voor je support. Leuk dat we onze samenwerking nog drie jaar hebben kunnen voortzetten bij de BMEP. Damiaan, dank voor je *niet*-dagelijkse begeleiding. Ik vind het knap hoe je altijd het overzicht bewaarde en op zoek ging naar het grotere verhaal. Jouw enthousiasme voor DBS en oog voor de klinische kant werkten aanstekelijk.

Hartelijk dank aan de leescommissie. Prof. Kuhn, dear Jens, thanks for taking the time to review my thesis and for coming over and taking part in my defence. I'm looking forward to having a nice discussion on the use of tractography in DBS. Prof. Nederveen, beste Aart, dank voor de beoordeling van mijn proefschrift en fijn dat ik kon aansluiten bij de mr-fysica groep op Z0. Prof. Forstmann, dear Birte, thanks for taking the time to review my thesis and the collaboration on the AHEAD diffusion MRI protocol. Dr. Beudel, beste Martijn, mijn dank voor de beoordeling van mijn proefschrift. Leuk om iemand die aan vergelijkbare vragen werkt bij de neurologie in mijn commissie te hebben. Dr. De Koning, beste Pelle, thanks voor het beoordelen van mijn proefschrift en het vertegenwoordigen van het DBS-team in mijn commissie.

Thanks to all the colleagues in the Van Wingen-group, collectively you've made the PhD more enjoyable. Paul, thanks for the many nice discussions, our fruitful collaboration, and being an awesome person. Nina, thanks for being one of the first

people to welcome me to the department and the many nice chats. Michelle, dankjewel voor de gezelligheid, van het AMC tot in Genève. Anouk, je hebt het het langst uitgehouden van al mijn kantoorgenoten. Dank voor alle humor en koffiemomenten. Egill, thanks for the fun times and sharing all those meals. Filipa, thanks for the fun and your enthusiasm. Nadine, dank voor de gezelligheid op kantoor en op reis; leuk dat we samen aan de misofonie hebben kunnen werken. Willem, thanks voor de gezelligheid. Freek, kantoorgenoot, thanks voor de gezelligheid. Weet je nog dat 2020 ver weg leek toen we begonnen? Rajat, thanks for being an inspiring researcher and a fun person to be around. Achmed, roomie!, thanks for the nice times. Leonardo, thanks for your passion for science and for your enthusiasm during all those *Ciao, Luka!*'s. Wieke, dank voor je gezelligheid. Shu, Selene, Dilan and Laurens, thanks for continuing to make the group a nice place after I left.

Dank aan alle DBS-onderzoekers. Zonder jullie was dit werk nooit zo klinisch relevant geworden en had ik nooit zo veel koffie gedronken en koekjes gegeten… Isidoor, van het wegwijzen van een jonge onderzoeker naar een hechte vriendschap. Ik ben blij dat we elkaar binnen en buiten het werk zo goed konden vinden. Maarten, dank voor je luisterend oor en de leuke tijd tijdens en na mijn promotieonderzoek. Leuk dat ik je optimalisatieverhaal mocht opleuken met een illustratie. Melisse, dank voor je ongebreidelde enthousiasme en het draaien van een complexe studie waar we veel van leren. Judy, thanks voor de gezelligheid binnen en buiten het onderzoek. Pieter, een dikke merci voor je enthousiasme en je humor – ook goed om te weten dat DBS kosteneffectief is. Ilse, thanks voor je mooie werk op het gebied van de klinische effectiviteit van DBS met ons nieuwe target. Zonder jouw database ook geen data-driven onderzoek. Grappig (en puur toeval) dat de titels van onze proefschriften op elkaar aansluiten. Roel, dank voor je inzichten en inzet voor de studie naar de klinische effectiviteit van DBS met ons nieuwe target.

Ook dank aan de rest van het DBS-team. Martijn, dank voor het wegwijs maken binnen de afdeling en je hart voor onderzoek binnen de DBS. Ik heb genoten van de mooie kans om naar je nieuwe lab te komen, ook al was er een sprint door Central Park voor nodig. Nienke, dank voor je betrokkenheid bij de patiënt en het onderzoek. Janine, dank voor de gezelligheid en de tijd die je steekt in de patiënt en bruikbare data. Mirjam, dankjewel voor de gezelligheid. Jaimy, dank voor de ondersteuning. Ralph, Ron, Geeske en alle anderen uit het DBS-team, dank voor de fijne werksfeer.

Speciale dank aan de DBS-neurochirurgen voor een prettige samenwerking. Het grootste deel van mijn onderzoek had betrekking op jullie werk en ik heb dan ook veel aan jullie gehad. Mooi dat de deur openstond op H2 en ik een stukje heb

kunnen bijdragen aan jullie vakgebied. Pepijn, dank voor het sparren en je enthousiasme over de tracking. Rick, bedankt voor het inkijkje in de OK en de vele discussies. Maarten, thanks voor je inzet voor de geavanceerde imaging in de DBS.

Ook aan de studenten die bij mij stage hebben gelopen ben ik dank verschuldigd. Thanks Chaira, Samuel, Eva en Isaac! Ik hoop dat jullie op een leuke en leerzame stage terugkijken. Veel succes met de volgende stappen in jullie carrières.

Thanks aan de overige collega-onderzoekers bij de psychiatrie die het werk op de afdeling leuker en interessanter maakten. Koen, kortstondige roomie, leuk dat je me betrokken hebt bij jouw onderzoek. Ik waardeer je Hollandse nuchterheid en enthousiasme. Collin, thanks for being such a cheerful colleague, we had a lot of fun in the hallways discussing anything. It was nice seeing you push to get the newest tech into the clinic. Rianne, thanks voor je vertrouwen in mijn imaging-kunde bij het doen van peer-reviews, leuk dat ik van je heb kunnen leren. Dirk, dank voor je inzicht en passie voor de DBS-elektrofysiologie; het was leuk om samen te werken. Nigel, thanks voor de goede samenwerking en het koppelen van de imaging aan de elektrofysiologie. Renée, dank voor je goede spirit; je maakte de 3e een stuk gezelliger. Thomas, dank voor het verlevendigen van de afdeling, van de leuke babbeltjes tot het rennen op de trap met je patiënten. Tim, thanks voor de gezelligheid op de afdeling en op congres.

Veel dank aan iedereen die het werk op de afdeling ondersteunde en mij veel zorg uit handen nam. Judith, dank voor je regelwerk en gezelligheid. Dankzij jou kreeg ik eindelijk toegang tot EPIC en mijn onderzoeksdata. Marianne, dank voor de formele en informele hulp in het promotietraject, het was altijd fijn om even te babbelen. Andrea, dank voor je inzet en hulp bij het afronden van mijn traject. Dank ook aan Lisette, Gaby, Ditte, Raquel, Leonie, Ingeborg, Dennis en alle anderen die mij hebben geholpen. Dank ook aan Arjan voor het beheren van ons rekencluster, je ondersteuning was top.

Mijn dank aan alle collega's van Z0, het was fijn om deel uit te maken van jullie groep. Jasper, van studiegenoot naar collega – thanks voor de gezelligheid binnen en buiten het AMC. Kerry, thanks for showing me your beautiful diffusion work, and sharing rooms abroad. Frans, dank voor de prettige samenwerking. Gustav, dank voor de peer support halverwege. Lukas, Eva, Luuk, Bram, Anouk, Koen, Bobby, Carmen, Melissa, Susi, Oliver, Laura, Mariah en alle andere medeonderzoekers van Z0, dank voor de fijne sfeer en de leerzame tijd.

Thanks ook aan de andere collega's op de AMC-campus. Ingo, dank voor je fundamentele onderzoek om DBS beter te kunnen begrijpen. Ons bezoek aan het AIAS zal ik niet snel vergeten. Dank aan prof. Nieuwenhuys, Rudolf, voor het delen

van uw kennis over neuroanatomie en voor de gastvrijheid. Chris, dank voor de gezelligheid, je fundamentele onderzoek en scherpe vragen. Thanks aan mijn eerste MRI-mentor Pieter, die paar maanden stage met jou vormden een uitstekende basis. Fijn dat we elkaar nog tegenkwamen op Spinoza. Jelle, dank voor de leuke tijd in het Spinoza en ver daarbuiten, vooral in het samen optrekken in Parijs. Diederick, hulde voor je blijvende ICT-support en de lol in het Spinoza. Wietske, je bent een inspirerende onderzoeker. Thanks voor de gezelligheid. Kai, dank voor alle leuke discussies die ontstaan zijn uit je soms onorthodoxe standpunten. Maartje, dank voor de fijne samenwerking, ik waardeer je doorzettingsvermogen en je geduld. Bob, thanks for all your inspiring work and your continued interest in young researchers.

Thanks to all the fun international colleagues who I've gotten to know at meetings and conferences, you're what makes science fun. Dear Francisco, Frank, it's nice how our joint interests extend far beyond diffusion MRI. I hope to be seeing you and your dog mug in the future. Patricio, I'm happy that you saw Jesus play in Barcelona. Thanks for all the laughs and your interesting stances on medical ethics. Prof. Mayberg, thanks for hosting me in your lab.

Fred, Mahsa, Albert, and Robbie, thanks for providing me with such a stimulating environment during my Master's internship. Even though the research topic was quite different, you put me on the right track to science. Thanks to all the fun and interesting people who are/were my colleagues while finishing this thesis, and thanks to everyone who I might have forgotten to thank…

Hartelijk dank aan al mijn vrienden voor de afleiding, atletiekmaatjes voor de ontspanning door inspanning, (voormalig) leraren en mentoren voor jullie bagage.

Thijs en Romy, mijn paranimfen, we zijn van ver gekomen. Vanaf het begin van de studie heb ik veel aan jullie gehad en ik ben jullie zeer dankbaar voor jullie vriendschap. Ik vind het ontzettend fijn dat jullie naast mij staan tijdens de verdediging.

Tobi, vriend van het eerste uur, dank voor al je afleiding en je support. Yo, Sebas, Anna, thanks voor alle *babbels*. Merci Marc en Katrijn, Alexander, Daan en Noor, Moes en Roos, Rolâââââând, Danny, Thomas en Joyce, Gijs, Michael, Koen, Bryan en de *kersies* voor jullie goede gezelschap. Bas, ontzettend bedankt voor je creativiteit, ik ben blij hoe mijn vage ideeën door jou in een mooi boekje zijn omgetoverd. Nort, dank voor je advies – het heeft zijn vruchten afgeworpen.

Speciale dank aan al mijn lieve (schoon)familie voor alle steun en enthousiaste pogingen om te begrijpen waar mijn onderzoek nou over ging. *Спасибо!*

Mama, dankjewel voor je warmte en je luisterend oor; zoals het hoort, komt alles voorbij aan de keukentafel. Papa, ik ben het nog steeds niet met je eens over jouw stelling over alfa's en bèta's. Dankjewel voor je nimmer aflatende belangstelling, ook al was dit onderzoek een ver-van-je-bedshow. Hetty, dank voor je gezelligheid en humor. Lasse, broertje, dank voor alle leuke avonturen. Kris en Anita, thanks voor al jullie steun, maar zeker ook de gezelligheid. Joy en Dylan, gezellig om bij de fam te horen.

Liefste Jessy, bedankt voor alles. Je ging me voor in je promotieonderzoek en ik kon mooi afkijken wat het is om een goede wetenschapper te zijn. Helaas zit het met je gezondheid niet mee; ik heb ontzettend veel bewondering hoe je daarmee omgaat. Je combineert intelligentie, ambitie en doorzettingsvermogen en bent de krachtigste vrouw die ik ken. Het is ontzettend fijn om jou mijn lief te noemen. Hoe je nog steeds om mijn flauwe grapjes lacht is mij een raadsel.